J. Mech. Phys. Solids 203 (2025) 106194

Contents lists available at ScienceDirect

Journal of the Mechanics and Physics of Solids

journal homepage: www.elsevier.com/locate/jmps

Large strain constitutive modelling of soft compressible and incompressible solids: Generalised isotropic and anisotropic viscoelasticity

Zeng Liu [a,b,*], Rogelio Ortigosa [c], Antonio J. Gil [d,**], Javier Bonet [a,b,*]

[a] Centre Internacional de Mètodes Numèrics en Enginyeria (CIMNE), Barcelona, Spain
[b] Departament de Enginyeria Civil i Ambiental (DECA), Universitat Politècnica de Catalunya, Barcelona, Spain
[c] Computational Mechanics and Scientific Computing Group, Technical University of Cartagena, Campus Muralla del Mar, 30202, Cartagena (Murcia), Spain
[d] Zienkiewicz Institute for Modelling, Data and AI, Faculty of Science and Engineering, Swansea University, Bay Campus, SA1 8EN, United Kingdom

ARTICLE INFO

Keywords:
Large strain
Finite viscoelasticity
Maxwell rheological model
Multiplicative decomposition

ABSTRACT

This paper discusses a new phenomenological continuum formulation for the constitutive modelling of viscoelastic materials at large strains. Following pioneering works in Sidoroff (1974), Lubliner (1985), Bergström (1998) and Reese and Govindjee (1997), the formulation shares some common ingredients with other phenomenological approaches, including the multiplicative decomposition of the deformation gradient into viscous and elastic contributions, the additive Maxwell-type decomposition of the strain energy density, and the definition of a set of kinematic internal state variables with their associated evolution laws. Our formulation departs from other state-of-the-art methodologies via three distinct novelties. First, and revisiting previous work by Bonet (2001), the paper introduces a thermodynamically consistent linear rate type evolution law in terms of stress-type variables, which resembles the return mapping algorithm typically used in elastoplasticity, facilitating the modelling link between both inelastic constitutive models. In this sense, the proposed viscoelastic evolution law can be identified with a classical plastic flow rule. Very importantly, the evolution law is shown to be compatible with the second law of thermodynamics by construction and have a closed-form solution in the case of incompressible viscoelasticity when using a prototypical neo-Hookean type of non-equilibrium strain energy density. Moreover, the paper shows how using the concept of a stress-driven dissipative potential, more general non-linear type of stress evolution laws can be straightforwardly constructed. Second, to facilitate the joint consideration of anisotropy and thermodynamic equilibrium, a frame indifferent stress free configuration is introduced which facilitates the definition of objective strain measures. Third, the methodology is extended from isotropy to transverse isotropy via the consideration of the appropriate structural tensor. The formulation is first displayed for the simple case of a single transversely isotropic invariant contribution with corresponding closed-form solution, and then straightforwardly extended to the consideration of the second transversely isotropic invariant, multiple families of fibres, or even more complex symmetry groups. To demonstrate the capability of the new framework, a specialised form of the eight-chain long-term strain energy (long term) and a neo-Hookean strain energy (non-equilibrium) have been adopted for the description of the mechanical behaviour

* Corresponding authors at: Centre Internacional de Mètodes Numèrics en Enginyeria (CIMNE), Barcelona, Spain.
** Corresponding author.
E-mail addresses: zliu@cimne.upc.edu (Z. Liu), a.j.gil@swansea.ac.uk (A.J. Gil), jbonet@cimne.upc.edu (J. Bonet).

https://doi.org/10.1016/j.jmps.2025.106194
Received 24 March 2025; Received in revised form 6 May 2025; Accepted 13 May 2025
Available online 2 June 2025

of VHB 4910 polymer, due to its use in current Electro-Active Polymers based soft robotics. Good agreement is found between in silico predictions and available experimental data on various tests, including loading–unloading cyclic tests, single-step relaxation tests and a multi-step relaxation test. Finally, biaxial loading–unloading cyclic and relaxation tests are presented to further showcase performance in anisotropic scenarios.

1. Introduction

Viscoelastic material models are widely adopted for the characterisation of the mechanical behaviour of polymers, soft biological tissues and many other soft smart (i.e. electro, magneto, chemo) active materials (Li et al., 2022; Wollner et al., 2023; Eleni et al., 2013; Freed and Rajagopal, 2016; Budday et al., 2017; Ghosh and Lopez-Pamies, 2021; Lenarda and Paggi, 2022; Liu et al., 2022; Dusane et al., 2023). To include dissipative mechanisms into their constitutive models, there have been two different classes of modelling approaches at the continuum length scale, as pointed out in Kumar and Lopez-Pamies (2016), Liu et al. (2021), Wijaya et al. (2023). The first approach is based on the hereditary integral, which generalises the concept of linear viscoelasticity theory to large deformations in terms of relaxation functions (Clifton et al., 2016; Haupt and Lion, 2002). In this approach, the model is usually formulated directly on the stress–strain relationship, and the viscous effects are taken into account via the hereditary integral of a relaxation function with the loading history for the description of the fading memory influence on the stress (Gurtin, 1968). The constrained mixture theory that has been developed for the remodelling of vascular growth can also be categorised into this hereditary-integral-based modelling framework (Humphrey and Rajagopal, 2002; Valentin et al., 2013). The second approach relies on the definition of so-called internal variables at the macroscopic level, which incorporate the physical insight of the microscopic scale. This *phenomenological* approach typically utilises the multiplicative decomposition of the deformation gradient into elastic and viscous components (Sidoroff, 1974; Bergström and Boyce, 1998; Lubliner, 1985; Reese and Govindjee, 1998; Huber and Tsakmakis, 2000; Bonet, 2001; Dal et al., 2020), and the evolution of internal variables generally leads to thermodynamically consistent dissipative behaviour (Bergström and Boyce, 1998; Naghdabadi et al., 2012). A Zener-type structure (Reese and Govindjee, 1998, 1997) is adopted and the inelastic deformation gradient resulting from the multiplicative decomposition is treated as the internal variable. The derivation of this model is similar to that of large strain elastoplasticity (Simo and Miehe, 1992). Note that this phenomenological approach can be generalised to involve multiple non-equilibrium contributions (Chockalingam et al., 2021). All in all, the second approach is more tractable than the first one and the model discussed here, as will be shown, belongs to this prevalent finite strain viscoelastic modelling approach.

Well known formulations (Lubliner, 1985; Bonet, 2001) exploit Maxwell type rheological models to provide physical insight to their more general continuum description, where each branch of the Maxwell-decomposition can be identified with a spring in series with a dashpot. The viscous strains in the dashpots represent the internal state variables that need to be determined for the comprehensive determination of the thermodynamic system. It is typically accepted (Kumar and Lopez-Pamies, 2016) that the strain energy of the system can be modelled via a two-potential framework, characterised by a long-term strain energy functional, that represents how the material stores energy through elastic deformation, and a non-equilibrium strain energy functional, that represent how the material dissipates energy through viscous deformation. In the finite strain continuum setting, nonlinear rate evolution laws for the internal variables are derived, in contrast with the linear relaxation laws that can be obtained in the simpler one-dimensional case. For ease of computational implementation, incremental forms of the evolution laws are derived in accordance with a selected time integration (typically implicit) scheme. Given the fact that soft materials can be either compressible or incompressible, suitable formulations are required in both cases (Wijaya et al., 2023), where the incompressibility constraint leads to an inevitable more complex nonlinear evolution law.

Additional efforts have been directed towards anisotropic viscoelasticity, generally modelled as an extension of the isotropic formulation via the use of structural tensors and the isotropicisation theorem (Ericksen and Rivlin, 1997; Limbert and Middleton, 2004; Pioletti et al., 1998). The anisotropic viscoelastic model proposed by Holzapfel et al. (2000) extends the isotropic convolution integral formulation established by Holzapfel (1996), incorporating a dependence of the equilibrium stress and overstress response on the invariants of the Cauchy–Green and structure tensors. Another physically based model has been formulated by Bischoff et al. (2004), specifically for highly extensible soft biological materials, which integrates the isotropic viscoelastic model of Bergström and Boyce (1998) and the orthotropic hyperelastic model developed by Bischoff et al. (2002). An alternative model has been developed in Nguyen et al. (2007) by the use of separate decompositions of the deformation gradient for the matrix and the fibre. Other works on the nonlinear viscoelastic modelling of fibre-reinforced composites using the multiplicative decomposition of deformation gradient can be found in Nedjar (2007), Liu et al. (2019), Sadik and Yavari (2024), Ciambella and Nardinocchi (2021).

In this work, we revisit previous work by one of the co-authors (Bonet, 2001) and advance the modelling approach thereby presented towards the general case of anisotropic viscoelasticity. With that in mind, we first introduce a thermodynamically consistent linear evolution law in terms of stress-type variables, which resembles the return mapping algorithm typically used in elastoplasticity (Simo and Hughes, 1998). As a result, the proposed viscoelastic evolution law can be identified with the classical plastic flow rule of other inelastic approaches. For the case of isochoric deformation, typical of viscoelastic polymers, the flow rule is suitably adapted to comply with this kinematic constraint. Very importantly, the evolution law is shown to have a closed-form solution in the case of incompressible viscoelasticity when using a prototypical neo-Hookean type of non-equilibrium strain energy density. With a view to facilitate the joint consideration of anisotropy and thermodynamic equilibrium, a frame indifferent

stress free configuration is introduced which facilitates the definition of objective strain measures with respect to the intermediate configuration. Moreover, with the aim of characterising materials endowed with anisotropic microstructures in the form of rank laminates (i.e. Electro-Active Polymers Ortigosa et al., 2022a), the methodology is extended from isotropy to transverse isotropy via the consideration of the appropriate $D_{\infty h}$ rank-one structural tensor (Zheng, 1994). We propose a physically insightful approach whereby the deformation gradient is also decomposed into the elastic and unique viscous parts for the one-dimensional fibre family as pointed out in Sansour (2008). Although the formulation is pursued in the examples shown for the simpler case of a single transversely isotropic invariant contribution (with corresponding closed-form solution), the methodology is straightforwardly extended to the consideration of the second transversely isotropic invariant, multiple families of fibres, or even more complex symmetry groups.

The paper is organised as follows. Section 2 reviews the basis of the linear rheological model in the one-dimensional setting. Section 3 presents the approach adopted for the modelling of compressible finite strain viscoelasticity, in which the unique viscous stretch tensor is defined as the internal variable that describes the viscous part of the deformation. A new evolution law is proposed to ensure positive viscous dissipation, and its incremental form is derived and solved. For the convenience of computational implementation, the tangent modulus of this formulation is given in Appendix B. Since the viscous deformation component for the vast majority of soft materials is assumed to be isochoric, incompressible finite strain viscoelasticity is formulated in Section 4. To ensure compliance with the incompressibility constraint, a modified evolution law is described so that thermodynamical consistency is also guaranteed in this case. Appendix C details the tangent modulus in this incompressible case. Section 5 presents the extension of the framework into anisotropic scenarios, with a focus on transverse isotropy, via the consideration of appropriate structural tensors. To validate the proposed methodology, Section 6 presents a specialised form of the theoretical framework using the eight-chain strain energy functional (long term) and an incompressible neo-Hookean strain energy functional (non-equilibrium). For calibration purposes, experimental data from various tests of VHB polymers at different strain rates are used. To demonstrate the validity of the anisotropic viscoelastic model, biaxial loading–unloading and relaxation tests are also presented in Section 7. Finally, the main contributions of this work are summarised in Section 8 with some additional useful material included in Appendices A–C.

2. One-dimensional Maxwell model

The proposed formulation starts from the generalised Maxwell model in the one-dimensional setting, also known as the Wiechert model, see Fig. 1. According to Bonet (2001), it is assumed that the total force f in this model can be written as

$$f = f_\infty + \sum_\alpha f_\alpha, \tag{1}$$

where f_∞ and f_α represent long-term and non-equilibrium components, respectively. For the convenient generalisation of this model to the three-dimensional case, we can rewrite the above equation in terms of the total free energy Ψ as

$$\Psi(x) = \Psi_\infty(x) + \sum_\alpha \Psi_\alpha\left(x,\ x_\alpha\right), \tag{2}$$

where x is the total displacement, x_α represents the viscous displacement, and Ψ_∞ and Ψ_α stand for the long-term and non-equilibrium energy terms, respectively. As shown in Fig. 1, the free energy can be expressed as

$$\Psi_\infty = \frac{1}{2}K_\infty x^2; \qquad \Psi_\alpha = \frac{1}{2}K_\alpha\left(x - x_\alpha\right)^2, \tag{3}$$

where K_∞ and K_α denote the stiffness of long-term and viscous components, respectively. It should be pointed out that the viscous displacements x_α are internal variables that need to be determined for the complete description of the system. The force equilibrium equation can be obtained by differentiating Eq. (3) with respect to the total displacement x, resulting in

$$f = \underbrace{K_\infty x}_{=f_\infty} + \sum_\alpha \underbrace{K_\alpha\left(x - x_\alpha\right)}_{=f_\alpha}, \tag{4}$$

where the above terms can be identified with those featuring in (1). As can be seen from Fig. 1, the force of each spring within the corresponding viscous element can be related to the rate of change of the viscous deformation, which can be expressed as

$$c_\alpha \dot{x}_\alpha = f_\alpha; \tag{5a}$$

$$f_\alpha = K_\alpha\left(x - x_\alpha\right), \tag{5b}$$

where $\dot{x}_\alpha$ denotes time differentiation of the viscous displacement x_α, and c_α stands for the linear viscosity that can be determined by the stiffness of the corresponding spring and the retardation time parameter τ_α as

$$c_\alpha = \tau_\alpha K_\alpha. \tag{6}$$

By combination of this equation and Eqs. (5a) and (5b), the evolution equation of the internal variable x_α can be rewritten as

$$\dot{x}_\alpha = \frac{1}{\tau_\alpha}\left(x - x_\alpha\right). \tag{7}$$

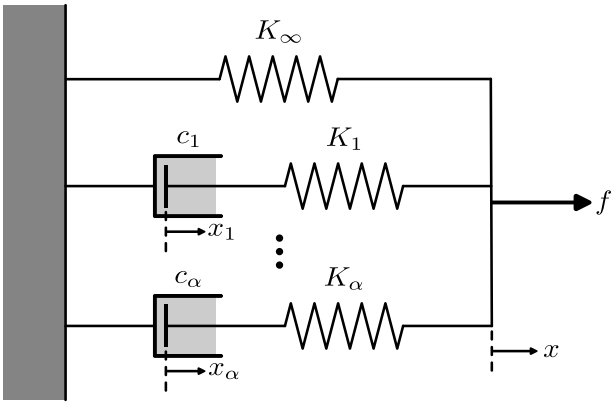

Fig. 1. Schematic diagram of the one-dimensional Maxwell model.

For the extension of this evolution law to the Lagrangian finite deformation setting, an alternative form of Eq. (7) is proposed by expressing Eq. (5b) as the relaxation of the non-equilibrium force component f_α at constant total displacement x, which is given by

$$\left.\frac{\mathrm{d}f_\alpha}{\mathrm{d}t}\right|_{x=\text{ const}} = -\frac{1}{\tau_\alpha} f_\alpha. \tag{8}$$

Note that combination of (5b) and (8) can easily lead to the evolution law of internal variable x_α (7) by straightforward transformation. However, it is worth mentioning here that the extension of (7) to the finite deformation case is non-trivial due to the fact that internal kinematic variables are usually nonlinearly constrained, while (8) here can be easily generalised into the three-dimensional Lagrangian setting as will be described in the following sections.

3. Compressible viscoelasticity at finite strains

This Section presents a theoretical framework for large strain compressible viscoelasticity, where the viscous deformation is not assumed isochoric at a first instance.

3.1. Continuum kinematics and multiplicative decomposition

Let $\mathcal{B}_0 \subset \mathbb{R}^3$ and $\mathcal{B}_t \subset \mathbb{R}^3$ denote the reference and current configurations of an arbitrary deformable continuum, respectively, with $\partial\mathcal{B}_0$ and $\partial\mathcal{B}_t$ their corresponding exterior boundaries with outward unit normals $\boldsymbol{N}$ and $\boldsymbol{n}$, and let $\boldsymbol{X} \in \mathcal{B}_0 \subset$ and $\boldsymbol{x} \in \mathcal{B}_t$ symbolise position vectors in their respective configurations. The motion of the material point $\boldsymbol{X}$ is denoted by $\boldsymbol{\varphi}(\boldsymbol{X}, t) : \mathcal{B}_0 \times [0, t] \to \mathbb{R}^3$ that maps into the corresponding position $\boldsymbol{x}$ during the time interval $[0, t]$. The deformation gradient tensor $\boldsymbol{F}$ is defined as $\boldsymbol{F} = \boldsymbol{\nabla}_0 \boldsymbol{\varphi}(\boldsymbol{X}, t)$, where $\boldsymbol{\nabla}_0$ represents the gradient in the reference configuration, and its determinant $J = \det\boldsymbol{F}$ denotes the Jacobian. In order to extend the one-dimensional Maxwell model to the large deformation three-dimensional setting, the deformation gradient $\boldsymbol{F}$ is typically decomposed into elastic $\boldsymbol{F}_{\mathrm{e}_\alpha}$ and viscous $\boldsymbol{F}_{\mathrm{v}_\alpha}$ components (Kröner, 1959; Lee, 1969; Anand, 1985; Bergström and Boyce, 1998; Reese and Govindjee, 1997)

$$\boldsymbol{F} = \boldsymbol{F}_{\mathrm{e}_\alpha} \boldsymbol{F}_{\mathrm{v}_\alpha}, \tag{9}$$

through the introduction of suitable intermediate (i.e. stress free) configurations (see Fig. 2). As it is illustrated, the number of viscous elements $\alpha = 1 \dots n_\alpha$ in this generalised Maxwell model can be arbitrary. Note that $\boldsymbol{F}_{\mathrm{v}_\alpha}$ denotes the internal variable of the corresponding viscous element α that determines the current state of the system, with thermo-dynamical equilibrium achieved when $\boldsymbol{F}_{\mathrm{v}_\alpha} = \boldsymbol{F}$. Moreover, to ensure that the proposed constitutive model is objective (i.e. frame invariant), suitable rotation free right Cauchy–Green deformation tensors can be defined as

$$\boldsymbol{C} = \boldsymbol{F}^{\mathrm{T}} \boldsymbol{F}; \tag{10a}$$

$$\boldsymbol{C}_{\mathrm{v}_\alpha} = \boldsymbol{F}_{\mathrm{v}_\alpha}^{\mathrm{T}} \boldsymbol{F}_{\mathrm{v}_\alpha}, \tag{10b}$$

where $\boldsymbol{C}$ and $\boldsymbol{C}_{\mathrm{v}_\alpha}$ denote the total and viscous right Cauchy–Green deformation tensors, respectively. It should be pointed out that unlike $\boldsymbol{C}$ and $\boldsymbol{C}_{\mathrm{v}_\alpha}$, the right Cauchy–Green deformation tensor $\boldsymbol{C}_{\mathrm{e}_\alpha} = \boldsymbol{F}_{\mathrm{e}_\alpha}^{\mathrm{T}} \boldsymbol{F}_{\mathrm{e}_\alpha}$ is not defined in the reference configuration, but at the intermediate (elastic free) configuration and, as such, it is not rotation free. Indeed, the multiplicative decomposition of the deformation gradient (9) has an internal redundant rotation, which means $\boldsymbol{F}$ can equally be written as

$$\boldsymbol{F} = \boldsymbol{F}_{\mathrm{e}_\alpha}^{*} \boldsymbol{F}_{\mathrm{v}_\alpha}^{*} \quad \text{with} \quad \boldsymbol{F}_{\mathrm{v}_\alpha}^{*} = \boldsymbol{Q} \boldsymbol{F}_{\mathrm{v}_\alpha} \quad \text{and} \quad \boldsymbol{F}_{\mathrm{e}_\alpha}^{*} = \boldsymbol{F}_{\mathrm{e}_\alpha} \boldsymbol{Q}^{\mathrm{T}}, \tag{11}$$

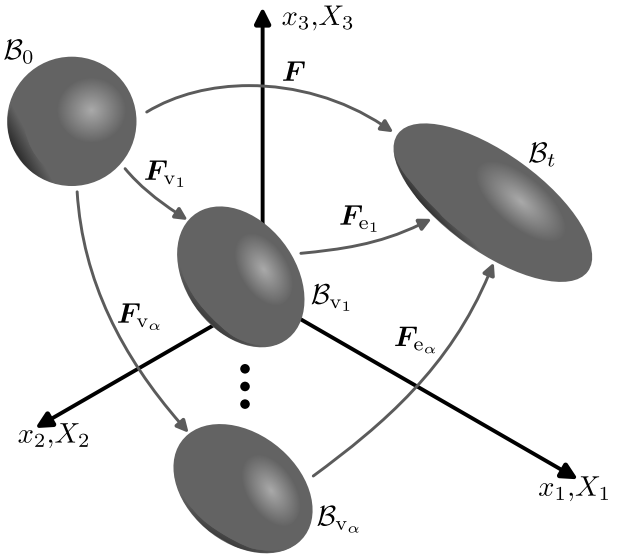

Fig. 2. Multiplicative decomposition of the deformation gradient.

where $\boldsymbol{Q} \in \mathrm{SO}(3)$ denotes an arbitrary rotation tensor. Following a similar idea to that of Holthusen et al. (2023), we propose to eliminate this redundant rotation by selecting $\boldsymbol{Q}$ as $\boldsymbol{R}_{\mathrm{v}_\alpha}^{\mathrm{T}}$, namely, the rotation tensor emanating from the right polar decomposition of the viscous deformation gradient tensor $\boldsymbol{F}_{\mathrm{v}_\alpha} = \boldsymbol{R}_{\mathrm{v}_\alpha} \boldsymbol{U}_{\mathrm{v}_\alpha}$. Hence, a unique multiplicative decomposition of the deformation gradient $\boldsymbol{F}$ can then be obtained as

$$\boldsymbol{F} = \boldsymbol{F}^*_{\mathrm{e}_\alpha} \boldsymbol{U}_{\mathrm{v}_\alpha}, \quad \boldsymbol{F}^*_{\mathrm{e}_\alpha} = \boldsymbol{F}_{\mathrm{e}_\alpha} \boldsymbol{R}_{\mathrm{v}_\alpha}, \tag{12}$$

whereby

$$\boldsymbol{C}_{\mathrm{e}_\alpha} = \boldsymbol{F}^{*\mathrm{T}}_{\mathrm{e}_\alpha} \boldsymbol{F}^*_{\mathrm{e}_\alpha} = \boldsymbol{U}^{-1}_{\mathrm{v}_\alpha} \boldsymbol{C} \boldsymbol{U}^{-1}_{\mathrm{v}_\alpha}, \tag{13}$$

and the symmetric viscous strain tensor $\boldsymbol{U}_{\mathrm{v}_\alpha}$ is also uniquely defined.

3.2. Strain energy function

By analogy with Eq. (2), a strain energy density of the system can be assumed as

$$\Psi\left(\boldsymbol{C},\ \boldsymbol{U}_{\mathrm{v}_\alpha}\right) = \Psi_\infty(\boldsymbol{C}) + \sum_\alpha \Psi_\alpha\left(\boldsymbol{C},\ \boldsymbol{U}_{\mathrm{v}_\alpha}\right), \tag{14}$$

where Ψ_∞ represents the long-term contribution and Ψ_α is the viscous element contribution defined in terms of $\boldsymbol{C}$ and $\boldsymbol{U}_{\mathrm{v}_\alpha}$. To guarantee that Ψ_α vanishes when $\boldsymbol{U}_{\mathrm{v}_\alpha}$ and $\boldsymbol{F}$ only differ by a rigid body rotation (i.e. thermo-dynamical equilibrium), we particularise the definition of Ψ_α as

$$\Psi_\alpha\left(\boldsymbol{C},\ \boldsymbol{U}_{\mathrm{v}_\alpha}\right) = \tilde{\Psi}_\alpha\left(\boldsymbol{C}_{\mathrm{e}_\alpha}\right), \tag{15}$$

where $\boldsymbol{C}_{\mathrm{e}_\alpha}$ is defined in (13) and the symbol $\tilde{\Psi}$ is used to emphasise the alternative functional dependency. Moreover, for the particular case of isotropic viscoelasticity, the strain energy contributions $\Psi_\infty(\boldsymbol{C})$ and $\tilde{\Psi}_\alpha(\boldsymbol{C}_{\mathrm{e}_\alpha})$ can be particularised in terms of their respective invariants $\{I_\bullet, II_\bullet, III_\bullet\}$, which will be implicitly assumed in what follows. Note that extension to the anisotropic case would imply the incorporation of structural tensors representative of their appropriate symmetry groups as further arguments of the strain energy density, which will be presented in a subsequent section.

3.3. Second Piola–Kirchhoff stress tensor

The second Piola–Kirchhoff stress tensor $\boldsymbol{S}$ can now be obtained from the directional derivative of the strain energy Ψ with respect to a perturbation $\delta\boldsymbol{C}$ whilst holding the internal state variable $\boldsymbol{U}_{\mathrm{v}_\alpha}$ constant (i.e. $D\,\Psi|_{\boldsymbol{U}_{\mathrm{v}_\alpha}=\mathrm{const}}[\delta\boldsymbol{C}] = \boldsymbol{S} : \frac{1}{2}\delta\boldsymbol{C}$), to yield

$$\boldsymbol{S} = 2\frac{\partial \Psi}{\partial \boldsymbol{C}} = \boldsymbol{S}_\infty + \sum_\alpha \boldsymbol{S}_\alpha, \quad \boldsymbol{S}_\infty = 2\frac{\partial \Psi_\infty}{\partial \boldsymbol{C}}, \quad \boldsymbol{S}_\alpha = 2\left.\frac{\partial \Psi_\alpha}{\partial \boldsymbol{C}}\right|_{\boldsymbol{U}_{\mathrm{v}_\alpha}=\mathrm{const}}, \tag{16}$$

where $\boldsymbol{S}_\infty$ represents the long-term stress tensor and $\boldsymbol{S}_\alpha$ denotes the viscous stress tensor of the corresponding Maxwell element and the symbol $(\bullet)|_{\boldsymbol{U}_{\mathrm{v}_\alpha}=\mathrm{const}}$ emphasises that the internal state variable $\boldsymbol{U}_{\mathrm{v}_\alpha}$ is held constant. Note that from (15) and the definition (13), stress $\boldsymbol{S}_\alpha$ will vanish when $\boldsymbol{U}_{\mathrm{v}_\alpha}$ only differs from $\boldsymbol{F}$ by a rigid body rotation. For the subsequent derivation, the elastic second Piola–Kirchhoff stress tensor of the viscous Maxwell element $\boldsymbol{S}_{\mathrm{e}_\alpha}$ is defined as

$$\boldsymbol{S}_{\mathrm{e}_\alpha} = 2\frac{\partial \tilde{\Psi}_\alpha\left(\boldsymbol{C}_{\mathrm{e}_\alpha}\right)}{\partial \boldsymbol{C}_{\mathrm{e}_\alpha}}. \tag{17}$$

It is now useful to relate stress $\boldsymbol{S}_\alpha$ $(16)_c$ to stress $\boldsymbol{S}_{\mathrm{e}_\alpha}$ (17) by noticing that

$$D\,\Psi_\alpha\big|_{\boldsymbol{U}_{\mathrm{v}_\alpha}=\mathrm{const}}[\delta\boldsymbol{C}] = D\tilde{\Psi}_\alpha[D\,\boldsymbol{C}_{\mathrm{e}_\alpha}\big|_{\boldsymbol{U}_{\mathrm{v}_\alpha}=\mathrm{const}}[\delta\boldsymbol{C}]], \tag{18}$$

and substituting the directional derivative of (13) with respect to $\delta\boldsymbol{C}$ into (18) results in

$$\boldsymbol{S}_{\mathrm{e}_\alpha} = \boldsymbol{U}_{\mathrm{v}_\alpha}\boldsymbol{S}_\alpha\boldsymbol{U}_{\mathrm{v}_\alpha}, \tag{19}$$

which establishes a necessary relationship between the Maxwell viscous contribution to the second Piola–Kirchhoff stress tensor and its elastic counterpart.

3.4. Viscous dissipation and evolution law

To fully determine the proposed viscoelastic model, an evolution law for the set of internal variables $\boldsymbol{U}_{\mathrm{v}_\alpha}(\alpha = 1 \dots n_\alpha)$ must be defined. Bonet (2001) introduces an evolution law based on the relaxation form of the viscous stress, that is, a natural extension of (8) to the three dimensional continua. This is accomplished by simply replacing the one-dimensional force and displacement in (8) with second Piola–Kirchhoff and right Cauchy–Green tensor counterparts, respectively. However, the non-satisfaction of *ab initio* positive viscous dissipation in Bonet (2001) (i.e. Coleman–Noll procedure Gurtin et al., 2010) motivates the further development of this theory in this work. As such, the rate of energy dissipation due to viscous effects is defined as

$$\begin{aligned}
\mathrm{D}_{\mathrm{vis}} &= -\sum_\alpha \frac{\partial \Psi_\alpha}{\partial \boldsymbol{U}_{\mathrm{v}_\alpha}} : \dot{\boldsymbol{U}}_{\mathrm{v}_\alpha} \\
&= -\sum_\alpha \left.\frac{\mathrm{d}\Psi_\alpha\left(\boldsymbol{C},\ \boldsymbol{U}_{\mathrm{v}_\alpha}\right)}{\mathrm{d}t}\right|_{\boldsymbol{F}=\mathrm{const}} \\
&= -\sum_\alpha \left.\frac{\mathrm{d}\tilde{\Psi}_\alpha\left(\boldsymbol{C}_{\mathrm{e}_\alpha}\left(\boldsymbol{C},\ \boldsymbol{U}_{\mathrm{v}_\alpha}\right)\right)}{\mathrm{d}t}\right|_{\boldsymbol{F}=\mathrm{const}} \\
&= -\sum_\alpha \frac{1}{2}\boldsymbol{S}_{\mathrm{e}_\alpha} : \left.\frac{\mathrm{d}\boldsymbol{C}_{\mathrm{e}_\alpha}\left(\boldsymbol{C},\ \boldsymbol{U}_{\mathrm{v}_\alpha}\right)}{\mathrm{d}t}\right|_{\boldsymbol{F}=\mathrm{const}},
\end{aligned} \tag{20}$$

where the explicit dependence of $\boldsymbol{C}_{\mathrm{e}_\alpha}$ on arguments $\{\boldsymbol{C},\ \boldsymbol{U}_{\mathrm{v}_\alpha}\}$ is displayed. To ensure that the evolution law is compatible with the second law of thermodynamics (Gurtin et al., 2010), the condition $\mathrm{D}_{\mathrm{vis}} \geq 0$ must be satisfied regardless of the current state of deformation and stress. In order to achieve this, note firstly that

$$\left.\frac{\mathrm{d}\boldsymbol{C}_{\mathrm{e}_\alpha}}{\mathrm{d}t}\right|_{\boldsymbol{F}=\mathrm{const}} = 2\mathbb{C}_{\mathrm{e}_\alpha}^{-1} : \left.\frac{\mathrm{d}\boldsymbol{S}_{\mathrm{e}_\alpha}}{\mathrm{d}t}\right|_{\boldsymbol{F}=\mathrm{const}}, \tag{21}$$

where $\mathbb{C}_{\mathrm{e}_\alpha} = 2\frac{\partial \boldsymbol{S}_{\mathrm{e}_\alpha}}{\partial \boldsymbol{C}_{\mathrm{e}_\alpha}}$ is the so-called fourth order (positive definite) Lagrangian elasticity tensor. Crucially, $\mathbb{C}_{\mathrm{e}_\alpha}$ and its inverse $\mathbb{C}_{\mathrm{e}_\alpha}^{-1}$ can be straightforwardly obtained for simple user defined strain energy densities (i.e. Saint-Venant, neo-Hookean) (Bonet et al., 2016). Using Eq. (21), the internal viscous dissipation can now be rewritten as

$$\mathrm{D}_{\mathrm{vis}} = -\sum_\alpha \boldsymbol{S}_{\mathrm{e}_\alpha} : \mathbb{C}_{\mathrm{e}_\alpha}^{-1} : \left.\frac{\mathrm{d}\boldsymbol{S}_{\mathrm{e}_\alpha}}{\mathrm{d}t}\right|_{\boldsymbol{F}=\mathrm{const}}, \tag{22}$$

where in order to ensure positive dissipation, the following general evolution law is proposed

$$\left.\frac{\mathrm{d}\boldsymbol{S}_{\mathrm{e}_\alpha}}{\mathrm{d}t}\right|_{\boldsymbol{F}=\mathrm{const}} = -\frac{1}{\tau_\alpha}\boldsymbol{S}_{\mathrm{e}_\alpha}; \qquad \tau_\alpha > 0, \tag{23}$$

where τ_α represents the relaxation time parameter that determines the rate of dissipation of the viscous stresses. For completeness, by the use of Eq. (23), the viscous dissipation can finally take the form of

$$\mathrm{D}_{\mathrm{vis}} = \sum_\alpha \frac{1}{\tau_\alpha}\boldsymbol{S}_{\mathrm{e}_\alpha} : \mathbb{C}_{\mathrm{e}_\alpha}^{-1} : \boldsymbol{S}_{\mathrm{e}_\alpha} \geq 0. \tag{24}$$

Since the elastic second Piola–Kirchhoff stress tensor $\boldsymbol{S}_{\mathrm{e}_\alpha}$ is a function of both the total deformation gradient $\boldsymbol{F}$ and viscous stretch $\boldsymbol{U}_{\mathrm{v}_\alpha}$, the left-hand side of (23) can be transformed as

$$\left.\frac{\partial \boldsymbol{S}_{\mathrm{e}_\alpha}}{\partial \boldsymbol{U}_{\mathrm{v}_\alpha}}\right|_{\boldsymbol{F}=\text{const}} : \dot{\boldsymbol{U}}_{\mathrm{v}_\alpha} = -\frac{1}{\tau_\alpha}\boldsymbol{S}_{\mathrm{e}_\alpha}, \tag{25}$$

thereby leading to the determination of the state variable $\boldsymbol{U}_{\mathrm{v}_\alpha}$ in the following nonlinear form

$$\dot{\boldsymbol{U}}_{\mathrm{v}_\alpha} = -\frac{1}{\tau_\alpha}\mathbb{M}_{\mathrm{e}_\alpha}^{-1} : \boldsymbol{S}_{\mathrm{e}_\alpha}, \tag{26}$$

where the fourth-order tensor $\mathbb{M}_{\mathrm{e}_\alpha}$ is defined by

$$\mathbb{M}_{\mathrm{e}_\alpha} = \left.\frac{\partial \boldsymbol{S}_{\mathrm{e}_\alpha}}{\partial \boldsymbol{U}_{\mathrm{v}_\alpha}}\right|_{\boldsymbol{F}=\text{const}}. \tag{27}$$

Interestingly, note that Eq. (26) is very similar to the plastic evolution equation in the context of maximum dissipation-based large strain elastoplasticity, as described in Simo (1988), Simo and Miehe (1992), facilitating thus the link between both inelastic approaches. It is straightforward to show that Eq. (26) corresponds to the plastic evolution equation in which the non-equilibrium strain energy function is replaced with the yield surface function and the elastic regime has been collapsed to the original state. In this sense, Eq. (23) can be also generalised into the plastic case by simply replacing the right-hand side with an appropriate flow rule. It is important to emphasise that the fourth tensor $\mathbb{M}_{\mathrm{e}_\alpha}$ encapsulates a nonlinear dependence on both the strain and the internal state variables.

It should also be pointed out that although the evolution Eq. (26) for the state variables $\boldsymbol{U}_{\mathrm{v}_\alpha}$ is nonlinear, the relaxation law embodied by Eq. (23) is generally linear (similar to the idea pursued in Simo 1987) except when the parameter τ_α is also a function of the stresses. Note that the only requirement to ensure positive dissipation is that τ_α is positive, but not necessarily constant, that is, $\tau_\alpha = f(\|\boldsymbol{S}_{\mathrm{e}_\alpha}\|)$, with f a non-negative function. Furthermore, more general fully nonlinear evolution laws can be developed using the concept of a dissipation potential as described in the Remark below.

Remark 1. Note that the evolution law selected in (23) is just one example of the myriad of possibilities available, and more complex *nonlinear* evolution laws can also be formulated if needed. For this purpose, the proposed formulation can be expressed in terms of a dissipation potential Φ function of the time rate of the elastic second Piola–Kirchhoff stress tensor $\boldsymbol{S}_{\mathrm{e}_\alpha}$, opening the door to any other user-defined stress-driven evolution law. Specifically, consider a stress-driven dissipation potential defined as $\Phi = \Phi(\dot{\boldsymbol{S}}_{\mathrm{e}_\alpha})$, with $\dot{\boldsymbol{S}}_{\mathrm{e}_\alpha} := \left.\frac{d\boldsymbol{S}_{\mathrm{e}_\alpha}}{dt}\right|_{\boldsymbol{F}=\text{const}}$ and Φ being a non-negative convex function, satisfying $\Phi(\boldsymbol{0}) = 0$[1]. The convexity of $\Phi(\dot{\boldsymbol{S}}_{\mathrm{e}_\alpha})$ implies that

$$\frac{\partial \Phi}{\partial \dot{\boldsymbol{S}}_{\mathrm{e}_\alpha}} : \dot{\boldsymbol{S}}_{\mathrm{e}_\alpha} \geq 0. \tag{28}$$

Therefore, choosing evolution laws constructed as

$$\frac{\partial \Phi}{\partial \dot{\boldsymbol{S}}_{\mathrm{e}_\alpha}} = -\mathbb{C}_{\mathrm{e}_\alpha}^{-1} : \boldsymbol{S}_{\mathrm{e}_\alpha}, \tag{29}$$

implies that the viscous dissipation in (22) is non-negative. One of the simplest dissipation potentials that can be defined is

$$\Phi(\dot{\boldsymbol{S}}_{\mathrm{e}_\alpha}) = \frac{\tau_\alpha}{2}\dot{\boldsymbol{S}}_{\mathrm{e}_\alpha} : \mathbb{C}_{\mathrm{e}_\alpha}^{-1} : \dot{\boldsymbol{S}}_{\mathrm{e}_\alpha}, \tag{30}$$

from which upon substitution into (29) and exploiting the positive definiteness of $\mathbb{C}_{\mathrm{e}_\alpha}^{-1}$ reduces to the evolution Eq. (23). Naturally, alternative dissipative potentials can be used instead of (30) resulting into more complex evolution laws to that in (23), all compliant with the second law of thermodynamics.

3.5. Incremental evolution law

For the sake of computational implementation, Eq. (26) would need to be integrated in time so as to update the state variables $\boldsymbol{U}_{\mathrm{v}_\alpha}$ from time step n to time step $n+1$. However, the direct use of this equation is highly cumbersome, and thus it is preferable to transform the left-hand side of Eq. (23) into an incremental form, which when using a classical (first order) backward Euler scheme renders

$$\left.\frac{\mathrm{d}\boldsymbol{S}_{\mathrm{e}_\alpha}}{\mathrm{d}t}\right|_{\boldsymbol{F}=\text{const}} = \frac{1}{\Delta t}\left(\boldsymbol{S}_{\mathrm{e}_\alpha}^{n+1} - \boldsymbol{S}_{\mathrm{e}_\alpha}^{*}\right), \tag{31}$$

[1] Strictly speaking, given that this dissipation potential is formulated in terms of stress rates it could be more precisely described as a *complementary* dissipation potential.

where Δt denotes the time step size, and the stress tensors $\boldsymbol{S}_{\mathrm{e}_\alpha}^{n+1}$ and $\boldsymbol{S}_{\mathrm{e}_\alpha}^{*}$ are defined by

$$\boldsymbol{S}_{\mathrm{e}_\alpha}^{*} = \boldsymbol{S}_{\mathrm{e}_\alpha}\left(\boldsymbol{C}^{n+1},\ \boldsymbol{U}_{\mathrm{v}_\alpha}^{n}\right) \quad \text{and} \quad \boldsymbol{S}_{\mathrm{e}_\alpha}^{n+1} = \boldsymbol{S}_{\mathrm{e}_\alpha}\left(\boldsymbol{C}^{n+1},\ \boldsymbol{U}_{\mathrm{v}_\alpha}^{n+1}\right), \tag{32}$$

where the upper script n and $n+1$ indicate evaluation in their corresponding time steps. Note that $\boldsymbol{S}_{\mathrm{e}_\alpha}^{*}$ represents the state of stress attained from the assumption that there is no viscous deformation taking place from time step n to $n+1$. Alternatively, it can also be interpreted as the state of stress attained when the deformation from time step n to $n+1$ takes place instantaneously[2]. In the context of viscoelasticity, the stress relaxation is inevitable and the final stress can be derived by substituting (31) into (23), resulting in

$$\frac{1}{\Delta t}\left(\boldsymbol{S}_{\mathrm{e}_\alpha}^{n+1} - \boldsymbol{S}_{\mathrm{e}_\alpha}^{*}\right) = -\frac{1}{\tau_\alpha}\boldsymbol{S}_{\mathrm{e}_\alpha}^{n+1}, \tag{33}$$

which after simple rearrangement results in

$$\boldsymbol{S}_{\mathrm{e}_\alpha}^{n+1} = \gamma_\alpha \boldsymbol{S}_{\mathrm{e}_\alpha}^{*}; \qquad \gamma_\alpha = \frac{\tau_\alpha}{\tau_\alpha + \Delta t}. \tag{34}$$

Note that the final relaxation stress $\boldsymbol{S}_{\mathrm{e}_\alpha}^{n+1}$ is proportional to the instantaneous stress $\boldsymbol{S}_{\mathrm{e}_\alpha}^{*}$ [3] and compared with the direct time integration of Eqs. (26)–(27), computational implementation of (34) is considerably simpler. Once the final relaxation stress $\boldsymbol{S}_{\mathrm{e}_\alpha}^{n+1}$ is computed, the elastic right-Cauchy–Green strain tensor $\boldsymbol{C}_{\mathrm{e}_\alpha}^{n+1}$ can be determined making use of the user-defined strain energy density $\tilde{\Psi}_\alpha$. After obtaining $\boldsymbol{C}_{\mathrm{e}_\alpha}^{n+1}$, the corresponding viscous state variable $\boldsymbol{U}_{\mathrm{v}_\alpha}^{n+1}$ can be derived from (13). It is possible to show by direct substitution that the symmetric viscous stretch tensor $\boldsymbol{U}_{\mathrm{v}_\alpha}^{n+1}$ can be obtained as

$$\boldsymbol{U}_{\mathrm{v}_\alpha}^{n+1} = \left(\boldsymbol{U}_{\mathrm{e}_\alpha}^{n+1}\right)^{-1}\left(\boldsymbol{U}_{\mathrm{e}_\alpha}^{n+1}\boldsymbol{C}^{n+1}\boldsymbol{U}_{\mathrm{e}_\alpha}^{n+1}\right)^{\frac{1}{2}}\left(\boldsymbol{U}_{\mathrm{e}_\alpha}^{n+1}\right)^{-1}; \qquad \boldsymbol{U}_{\mathrm{e}_\alpha}^{n+1} = \left(\boldsymbol{C}_{\mathrm{e}_\alpha}^{n+1}\right)^{\frac{1}{2}}. \tag{35}$$

The numerical procedure for the calculation of the internal variable $\boldsymbol{U}_{\mathrm{v}_\alpha}^{n+1}$ is outlined in Algorithm 1.

Algorithm 1 Numerical procedure for the calculation of the internal variable in the compressible case.

for $Time\ Increment = 1, 2, \ldots$ **do**
  for $Iteration = 1, 2, \ldots$ **do**
    Calculate the right Cauchy–Green strain tensor at the current time increment $\boldsymbol{C}^{n+1}$
    Compute the instantaneous stress tensor $\boldsymbol{S}_{\mathrm{e}_\alpha}^{*}$
    Compute the stress relaxation $\boldsymbol{S}_{\mathrm{e}_\alpha}^{n+1}$ via Eq. (34)
    Obtain the elastic right Cauchy–Green tensor $\boldsymbol{C}_{\mathrm{e}_\alpha}^{n+1}$ via stress energy density $\tilde{\Psi}_\alpha$
    Determine the internal variable $\boldsymbol{U}_{\mathrm{v}_\alpha}^{n+1}$ according to Eq. (35)
  end for
  Store the internal variable $\boldsymbol{U}_{\mathrm{v}_\alpha}^{n+1}$ as history variable
end for

Notice that for the case of a simple Saint-Venant–Kirchhoff material model, computation of $\boldsymbol{C}_{\mathrm{e}_\alpha}^{n+1}$ accepts a closed-form solution, whilst for other more nonlinear models (i.e. neo-Hookean), a simple Newton–Raphson scheme can be needed. Specifically, in the case of the simple Saint-Venant–Kirchhoff material model, (34) results in

$$\frac{1}{2}\lambda_\alpha\left(\mathrm{tr}\boldsymbol{C}_{\mathrm{e}_\alpha}^{n+1} - 3\right)\boldsymbol{I} + \mu_\alpha\left(\boldsymbol{C}_{\mathrm{e}_\alpha}^{n+1} - \boldsymbol{I}\right) = \gamma_\alpha \boldsymbol{S}_{\mathrm{e}_\alpha}^{*}, \tag{36}$$

expressed in terms of the lame coefficients λ_α and μ_α, which admits a closed-form solution for $\boldsymbol{C}_{\mathrm{e}_\alpha}^{n+1}$. Analogously, in the case of a neo-Hookean material model, (34) takes the explicit form of

$$\mu_\alpha\left(\boldsymbol{I} - \left(\boldsymbol{C}_{\mathrm{e}_\alpha}^{n+1}\right)^{-1}\right) + \frac{\lambda_\alpha}{2}\ln\left(\det \boldsymbol{C}_{\mathrm{e}_\alpha}^{n+1}\right)\left(\boldsymbol{C}_{\mathrm{e}_\alpha}^{n+1}\right)^{-1} = \gamma_\alpha \boldsymbol{S}_{\mathrm{e}_\alpha}^{*}, \tag{37}$$

which can be easily solved for $\boldsymbol{C}_{\mathrm{e}_\alpha}^{n+1}$ via a Newton–Raphson type of iterative solution scheme.

4. Incompressible viscoelasticity at finite strains

In the previous Section, the viscous stretch tensor $\boldsymbol{U}_{\mathrm{v}_\alpha}$ can in general contain both volumetric and distortional components. However, for many viscoelastic materials, the viscous deformation is usually assumed isochoric, and so in this section we will present a modified theory for incompressible viscoelasticity at finite strains.

[2] In the case of elastoplasticity, this term is known as the trial stress that may or may not satisfy the yield inequality.
[3] This projection can be identified with the radial return scheme in the context of elastoplasticity.

4.1. Volume-preserving constraints

Incompressibility of the viscous stretch contribution $\boldsymbol{U}_{\mathrm{v}_\alpha}$ implies that $\det\boldsymbol{U}_{\mathrm{v}_\alpha} = 1$ or, alternatively, by recalling (9), that

$$J_{\mathrm{e}_\alpha} = \det\boldsymbol{F}_{\mathrm{e}_\alpha} = \det\boldsymbol{F} = J. \tag{38}$$

Time differentiation of above kinematic constraint (38) leads to

$$\boldsymbol{C}_{\mathrm{e}_\alpha}^{-1} : \left.\frac{\mathrm{d}\boldsymbol{C}_{\mathrm{e}_\alpha}}{\mathrm{d}t}\right|_{\boldsymbol{F}=\mathrm{const}} = 0, \tag{39}$$

which arises as a kinematic constraint for the time evolution of the elastic right Cauchy–Green tensor $\boldsymbol{C}_{\mathrm{e}_\alpha}$. Correspondingly, the Maxwell strain energy density Ψ_α must be defined to only penalise distortional contributions, that is

$$\Psi_\alpha(\boldsymbol{C},\ \boldsymbol{U}_{\mathrm{v}_\alpha}) = \hat{\tilde{\Psi}}_\alpha\left(\boldsymbol{C}_{\mathrm{e}_\alpha}\right) = \tilde{\Psi}_\alpha\left(\hat{\boldsymbol{C}}_{\mathrm{e}_\alpha}\right); \qquad \hat{\boldsymbol{C}}_{\mathrm{e}_\alpha} = J_{\mathrm{e}_\alpha}^{-\frac{2}{3}}\boldsymbol{C}_{\mathrm{e}_\alpha}, \tag{40}$$

whereby[4] the (deviatoric) second Piola–Kirchhoff elastic stress $\boldsymbol{S}'_{\mathrm{e}_\alpha} = 2\frac{\partial\hat{\tilde{\Psi}}_\alpha\left(\boldsymbol{C}_{\mathrm{e}_\alpha}\right)}{\partial\boldsymbol{C}_{\mathrm{e}_\alpha}}$ can be shown to verify[5]

$$\boldsymbol{S}'_{\mathrm{e}_\alpha} : \boldsymbol{C}_{\mathrm{e}_\alpha} = 0, \tag{41}$$

which can be understood as an alternative kinetic (i.e. stress based) constraint to those of (38) or (39) to fulfil incompressibility[6]. Further differentiation of this constraint and application of (39) results in an alternative incompressibility constraint

$$\boldsymbol{C}_{\mathrm{e}_\alpha} : \mathbb{C}_{\mathrm{e}_\alpha} : \boldsymbol{C}_{\mathrm{e}_\alpha} = 0, \tag{42}$$

in terms of the fourth order elasticity tensor $\mathbb{C}_{\mathrm{e}_\alpha}$[7]. Note that, due to its deviatoric nature, $\mathbb{C}_{\mathrm{e}_\alpha}$ is not strictly positive definite (refer to (42)) and cannot thus be directly inverted, so the evolution law in (22) needs to be suitably adapted, which will be presented in the following section.

4.2. Modified viscous dissipation and evolution law

A straightforward way to guarantee the invertibility of the singular fourth order elasticity tensor $\mathbb{C}_{\mathrm{e}_\alpha}$ can be obtained via the following additive extension

$$\bar{\mathbb{C}}_{\mathrm{e}_\alpha} = 2\frac{\partial\boldsymbol{S}'_{\mathrm{e}_\alpha}}{\partial\boldsymbol{C}_{\mathrm{e}_\alpha}} + m\boldsymbol{C}_{\mathrm{e}_\alpha}^{-1}\otimes\boldsymbol{C}_{\mathrm{e}_\alpha}^{-1}, \tag{43}$$

where m denotes an arbitrary positive constant adopting the role of an artificial bulk modulus which guarantees the positive definiteness of the newly defined enhanced elasticity tensor $\bar{\mathbb{C}}_{\mathrm{e}_\alpha}$. It is clear now that application of (42) into $\bar{\mathbb{C}}_{\mathrm{e}_\alpha}$ renders $9m > 0$. As a result, Eq. (21) is re-defined as

$$\left.\frac{\mathrm{d}\boldsymbol{C}_{\mathrm{e}_\alpha}}{\mathrm{d}t}\right|_{\boldsymbol{F}=\mathrm{const}} = 2\bar{\mathbb{C}}_{\mathrm{e}_\alpha}^{-1} : \left.\frac{\mathrm{d}\boldsymbol{S}'_{\mathrm{e}_\alpha}}{\mathrm{d}t}\right|_{\boldsymbol{F}=\mathrm{const}}. \tag{44}$$

The evolution law for $\boldsymbol{S}'_{\mathrm{e}_\alpha}$ embodied by Eq. (23) in the compressible case, can now be adjusted in order to comply with the incompressibility constraint Eq. (39). This can be carried out via the use of a scalar parameter λ_α (i.e. Lagrange multiplier) to give

$$\left.\frac{\mathrm{d}\boldsymbol{S}'_{\mathrm{e}_\alpha}}{\mathrm{d}t}\right|_{\boldsymbol{F}=\mathrm{const}} = -\frac{1}{\tau_\alpha}\left(\boldsymbol{S}'_{\mathrm{e}_\alpha} - \lambda_\alpha\boldsymbol{C}_{\mathrm{e}_\alpha}^{-1}\right), \tag{45}$$

where the last term on the right hand side represent a possible volumetric stress contribution. Using Eqs. (39) and (44) along with above Eq. (45), the value of λ_α can be obtained after simple algebra as

$$\lambda_\alpha = \frac{\boldsymbol{S}'_{\mathrm{e}_\alpha} : \bar{\mathbb{C}}_{\mathrm{e}_\alpha}^{-1} : \boldsymbol{C}_{\mathrm{e}_\alpha}^{-1}}{\boldsymbol{C}_{\mathrm{e}_\alpha}^{-1} : \bar{\mathbb{C}}_{\mathrm{e}_\alpha}^{-1} : \boldsymbol{C}_{\mathrm{e}_\alpha}^{-1}}, \tag{46}$$

[4] For the particular isotropic case, the strain energy $\tilde{\Psi}_\alpha$ depends on $\hat{\boldsymbol{C}}_{\mathrm{e}_\alpha}$ via its first two invariants $\{I_{\hat{\boldsymbol{C}}_{\mathrm{e}_\alpha}}, II_{\hat{\boldsymbol{C}}_{\mathrm{e}_\alpha}}\}$.

[5] As standard, the deviatoric nature of the stress tensor is emphasised using the superscript $'$ symbol.

[6] This kinetic constraint results from the homogeneous nature of order 0 of the Maxwell strain energy function $\tilde{\Psi}_\alpha$, that is, $\tilde{\Psi}_\alpha(\boldsymbol{C}_{\mathrm{e}_\alpha}) = \tilde{\Psi}_\alpha(\alpha\boldsymbol{C}_{\mathrm{e}_\alpha})$, for any arbitrary constant α (Bonet et al., 2016).

[7] Constraints (41) and (42) can be easily obtained by computing first and second derivatives of $\tilde{\Psi}_\alpha(\alpha\boldsymbol{C}_{\mathrm{e}_\alpha})$ with respect to α, evaluated at $\alpha = 1$.

from where the positive dissipation Eq. (22) now becomes

$$\begin{aligned} \mathrm{D}_{\mathrm{vis}} &= -\sum_{\alpha} \boldsymbol{S}'_{\mathrm{e}_\alpha} : \bar{\mathbb{C}}^{-1}_{\mathrm{e}_\alpha} : \left.\frac{\mathrm{d}\boldsymbol{S}'_{\mathrm{e}_\alpha}}{\mathrm{d}t}\right|_{\boldsymbol{F}=\mathrm{const}} \\ &= \sum_{\alpha} \frac{1}{\tau_\alpha} \boldsymbol{S}'_{\mathrm{e}_\alpha} : \bar{\mathbb{C}}^{-1}_{\mathrm{e}_\alpha} : \left(\boldsymbol{S}'_{\mathrm{e}_\alpha} - \frac{\boldsymbol{S}'_{\mathrm{e}_\alpha} : \bar{\mathbb{C}}^{-1}_{\mathrm{e}_\alpha} : \boldsymbol{C}^{-1}_{\mathrm{e}_\alpha}}{\boldsymbol{C}^{-1}_{\mathrm{e}_\alpha} : \bar{\mathbb{C}}^{-1}_{\mathrm{e}_\alpha} : \boldsymbol{C}^{-1}_{\mathrm{e}_\alpha}} \boldsymbol{C}^{-1}_{\mathrm{e}_\alpha} \right) \\ &= \sum_{\alpha} \frac{1}{\tau_\alpha} \frac{(\boldsymbol{S}'_{\mathrm{e}_\alpha} : \bar{\mathbb{C}}^{-1}_{\mathrm{e}_\alpha} : \boldsymbol{S}'_{\mathrm{e}_\alpha})(\boldsymbol{C}^{-1}_{\mathrm{e}_\alpha} : \bar{\mathbb{C}}^{-1}_{\mathrm{e}_\alpha} : \boldsymbol{C}^{-1}_{\mathrm{e}_\alpha}) - (\boldsymbol{S}'_{\mathrm{e}_\alpha} : \bar{\mathbb{C}}^{-1}_{\mathrm{e}_\alpha} : \boldsymbol{C}^{-1}_{\mathrm{e}_\alpha})^2}{\boldsymbol{C}^{-1}_{\mathrm{e}_\alpha} : \bar{\mathbb{C}}^{-1}_{\mathrm{e}_\alpha} : \boldsymbol{C}^{-1}_{\mathrm{e}_\alpha}} \\ &\geq 0, \end{aligned} \tag{47}$$

and the positive value of the numerator is a consequence of the Cauchy–Schwarz inequality. An alternative derivation of the evolution law (45) and the value of the Lagrange multiplier (46) can be found in Appendix A.

4.3. Incremental equations of the modified evolution law

Following a similar procedure to that described in Section 3.5, Eq. (45) can be integrated in time (i.e. first order backward Euler) as

$$\frac{1}{\Delta t}(\boldsymbol{S}'^{n+1}_{\mathrm{e}_\alpha} - \boldsymbol{S}'^{*}_{\mathrm{e}_\alpha}) = -\frac{1}{\tau_\alpha}\left(\boldsymbol{S}'^{n+1}_{\mathrm{e}_\alpha} - \lambda^{n+1}_{\alpha} \left(\boldsymbol{C}^{n+1}_{\mathrm{e}_\alpha} \right)^{-1} \right), \tag{48}$$

where $\boldsymbol{S}'^{*}_{\mathrm{e}_\alpha}$ and $\boldsymbol{S}'^{n+1}_{\mathrm{e}_\alpha}$ are defined as

$$\boldsymbol{S}'^{*}_{\mathrm{e}_\alpha} = \boldsymbol{S}'_{\mathrm{e}_\alpha}\left(\boldsymbol{C}^{n+1},\ \boldsymbol{U}^{n}_{\mathrm{v}_\alpha} \right) \quad \text{and} \quad \boldsymbol{S}'^{n+1}_{\mathrm{e}_\alpha} = \boldsymbol{S}'_{\mathrm{e}_\alpha}\left(\boldsymbol{C}^{n+1},\ \boldsymbol{U}^{n+1}_{\mathrm{v}_\alpha} \right), \tag{49}$$

and λ^{n+1}_{α} can be incrementally obtained by enforcing the constraint

$$\det \boldsymbol{C}^{n+1}_{\mathrm{e}_\alpha} = J^2_{n+1}, \tag{50}$$

rather than using Eq. (46), which only enforces the rate form of the incompressibility constraint[8]. Notably, Eqs. (48) and (50) represent an implicit system of nonlinear equations for the solution of $\boldsymbol{U}^{n+1}_{\mathrm{v}_\alpha}$ and λ^{n+1}_{α} in terms of $\mathbf{C}^{n+1}$ and $\boldsymbol{U}^{n}_{\mathrm{v}_\alpha}$. Its solution process can be broken-down as previously done in Section 3.5. Specifically, provided $\mathbf{C}^{n+1}$ and $\boldsymbol{U}^{n}_{\mathrm{v}_\alpha}$, Eqs. (48) and (50) can be first solved in terms of $\boldsymbol{C}^{n+1}_{\mathrm{e}_\alpha}$ and λ^{n+1}_{α} prior definition of the trial stress tensor $\boldsymbol{S}'^{*}_{\mathrm{e}_\alpha}$ and with knowledge of the Maxwell viscous strain energy density $\hat{\bar{\Psi}}_\alpha$. Subsequently, the viscous stretch tensor $\boldsymbol{U}^{n+1}_{\mathrm{v}_\alpha}$ can be evaluated by using Eq. (35). The numerical procedure for the calculation of the internal variable $\boldsymbol{U}^{n+1}_{\mathrm{v}_\alpha}$ is outlined in Algorithm 2.

Algorithm 2 Numerical procedure for the calculation of the internal variable in the incompressible case.

1: **for** $Time\ Increment = 1, 2, \ldots$ **do**
2: **for** $Iteration = 1, 2, \ldots$ **do**
3: Calculate the right Cauchy–Green strain tensor at the current time increment $\boldsymbol{C}^{n+1}$
4: Compute the instantaneous stress tensor $\boldsymbol{S}'^{*}_{\mathrm{e}_\alpha}$
5: Obtain the elastic right Cauchy–Green tensor $\boldsymbol{C}^{n+1}_{\mathrm{e}_\alpha}$ by the solution of Eq. (48) and Eq. (50)
6: Determine the internal variable $\boldsymbol{U}^{n+1}_{\mathrm{v}_\alpha}$ according to Eq. (35)
7: **end for**
8: Store the internal variable $\boldsymbol{U}^{n+1}_{\mathrm{v}_\alpha}$ as history variable
9: **end for**

Nonetheless, it is instructive to demonstrate the technique for the selected case of an incompressible viscous strain energy density neo-Hookean model, which can be solved analytically. Firstly, by re-arranging Eq. (48), it yields

$$\boldsymbol{S}'^{n+1}_{\mathrm{e}_\alpha} - \bar{\eta}^{n+1}\left(\boldsymbol{C}^{n+1}_{\mathrm{e}_\alpha} \right)^{-1} = \gamma_\alpha \boldsymbol{S}'^{*}_{\mathrm{e}_\alpha}; \qquad \bar{\eta}^{n+1} = \frac{\Delta t}{\tau_\alpha + \Delta t}\lambda^{n+1}_{\alpha}; \qquad \gamma_\alpha = \frac{\tau_\alpha}{\tau_\alpha + \Delta t}. \tag{51}$$

For an incompressible new-Hookean strain energy density, the expression for the second Piola–Kirchhoff stress tensor (Bonet et al., 2016) can be substituted into $(51)_a$ to give

$$\mu_\alpha J^{-\frac{2}{3}}_{n+1}\left(\boldsymbol{I} - \frac{1}{3}\mathrm{tr}\boldsymbol{C}^{n+1}_{\mathrm{e}_\alpha}\left(\boldsymbol{C}^{n+1}_{\mathrm{e}_\alpha} \right)^{-1} \right) - \bar{\eta}^{n+1}\left(\boldsymbol{C}^{n+1}_{\mathrm{e}_\alpha} \right)^{-1} = \gamma_\alpha \boldsymbol{S}'^{*}_{\mathrm{e}_\alpha}, \tag{52}$$

[8] This is similar to classical time integration return mapping approaches in elastoplasticity (Simo, 1988; Simo and Miehe, 1992) for the computation of the algorithmic tangent modulus.

where μ_α is the selected shear modulus and, after some simple algebra, above Eq. (52) can be re-arranged to yield

$$\boldsymbol{C}_{\mathrm{e}_\alpha}^{n+1} = \bar{\gamma}_{n+1}\left(\boldsymbol{I} - \frac{\gamma_\alpha}{\mu_\alpha} J_{n+1}^{\frac{2}{3}} \boldsymbol{S}'^{*}_{\mathrm{e}_\alpha}\right)^{-1}, \tag{53}$$

in terms of a yet unknown coefficient $\bar{\gamma}^{n+1}$ formulated as

$$\bar{\gamma}^{n+1} = \frac{\mu_\alpha \mathrm{tr}\boldsymbol{C}_{\mathrm{e}_\alpha}^{n+1} + 3\bar{\eta}^{n+1} J_{n+1}^{\frac{2}{3}}}{3\mu_\alpha}. \tag{54}$$

In order to determine $\bar{\gamma}^{n+1}$, we can enforce

$$\det \boldsymbol{C}_{\mathrm{e}_\alpha}^{n+1} = \frac{\bar{\gamma}_{n+1}^3}{\det\left(\boldsymbol{I} - \frac{\gamma_\alpha}{\mu_\alpha} J_{n+1}^{\frac{2}{3}} \boldsymbol{S}'^{*}_{\mathrm{e}_\alpha}\right)} = J_{n+1}, \tag{55}$$

leading to the explicit evaluation of coefficient $\bar{\gamma}^{n+1}$ as

$$\bar{\gamma}_{n+1} = J_{n+1}^{\frac{2}{3}}\left(\det\left(\boldsymbol{I} - \frac{\gamma_\alpha}{\mu_\alpha} J_{n+1}^{\frac{2}{3}} \boldsymbol{S}'^{*}_{\mathrm{e}_\alpha}\right)\right)^{\frac{1}{3}}, \tag{56}$$

which along with (53) provides a computationally efficient closed-form expression for $\boldsymbol{C}_{\mathrm{e}_\alpha}^{n+1}$.

5. Extension to anisotropic viscoelasticity at finite strains

5.1. Continuum kinematics of the anisotropic part

We follow Liu et al. (2019) and assume that the anisotropic viscous part can be assumed independent of the isotropic viscous contribution (already presented in Sections 3 and 4), and can thus be dealt with separately. Specifically, an isotropic approach will be used to describe the matrix component, whereas a transverse isotropic approach will be used to describe a single family of viscous fibres. Analogously to (12), we assume a multiplicative decomposition of the deformation gradient $\boldsymbol{F}$ into elastic $\boldsymbol{F}_{\mathrm{e}_\beta}^{\mathrm{f}}$ and β-Maxwell (rotation free) viscous $\boldsymbol{U}_{\mathrm{v}_\beta}^{\mathrm{f}}$ components as

$$\boldsymbol{F} = \boldsymbol{F}_{\mathrm{e}_\beta}^{\mathrm{f}} \boldsymbol{U}_{\mathrm{v}_\beta}^{\mathrm{f}}, \tag{57}$$

through the introduction of suitable intermediate stress free configurations (see Fig. 3), and where the super script $\bullet^{\mathrm{f}}$ is used to emphasise the fibre nature. As in isotropic viscoelasticity, the number of viscous elements $\beta = 1 \dots n_\beta$ for the anisotropic part can also be selected arbitrarily. To guarantee that the proposed constitutive model is objective, the strain energy density is defined in terms of the total right Cauchy–Green strain tensor $\boldsymbol{C}$ and the viscous stretch tensor $\boldsymbol{U}_{\mathrm{v}_\beta}^{\mathrm{f}}$ (or $\boldsymbol{C}_{\mathrm{v}_\beta}^{\mathrm{f}} = \boldsymbol{U}_{\mathrm{v}_\beta}^{\mathrm{f}} \boldsymbol{U}_{\mathrm{v}_\beta}^{\mathrm{f}}$). It is pertinent to point out that $\boldsymbol{U}_{\mathrm{v}_\beta}^{\mathrm{f}}$ signifies the internal variable associated with the respective viscous β-Maxwell element of the fibre family, which determines the current state of viscous deformation. Moreover, to facilitate the satisfaction of thermodynamic equilibrium, it is convenient to introduce the right Cauchy–Green strain tensor in the intermediate configuration $\boldsymbol{C}_{\mathrm{e}_\beta}^{\mathrm{f}}$ as

$$\boldsymbol{C}_{\mathrm{e}_\beta}^{\mathrm{f}} = (\boldsymbol{F}_{\mathrm{e}_\beta}^{\mathrm{f}})^{\mathrm{T}} \boldsymbol{F}_{\mathrm{e}_\beta}^{\mathrm{f}} = (\boldsymbol{U}_{\mathrm{v}_\beta}^{\mathrm{f}})^{-1} \boldsymbol{C} (\boldsymbol{U}_{\mathrm{v}_\beta}^{\mathrm{f}})^{-1}, \tag{58}$$

which reduces to the identity when $\boldsymbol{U}_{\mathrm{v}_\beta}^{\mathrm{f}}$ and $\boldsymbol{F}$ only differ by a rigid body rotation. To account for a transverse isotropic behaviour in a single family of fibres, we consider the symmetry group $\mathcal{D}_{\infty h}$ characterised by the rank-one second order structural tensor $\boldsymbol{a}_0 \otimes \boldsymbol{a}_0$ defined in the initial material configuration[9], where $\boldsymbol{a}_0$ denotes a unit vector aligned with the fibre orientation (Zheng, 1994).

As shown in Fig. 3, the fibre family is embedded in the isotropic matrix, and its direction in the reference configuration $\mathcal{B}_0$ is defined by the unit vector $\boldsymbol{a}_0$. Deformation of the fibre leads in the β-Maxwell viscous element to unit vectors $\tilde{\boldsymbol{a}}_\beta$ and $\boldsymbol{a}$, defined in the intermediate and current configurations, respectively, which can be formulated as

$$\tilde{\boldsymbol{a}}_\beta = \frac{\boldsymbol{U}_{\mathrm{v}_\beta}^{\mathrm{f}} \boldsymbol{a}_0}{\lambda_{\mathrm{v}_\beta}^{\mathrm{f}}}; \qquad \lambda_{\mathrm{v}_\beta}^{\mathrm{f}} = \sqrt{\boldsymbol{C}_{\mathrm{v}_\beta}^{\mathrm{f}} : \boldsymbol{a}_0 \otimes \boldsymbol{a}_0}, \tag{59}$$

and

$$\boldsymbol{a} = \frac{\boldsymbol{F}\boldsymbol{a}_0}{\lambda^{\mathrm{f}}}; \qquad \lambda^{\mathrm{f}} = \sqrt{\boldsymbol{C} : \boldsymbol{a}_0 \otimes \boldsymbol{a}_0}. \tag{60}$$

For completeness, notice that an alternative representation of (60) can be given by

$$\boldsymbol{a} = \frac{\boldsymbol{F}_{\mathrm{e}_\beta}^{\mathrm{f}} \tilde{\boldsymbol{a}}_\beta}{\lambda_{\mathrm{e}_\beta}^{\mathrm{f}}}; \qquad \lambda_{\mathrm{e}_\beta}^{\mathrm{f}} = \sqrt{\boldsymbol{C}_{\mathrm{e}_\beta}^{\mathrm{f}} : \tilde{\boldsymbol{a}}_\beta \otimes \tilde{\boldsymbol{a}}_\beta}. \tag{61}$$

[9] Note that according to Zheng (1994), there exist five types of transverse isotropy.

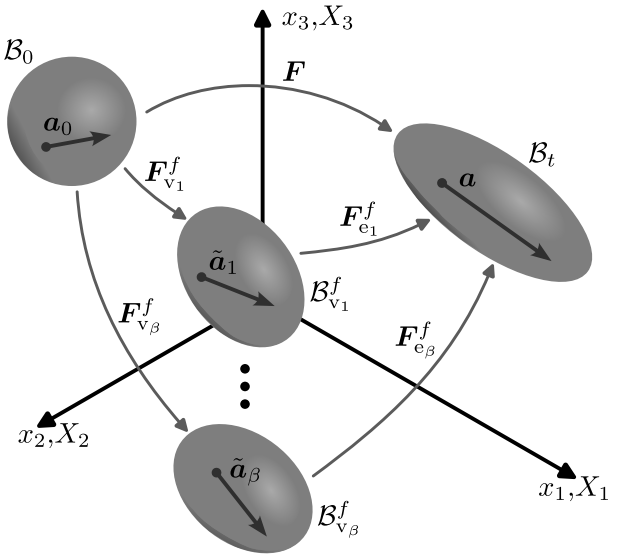

Fig. 3. Deformation decomposition for the anisotropic part and kinematics of the fibre orientation.

It is straightforward to see that $\lambda^{\mathrm{f}}_{\mathrm{e}_\beta} = \lambda^{\mathrm{f}}/\lambda^{\mathrm{f}}_{\mathrm{v}_\beta}$ via substitution of (59) and (60) into (61). Moreover, the anisotropy introduced by the structural tensor (of the symmetry group $\mathcal{D}_{\infty h}$) can indistinctively be formulated based on $\boldsymbol{a}_0 \otimes \boldsymbol{a}_0$, $\tilde{\boldsymbol{a}}_\beta \otimes \tilde{\boldsymbol{a}}_\beta$ or $\boldsymbol{a} \otimes \boldsymbol{a}$, which will be used in the following section.

Remark 2. The extension into a set of n_{f} fibres is straightforward by simply considering a set of rank-one second order tensors $\boldsymbol{a}^{\mathrm{f}_i}_0 \otimes \boldsymbol{a}^{\mathrm{f}_i}_0$ with $i = 1 \dots n_{\mathrm{f}}$. In this case, and for the i – th family of fibres, the deformation gradient tensor for the β-Maxwell element accepts the following multiplicative decomposition

$$\boldsymbol{F} = \boldsymbol{F}^{\mathrm{f}_i}_{\mathrm{e}_\beta} \boldsymbol{U}^{\mathrm{f}_i}_{\mathrm{v}_\beta}; \quad i = 1 \dots n_{\mathrm{f}}; \quad \beta = 1 \dots n_\beta. \tag{62}$$

As a result, similar equations to (59)–(61) can be straightforwardly obtained in terms of vectors $\boldsymbol{a}^{\mathrm{f}_i}_0, \tilde{\boldsymbol{a}}^{\mathrm{f}_i}_\beta, \boldsymbol{a}^{\mathrm{f}_i}$ and stretches $\lambda^{\mathrm{f}_i}_{\mathrm{v}_\beta}, \lambda^{\mathrm{f}_i}, \lambda^{\mathrm{f}_i}_{\mathrm{e}_\beta}$, with $i = 1 \dots n_{\mathrm{f}}$.

5.2. Strain energy density and second Piola–Kirchhoff stress

As in Ericksen and Rivlin (1997), Sansour (2008), we postulate an additive decomposition of the strain energy density into isotropic (refer to Eqs. (14)–(15)) and anisotropic contributions. For the latter, and by making use of the isotropicisation theorem (Zheng, 1994; Horák et al., 2023), the free energy density is described by an isotropic strain energy density $\Psi^{\mathrm{aniso}}(\boldsymbol{C}, \boldsymbol{a}_0 \otimes \boldsymbol{a}_0, \boldsymbol{U}^{\mathrm{f}}_{\mathrm{v}_1}, \dots, \boldsymbol{U}^{\mathrm{f}}_{\mathrm{v}_{n_\beta}})$ in terms of the total right Cauchy–Green tensor, the structural tensor in the reference configuration, and the viscous internal variables. Furthermore, it is postulated that the anisotropic free energy density can be decomposed additively into a component $\Psi^{\mathrm{aniso}}_\infty(\boldsymbol{C}, \boldsymbol{a}_0 \otimes \boldsymbol{a}_0)$ associated with the equilibrium state that accounts for the time-invariant stress response, and a sum of n_β viscous β-element contributions $\Psi^{\mathrm{aniso}}_\beta(\boldsymbol{C}, \boldsymbol{a}_0 \otimes \boldsymbol{a}_0, \boldsymbol{U}^{\mathrm{f}}_{\mathrm{v}_\beta})$ associated with the non-equilibrium states that govern the time-dependent aspect of the stress response, see Bergström and Boyce (1998), Bonet (2001). To guarantee that $\Psi^{\mathrm{aniso}}_\beta$ vanishes when $\boldsymbol{U}^{\mathrm{f}}_{\mathrm{v}_\beta}$ and $\boldsymbol{F}$ only differ by a rigid body rotation (i.e. thermo-dynamical equilibrium), we particularise the definition of $\Psi^{\mathrm{aniso}}_\beta$ as

$$\Psi^{\mathrm{aniso}}_\beta(\boldsymbol{C}, \boldsymbol{a}_0 \otimes \boldsymbol{a}_0, \boldsymbol{U}^{\mathrm{f}}_{\mathrm{v}_\beta}) = \tilde{\Psi}^{\mathrm{aniso}}_\beta(\boldsymbol{C}^{\mathrm{f}}_{\mathrm{e}_\beta}, \tilde{\boldsymbol{a}}_\beta \otimes \tilde{\boldsymbol{a}}_\beta), \tag{63}$$

where the strain energy density arguments are re-written with respect to the intermediate configuration (see right hand side of (63)). The two invariants responsible for the transverse isotropic behaviour (Horák et al., 2023) can be defined as the following integrity basis

$$I^{\mathrm{f}} = \mathrm{tr}[\boldsymbol{C}(\boldsymbol{a}_0 \otimes \boldsymbol{a}_0)]; \qquad II^{\mathrm{f}} = \mathrm{tr}[(\boldsymbol{C})^2(\boldsymbol{a}_0 \otimes \boldsymbol{a}_0)], \tag{64}$$

for the time-invariant stress response and

$$I^{\mathrm{f}}_{\mathrm{e}_\beta} = \mathrm{tr}[\boldsymbol{C}^{\mathrm{f}}_{\mathrm{e}_\beta}(\tilde{\boldsymbol{a}}_\beta \otimes \tilde{\boldsymbol{a}}_\beta)]; \qquad II^{\mathrm{f}}_{\mathrm{e}_\beta} = \mathrm{tr}[(\boldsymbol{C}^{\mathrm{f}}_{\mathrm{e}_\beta})^2(\tilde{\boldsymbol{a}}_\beta \otimes \tilde{\boldsymbol{a}}_\beta)], \tag{65}$$

for the non-equilibrium response. As such, the anisotropic strain energy density, including both long term and non-equilibrium contributions, can be further reduced to

$$\Psi_\infty^{\text{aniso}}(\boldsymbol{C}, \boldsymbol{a}_0 \otimes \boldsymbol{a}_0) + \sum_\beta \tilde{\Psi}_\beta^{\text{aniso}}(\boldsymbol{C}_{\text{e}_\beta}^{\text{f}}, \tilde{\boldsymbol{a}}_\beta \otimes \tilde{\boldsymbol{a}}_\beta) = \bar{\Psi}_\infty^{\text{aniso}}(I^{\text{f}}, II^{\text{f}}) + \sum_\beta \bar{\Psi}_\beta^{\text{aniso}}(I_{\text{e}_\beta}^{\text{f}}, II_{\text{e}_\beta}^{\text{f}}), \tag{66}$$

where the two terms on the right hand side of above equation are now written only in terms of the transverse isotropic invariants, resulting in a complete strain energy density given by

$$\begin{aligned}\Psi\left(\boldsymbol{C}, \boldsymbol{a}_0 \otimes \boldsymbol{a}_0, \boldsymbol{U}_{\text{v}_1}, \dots, \boldsymbol{U}_{\text{v}_{n_\alpha}}, \boldsymbol{U}_{\text{v}_1}^{\text{f}}, \dots, \boldsymbol{U}_{\text{v}_{n_\beta}}^{\text{f}}\right) &= \Psi_\infty(\boldsymbol{C}) + \sum_\alpha \Psi_\alpha\left(\boldsymbol{C}, \boldsymbol{U}_{\text{v}_\alpha}\right) \\ &+ \bar{\Psi}_\infty^{\text{aniso}}(I^{\text{f}}) + \sum_\beta \bar{\Psi}_\beta^{\text{aniso}}(I_{\text{e}_\beta}^{\text{f}}) + \bar{\Psi}_\infty^{\text{aniso}}(II^{\text{f}}) + \sum_\beta \bar{\Psi}_\beta^{\text{aniso}}(II_{\text{e}_\beta}^{\text{f}}),\end{aligned} \tag{67}$$

where isotropic and transversely isotropic (first and second invariant) contributions can be easily identified.

Remark 3. The extension into a set of n_{f} fibres is formulated as

$$\begin{aligned}&\Psi\left(\boldsymbol{C}, \boldsymbol{a}_0^{\text{f}_1} \otimes \boldsymbol{a}_0^{\text{f}_1}, \dots, \boldsymbol{a}_0^{\text{f}_{n_\text{f}}} \otimes \boldsymbol{a}_0^{\text{f}_{n_\text{f}}}, \boldsymbol{U}_{\text{v}_1}, \dots, \boldsymbol{U}_{\text{v}_{n_\alpha}}, \boldsymbol{U}_{\text{v}_1}^{\text{f}_1}, \dots, \boldsymbol{U}_{\text{v}_{n_\beta}}^{\text{f}_1}, \dots, \boldsymbol{U}_{\text{v}_1}^{\text{f}_{n_\text{f}}}, \dots, \boldsymbol{U}_{\text{v}_{n_\beta}}^{\text{f}_{n_\text{f}}}\right) = \Psi_\infty(\boldsymbol{C}) + \\ &\sum_\alpha \Psi_\alpha\left(\boldsymbol{C}, \boldsymbol{U}_{\text{v}_\alpha}\right) + \sum_i \bar{\Psi}_\infty^{\text{aniso}}(I^{\text{f}_i}) + \sum_i \sum_\beta \bar{\Psi}_\beta^{\text{aniso}}(I_{\text{e}_\beta}^{\text{f}_i}) + \sum_i \bar{\Psi}_\infty^{\text{aniso}}(II^{\text{f}_i}) + \sum_i \sum_\beta \bar{\Psi}_\beta^{\text{aniso}}(II_{\text{e}_\beta}^{\text{f}_i}),\end{aligned} \tag{68}$$

where summation terms over the number of families of fibres can be seen.

Remark 4. An extension into more complex symmetry groups (i.e. composites) can be realised by adding suitable invariants to the integrity basis. As an example, for the consideration of orthotropy under three preferred orthonormal directions defined by $\{\boldsymbol{a}_{0,1}^{\text{f}_i}, \boldsymbol{a}_{0,2}^{\text{f}_i}, \boldsymbol{a}_{0,3}^{\text{f}_i}\}$ within a composite family, the following invariants define the integrity basis (with other invariants related via functional dependency) (Ellmer et al., 2024)

$$I^{\text{f}_i} = \text{tr}[\boldsymbol{C}(\boldsymbol{a}_{0,1}^{\text{f}_i} \otimes \boldsymbol{a}_{0,1}^{\text{f}_i})]; \qquad II^{\text{f}_i} = \text{tr}[(\boldsymbol{C})^2(\boldsymbol{a}_{0,1}^{\text{f}_i} \otimes \boldsymbol{a}_{0,1}^{\text{f}_i})]; \qquad III^{\text{f}_i} = \text{tr}[(\boldsymbol{C})(\boldsymbol{a}_{0,2}^{\text{f}_i} \otimes \boldsymbol{a}_{0,2}^{\text{f}_i})], \tag{69}$$

for the time-invariant response, and

$$I_{\text{e}_\beta}^{\text{f}_i} = \text{tr}[\boldsymbol{C}_{\text{e}_\beta}^{\text{f}_i}(\boldsymbol{a}_{0,1}^{\text{f}_i} \otimes \boldsymbol{a}_{0,1}^{\text{f}_i})]; \qquad II_{\text{e}_\beta}^{\text{f}_i} = \text{tr}[(\boldsymbol{C}_{\text{e}_\beta}^{\text{f}_i})^2(\boldsymbol{a}_{0,1}^{\text{f}_i} \otimes \boldsymbol{a}_{0,1}^{\text{f}_i})]; \qquad III_{\text{e}_\beta}^{\text{f}_i} = \text{tr}[(\boldsymbol{C}_{\text{e}_\beta}^{\text{f}_i})(\boldsymbol{a}_{0,2}^{\text{f}_i} \otimes \boldsymbol{a}_{0,2}^{\text{f}_i})], \tag{70}$$

for the non-equilibrium response. Thus, the strain energy density function for a symmetry defined by a family of orthotropic composites can be defined as

$$\begin{aligned}&\Psi\left(\boldsymbol{C}, \boldsymbol{a}_0^{\text{f}_1} \otimes \boldsymbol{a}_0^{\text{f}_1}, \dots, \boldsymbol{a}_0^{\text{f}_{n_\text{f}}} \otimes \boldsymbol{a}_0^{\text{f}_{n_\text{f}}}, \boldsymbol{U}_{\text{v}_1}, \dots, \boldsymbol{U}_{\text{v}_{n_\alpha}}, \boldsymbol{U}_{\text{v}_1}^{\text{f}_1}, \dots, \boldsymbol{U}_{\text{v}_{n_\beta}}^{\text{f}_1}, \dots, \boldsymbol{U}_{\text{v}_1}^{\text{f}_{n_\text{f}}}, \dots, \boldsymbol{U}_{\text{v}_{n_\beta}}^{\text{f}_{n_\text{f}}}\right) = \Psi_\infty(\boldsymbol{C}) + \\ &\sum_\alpha \Psi_\alpha\left(\boldsymbol{C}, \boldsymbol{U}_{\text{v}_\alpha}\right) + \sum_i \bar{\Psi}_\infty^{\text{aniso}}(I^{\text{f}_i}) + \sum_i \sum_\beta \bar{\Psi}_\beta^{\text{aniso}}(I_{\text{e}_\beta}^{\text{f}}) + \sum_i \bar{\Psi}_\infty^{\text{aniso}}(II^{\text{f}_i}) + \sum_i \sum_\beta \bar{\Psi}_\beta^{\text{aniso}}(II_{\text{e}_\beta}^{\text{f}_i}) + \\ &\sum_i \bar{\Psi}_\infty^{\text{aniso}}(III^{\text{f}_i}) + \sum_i \sum_\beta \bar{\Psi}_\beta^{\text{aniso}}(III_{\text{e}_\beta}^{\text{f}_i}).\end{aligned} \tag{71}$$

For simplicity, and without loss of generality in what follows, the strain energy density will be particularised for the case of a single transverse isotropic family, and where contributions stemming from the second invariants $\{II^{\text{f}}, II_{\text{e}_\beta}^{\text{f}}\}$ will be considered negligible in comparison with those stemming from the first invariants $\{I^{\text{f}}, I_{\text{e}_\beta}^{\text{f}}\}$. Moreover, from $(61)_b$, it is easy to see that $I_{\text{e}_\beta}^{\text{f}} = (\lambda_{\text{e}_\beta}^{\text{f}})^2 = (\lambda^{\text{f}}/\lambda_{\text{v}_\beta}^{\text{f}})^2$ and that $I^{\text{f}} = (\lambda^{\text{f}})^2$. Finally, for completeness, the overall strain density function of the composite can be written as

$$\Psi\left(\boldsymbol{C}, \boldsymbol{a}_0 \otimes \boldsymbol{a}_0, \boldsymbol{U}_{\text{v}_1}, \dots, \boldsymbol{U}_{\text{v}_{n_\alpha}}, \boldsymbol{U}_{\text{v}_1}^{\text{f}}, \dots, \boldsymbol{U}_{\text{v}_{n_\beta}}^{\text{f}}\right) = \Psi_\infty(\boldsymbol{C}) + \sum_\alpha \Psi_\alpha\left(\boldsymbol{C}, \boldsymbol{U}_{\text{v}_\alpha}\right) + \bar{\Psi}_\infty^{\text{aniso}}(I^{\text{f}}) + \sum_\beta \bar{\Psi}_\beta^{\text{aniso}}(I_{\text{e}_\beta}^{\text{f}}). \tag{72}$$

The second Piola–Kirchhoff stress tensor (refer to (16)) can be obtained as

$$\boldsymbol{S} = \boldsymbol{S}_\infty + \sum_\alpha \boldsymbol{S}_\alpha + \boldsymbol{S}_\infty^{\text{f}} + \sum_\beta \boldsymbol{S}_\beta^{\text{f}}, \tag{73}$$

where, similarly to (16), for the evaluation of $\boldsymbol{S}_\beta^{\text{f}}$ the internal state variable $\boldsymbol{U}_{\text{v}_\alpha}^{\text{f}}$ is held constant, resulting in

$$\boldsymbol{S}_\infty^{\text{f}} = 2\frac{\partial \bar{\Psi}_\infty^{\text{aniso}}}{\partial I^{\text{f}}}\boldsymbol{a}_0 \otimes \boldsymbol{a}_0; \qquad \boldsymbol{S}_\beta^{\text{f}} = \frac{S_{\text{e}_\beta}^{\text{f}}}{(\lambda_{\text{v}_\beta}^{\text{f}})^2}\boldsymbol{a}_0 \otimes \boldsymbol{a}_0; \qquad S_{\text{e}_\beta}^{\text{f}} = 2\frac{\partial \bar{\Psi}_\beta^{\text{aniso}}}{\partial I_{\text{e}_\beta}^{\text{f}}}, \tag{74}$$

where it is easy to observe the similarities between $(74)_{b,c}$ with (19) previously obtained.

5.3. Evolution law of the anisotropic viscous part

To fully determine the viscoelastic model, an evolution law for the set of internal variables $\lambda^{\mathrm{f}}_{\mathrm{v}_\beta}$ ($\beta = 1 \dots n_\beta$) must be determined. These will be complementary to the set of evolution laws already presented in previous sections for the isotropic contribution (compressible/incompressible). Following standard thermodynamic principles, the anisotropic viscous contribution is obtained as

$$\begin{aligned}
\mathrm{D}^{\mathrm{f}}_{\mathrm{vis}} &= -\sum_\beta \frac{\partial \Psi^{\mathrm{aniso}}_\beta}{\partial \boldsymbol{U}^{\mathrm{f}}_{\mathrm{v}_\beta}} : \dot{\boldsymbol{U}}^{\mathrm{f}}_{\mathrm{v}_\beta} \\
&= -\sum_\beta \left. \frac{\mathrm{d}\Psi^{\mathrm{aniso}}_\beta\left(\boldsymbol{C}, \boldsymbol{a}_0 \otimes \boldsymbol{a}_0, \boldsymbol{U}^{\mathrm{f}}_{\mathrm{v}_\beta}\right)}{\mathrm{d}t} \right|_{\boldsymbol{F}=\mathrm{const}} \\
&= -\sum_\beta \left. \frac{\mathrm{d}\bar{\Psi}^{\mathrm{aniso}}_\beta\left(I^{\mathrm{f}}_{\mathrm{e}_\beta}\left(\boldsymbol{C}, \boldsymbol{a}_0 \otimes \boldsymbol{a}_0, \boldsymbol{U}^{\mathrm{f}}_{\mathrm{v}_\beta}\right)\right)}{\mathrm{d}t} \right|_{\boldsymbol{F}=\mathrm{const}} \\
&= -\sum_\beta \frac{1}{2}\left(2\frac{\partial \bar{\Psi}^{\mathrm{aniso}}_\beta}{\partial I^{\mathrm{f}}_{\mathrm{e}_\beta}}\right) \left. \frac{\mathrm{d}I^{\mathrm{f}}_{\mathrm{e}_\beta}\left(\boldsymbol{C}, \boldsymbol{a}_0 \otimes \boldsymbol{a}_0, \boldsymbol{U}^{\mathrm{f}}_{\mathrm{v}_\beta}\right)}{\mathrm{d}t} \right|_{\boldsymbol{F}=\mathrm{const}} \\
&= -\sum_\beta \frac{1}{2} S^{\mathrm{f}}_{\mathrm{e}_\beta} \left. \frac{\mathrm{d}I^{\mathrm{f}}_{\mathrm{e}_\beta}\left(\boldsymbol{C}, \boldsymbol{a}_0 \otimes \boldsymbol{a}_0, \boldsymbol{U}^{\mathrm{f}}_{\mathrm{v}_\beta}\right)}{\mathrm{d}t} \right|_{\boldsymbol{F}=\mathrm{const}},
\end{aligned} \tag{75}$$

where Eq. (74)$_c$ has been used in the penultimate line above and the explicit dependence of $I^{\mathrm{f}}_{\mathrm{e}_\beta}$ on its arguments is displayed. To ensure that the evolution law is compatible with the second law of thermodynamics (i.e. Coleman–Noll procedure), the condition $\mathrm{D}^{\mathrm{f}}_{\mathrm{vis}} \geq 0$ must be satisfied regardless of the current state of deformation and stress. In order to achieve this, note firstly that

$$\left. \frac{\mathrm{d}I^{\mathrm{f}}_{\mathrm{e}_\beta}}{\mathrm{d}t} \right|_{\boldsymbol{F}=\mathrm{const}} = \frac{2}{\mathbb{C}^{\mathrm{f}}_{\mathrm{e}_\beta}} \left. \frac{\mathrm{d}S^{\mathrm{f}}_{\mathrm{e}_\beta}}{\mathrm{d}t} \right|_{\boldsymbol{F}=\mathrm{const}}, \tag{76}$$

where $\mathbb{C}^{\mathrm{f}}_{\mathrm{e}_\beta} = 2\frac{\partial S^{\mathrm{f}}_{\mathrm{e}_\beta}}{\partial I^{\mathrm{f}}_{\mathrm{e}_\beta}}$ denotes the anisotropic elasticity value, which is user-defined positive. Substituting Eq. (76) into Eq. (75), the rate of viscous dissipation yields

$$\mathrm{D}^{\mathrm{f}}_{\mathrm{vis}} = -\sum_\beta \frac{S^{\mathrm{f}}_{\mathrm{e}_\beta}}{\mathbb{C}^{\mathrm{f}}_{\mathrm{e}_\beta}} \left. \frac{\mathrm{d}S^{\mathrm{f}}_{\mathrm{e}_\beta}}{\mathrm{d}t} \right|_{\boldsymbol{F}=\mathrm{const}}, \tag{77}$$

and to ensure positive anisotropic viscous dissipation, the following evolution law can be proposed

$$\left. \frac{\mathrm{d}S^{\mathrm{f}}_{\mathrm{e}_\beta}}{\mathrm{d}t} \right|_{\boldsymbol{F}=\mathrm{const}} = -\frac{1}{\tau^{\mathrm{f}}_\beta} S^{\mathrm{f}}_{\mathrm{e}_\beta}, \tag{78}$$

where τ^{f}_β represents the relaxation time parameter. By using this evolution law, the rate of viscous dissipation Eq. (77) finally takes the form of

$$\mathrm{D}^{\mathrm{f}}_{\mathrm{vis}} = \sum_\beta \frac{(S^{\mathrm{f}}_{\mathrm{e}_\beta})^2}{\tau^{\mathrm{f}}_\beta \mathbb{C}^{\mathrm{f}}_{\mathrm{e}_\beta}} \geq 0. \tag{79}$$

Note that for the case of more complex composites, and under the assumption of an additive decomposition such as that shown in (68) or (71), a set of evolution laws similar to that postulated in (78) can be established in terms of each of the invariants conforming the corresponding integrity basis, for each ith family and for each β-Maxwell element.

5.4. Incremental evolution law

The integration of the evolution Eq. (78) from time step n to time step $n+1$ can also be performed by the use of a backward Euler scheme, rendering

$$\frac{1}{\Delta t}(S^{\mathrm{f},n+1}_{\mathrm{e}_\beta} - S^{\mathrm{f}*}_{\mathrm{e}_\beta}) = -\frac{1}{\tau^{\mathrm{f}}_\beta} S^{\mathrm{f},n+1}_{\mathrm{e}_\beta}. \tag{80}$$

where Δt denotes the time step size and the stress values $S^{\mathrm{f},n+1}_{\mathrm{e}_\beta}$ and $S^{\mathrm{f}*}_{\mathrm{e}_\beta}$ are defined as

$$S^{\mathrm{f}*}_{\mathrm{e}_\beta} = S^{\mathrm{f}*}_{\mathrm{e}_\beta}\left(\boldsymbol{C}^{n+1}, \boldsymbol{a}_0 \otimes \boldsymbol{a}_0, \boldsymbol{U}^{\mathrm{f},n}_{\mathrm{v}_\beta}\right) \quad \text{and} \quad S^{\mathrm{f}}_{\mathrm{e}_\beta} = S^{\mathrm{f}}_{\mathrm{e}_\beta}\left(\boldsymbol{C}^{n+1}, \boldsymbol{a}_0 \otimes \boldsymbol{a}_0, \boldsymbol{U}^{\mathrm{f},n+1}_{\mathrm{v}_\beta}\right). \tag{81}$$

Note that the term $S^{\mathrm{f}*}_{\mathrm{e}_\beta}$ denotes the instantaneous stress state from the time step n to time step $n+1$ during which there is no anisotropic viscous deformation. Following an identical process to that included in Section 3.5, the following incremental stress update can be obtained

$$S^{\mathrm{f},n+1}_{\mathrm{e}_\beta} = \gamma^{\mathrm{f}}_\beta S^{\mathrm{f}*}_{\mathrm{e}_\beta}; \qquad \gamma^{\mathrm{f}}_\beta = \frac{\tau^{\mathrm{f}}_\beta}{\tau^{\mathrm{f}}_\beta + \Delta t}. \tag{82}$$

Once the final relaxation stress $S^{\mathrm{f},n+1}_{\mathrm{e}_\beta}$ is computed, the first invariant $I^{\mathrm{f}}_{\mathrm{e}_\beta}$ can be determined making use of the user-defined strain energy density $\bar{\Psi}^{\mathrm{aniso}}_\beta$, from which the viscous stretch $\lambda^{\mathrm{f}}_{\mathrm{v}_\beta}$ can be computed via

$$\lambda^{\mathrm{f}}_{\mathrm{v}_\beta} = \frac{(\boldsymbol{C}^{n+1} : (\boldsymbol{a}_0 \otimes \boldsymbol{a}_0))^{1/2}}{(I^{\mathrm{f},n+1}_{\mathrm{e}_\beta})^{1/2}}. \tag{83}$$

As a possible example, we can consider that the anisotropic viscoelastic strain energy density Ψ^{f}_β can be described by

$$\Psi^{\mathrm{f}}_\beta = \frac{1}{4} E_{\mathrm{f}} \left(\mathrm{e}^{I^{\mathrm{f}}_{\mathrm{e}_\beta} - 1} - I^{\mathrm{f}}_{\mathrm{e}_\beta} \right), \tag{84}$$

where E_{f} denotes the elastic parameter[10]. By substituting (84) into (82), the nonlinear equation for $I^{\mathrm{f}}_{\mathrm{e}_\beta}$ takes the form

$$\frac{1}{2} E_{\mathrm{f}} \left(\mathrm{e}^{I^{\mathrm{f}}_{\mathrm{e}_\beta} - 1} - 1 \right) = \gamma^{\mathrm{f}}_\beta S^{\mathrm{f}*}_{\mathrm{e}_\beta}, \tag{85}$$

and thus the elastic invariant of the anisotropic viscous element $I^{\mathrm{f}}_{\mathrm{e}_\beta}$ can be solved analytically,

$$I^{\mathrm{f}}_{\mathrm{e}_\beta} = 1 + \ln \left(2 \frac{\gamma^{\mathrm{f}}_\beta}{E_{\mathrm{f}}} S^{\mathrm{f}*}_{\mathrm{e}_\beta} + 1 \right). \tag{86}$$

The procedure for the calculation of anisotropic viscous internal variables is outlined in Algorithm 3.

Algorithm 3 Numerical procedure for the calculation of the anisotropic viscous internal variable.

```
for Time Increment = 1, 2, ... do
    for Iteration = 1, 2, ... do
        Calculate the right Cauchy–Green strain tensor at the current time increment C
        Compute the instantaneous stress S^{f*}_{e_β}
        Obtain the elastic invariant I^{f}_{e_β} by the solution of Eq. (82)
        Determine the internal variable λ^{f}_{v_β} according to Eq. (83)
    end for
    Store the internal variable λ^{f}_{v_β} as history variable
end for
```

6. Calibration and experimental validation of isotropic viscoelasticity

The proposed viscoelasticity theory is very general and can be applied to a wide variety of compressible and incompressible materials by adopting specialised forms of strain energy density functions. To validate this new conceptual approach for viscoelasticity modelling with available experimental data, the eight-chain strain energy function (Arruda and Boyce, 1993) is chosen as a particular example of the long-term component to describe the ground state elastic behaviour of the VHB 4910 polymer. VHB 4910 is a typical viscoelastic polymeric material that has potential use in producing Electro-Active and Magneto-Active devices (Ortigosa et al., 2023, 2022b,a; Martínez-Frutos et al., 2021b,a), and the comprehensive experimental data from mechanical characterisation of its viscoelastic behaviour can be found in Hossain et al. (2012), which will be adopted here to calibrate and validate the proposed theoretical framework. In the eight-chain model, the long-term strain energy function Ψ_∞ can be decomposed into volumetric $\Psi^{\mathrm{vol}}_\infty$ and isochoric parts $\Psi^{\mathrm{iso}}_\infty$ as

$$\Psi_\infty = \Psi^{\mathrm{vol}}_\infty(J) + \hat{\Psi}_\infty(\boldsymbol{C}); \qquad \hat{\Psi}_\infty(\boldsymbol{C}) = \Psi_\infty(\hat{\boldsymbol{C}}); \qquad \hat{\boldsymbol{C}} = J^{-2/3}\boldsymbol{C}, \tag{87}$$

where the volumetric part of the long-term strain energy $\Psi^{\mathrm{vol}}_\infty$ can be simply given by Bonet et al. (2016), Holzapfel (2002)

$$\Psi^{\mathrm{vol}}_\infty = \frac{1}{2}\kappa(J-1)^2, \tag{88}$$

where κ serves as the so-called bulk modulus. According to Arruda and Boyce (1993), this model is established on the basis of the underlying molecular network structure of the polymeric material and non-Gaussian behaviour of the individual chains. It can

[10] An alternative strain energy density used by other authors can be given by $\Psi^{\mathrm{f}}_\beta = \frac{1}{4} E_{\mathrm{f}} \left(\mathrm{e}^{(I^{\mathrm{f}}_{\mathrm{e}_\beta} - 1)^2} - 1 \right)$ (Garcia-Blanco et al., 2019b,a).

accurately capture the ultimate network deformation of polymers with only two material parameters including the shear modulus μ and the number of segments per chain N. The isochoric part of the long-term strain energy can be obtained as (Arruda and Boyce, 1993)

$$\Psi_{\infty}(\hat{\boldsymbol{C}}) = \mu N \left[\beta \mathcal{L}^{-1}(\beta) + \ln\left(\frac{\mathcal{L}^{-1}(\beta)}{\sinh \mathcal{L}^{-1}(\beta)}\right)\right], \tag{89}$$

where $\mathcal{L}^{-1}$ is the inverse Langevin function and the parameter β is defined as

$$\beta = \sqrt{\frac{1}{3N}\mathrm{tr}\hat{\boldsymbol{C}}}, \tag{90}$$

which closes the definition of the isotropic long term strain energy density function. From the experimental viewpoint, given the definition of uniaxial tension (along $\boldsymbol{E}_1$), the specimen is elongated only in the loading direction while it is free to move in the other two directions $\{\boldsymbol{E}_2, \boldsymbol{E}_3\}$. Taking also into account the assumption of incompressibility and symmetry of principal stretches as explained in Liu et al. (2019), Hossain et al. (2012), the matrix representation of the complete deformation gradient $\boldsymbol{F}$ to be used reads

$$\boldsymbol{F} = \begin{bmatrix} \lambda_L & 0 & 0 \\ 0 & \lambda_L^{-\frac{1}{2}} & 0 \\ 0 & 0 & \lambda_L^{-\frac{1}{2}} \end{bmatrix}, \tag{91}$$

where λ_L is the ratio between the length of the deformed specimen and the initial undeformed length.

6.1. Calibration

To identify the long-term parameters μ and N for the determination of the equilibrium response, experimental data from single-step relaxation tests are adopted for the corresponding calibration. The stress values reached asymptotically at the end of the holding stage during the testing process are treated as the equilibrium values for each deformation level. By suitable statistical fitting against the experimental data obtained from the single-step relaxation tests, the optimised long-term parameters μ and N are determined as 13.67 kPa and 7.86e5, respectively. Note that these two long-term parameters will be kept constant for the subsequent calibration and validation.

For the identification of the viscous parameters, the number of viscous branches that is equivalent to that of Maxwell elements needs to be determined firstly, which is of great significance for the description of the nonlinear viscoelastic material behaviour. Each Maxwell element contains two extra parameters that require determination, i.e. the viscous modulus μ_α and the relaxation time τ_α. The experimental data obtained from the loading–unloading cyclic tests at the two different strain rates, 0.01 s^{-1} and 0.05 s^{-1}, is chosen for calibration purpose here, and it will be used for the construction of the objective (i.e. loss) function during the parameter optimisation process. Three sets of data at deformation levels of 50%, 100% and 200% are available, and one of them will be selected for calibration (i.e. training) while the other two will be used for validation. The set of viscous parameters μ_α and τ_α are obtained by minimising the discrepancy between the loading–unloading nominal stress versus elongation curves obtained from both experiments and simulation. As pointed out in Linder et al. (2011), this optimisation procedure is known as the simultaneous minimisation for the parameter identification.

The fittings with two, three and four viscous branches for the loading–unloading cyclic test at deformation levels of 50%, 100% and 200% under two different loading strain rates of 0.05 s^{-1} and 0.01 s^{-1} are shown in Fig. 4, Fig. 5 and Fig. 6, respectively. The optimised parameter sets using `MatLab` built-in optimisation routine `lsqnonlin` (Anon, 2024) are listed in Table 1, Table 2 and Table 3, respectively. To quantify the difference between the fitting modelling curve and corresponding experimental data, the normalised root mean square error (NRMSE) is calculated and listed in Table 4. Note that the increase in the number of viscous branches from three to four does not significantly improve the fitting accuracy for all the three different fittings using data at deformation levels of 50%, 100% and 200%. Therefore, it is assumed three viscous branches are sufficient to describe the viscoelastic behaviour of the polymeric material here. Moreover, it is also seen from Table 4 that the fitting result using data at deformation level 200% is the best, so the complete set of identified parameters in Table 3 will be used to validate the proposed model with other experimental results that are not used in the calibration procedure (including data from the loading–unloading cyclic tests at deformation levels of 50% and 100%).

6.2. Validation of the loading–unloading cyclic tests

In this Section, the experimental results for the loading–unloading cyclic tests at deformation levels of 50% and 100% under the two strain rates of 0.05 s^{-1} and 0.01 s^{-1} are used to validate the model with the identified parameters above, as shown in Figs. 7(a) and 8(a). The comparison between experiments and in-silico simulation for deformation levels of 50% and 100% are shown in Figs. 7(b) and 8(b), respectively. Although there is some difference between simulation and experiments for the deformation level of 50% during the unloading stage, the overall prediction of the model for the cyclic tests at the two different strain rates of 0.05 s^{-1} and 0.01 s^{-1} is very good. It should be pointed out that the loading–unloading cyclic tests are typical in case of the characterisation of rate-dependent behaviour of viscoelastic polymers. Note that the proposed model can predict the dissipative behaviour with varying hysteresis loops for the tests at deformation levels of both 50% and 100% with satisfactory accuracy. Furthermore, the nonlinear rate-dependency of the cyclic tests during the loading stage due to the viscosity of polymers can also be captured by the proposed model, which clearly demonstrates its effectiveness.

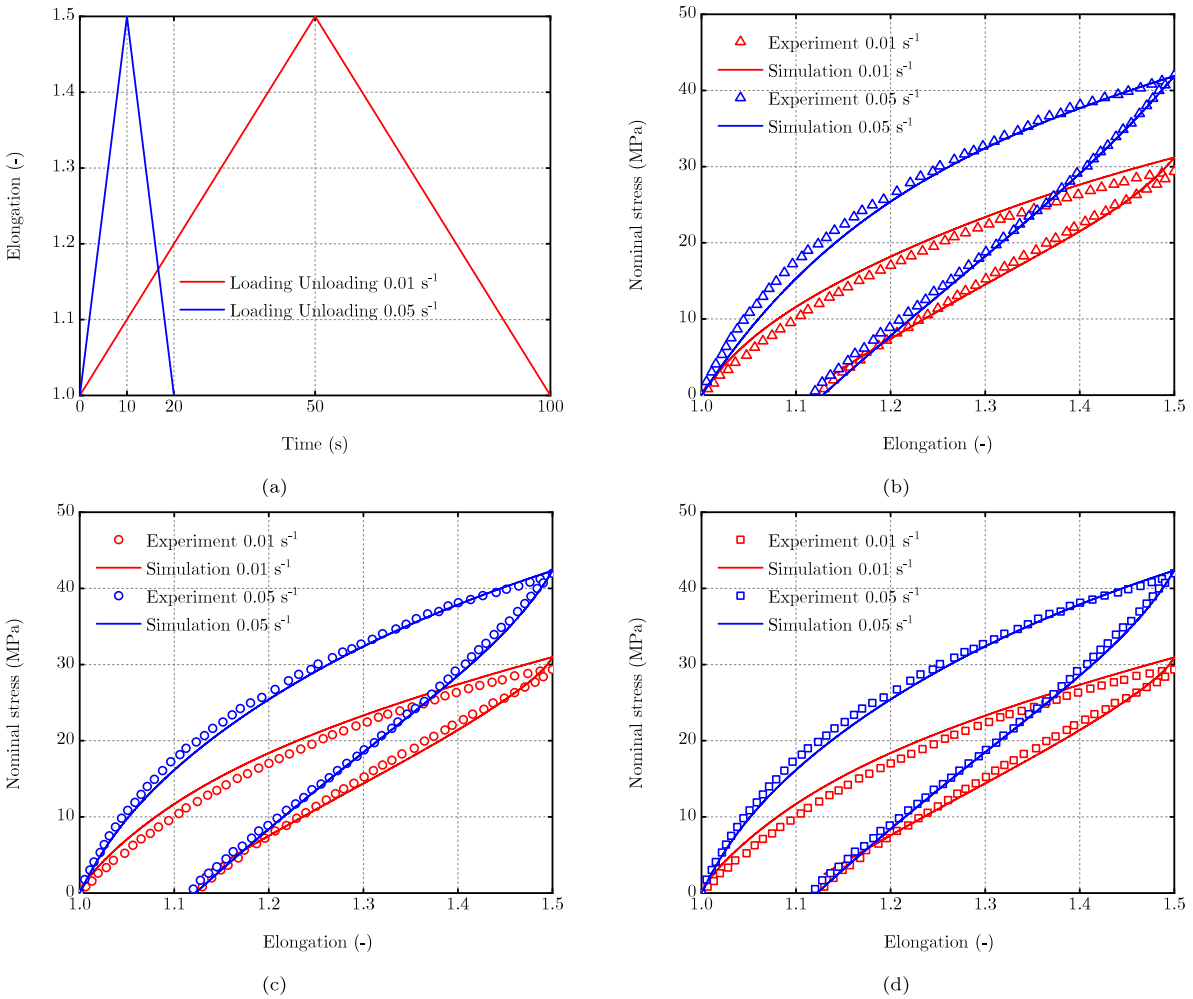

Fig. 4. (a) The loading history evolution curves and fitting nominal stress versus elongation curves using (b) two viscous branches, (c) three viscous branches and (d) four viscous branches for the loading–unloading cyclic tests at deformation level of 50% under strain rates of 0.01 s^{-1} and 0.05 s^{-1}.

Table 1
Identified viscous parameters using experimental data at deformation level of 50%.

	Two branches	Three branches	Four branches
μ_1 (kPa)	46.76	31.53	32.28
τ_1 (s)	4.21	10.72	11.64
μ_2 (kPa)	27.30	56.39	57.52
τ_2 (s)	144.76	0.82	0.86
μ_3 (kPa)	–	19.81	2.92
τ_3 (s)	–	498.83	996.23
μ_4 (kPa)	–	–	15.54
τ_4 (s)	–	–	994.36

6.3. Validation of single-step relaxation tests

The single-step relaxation test is an alternative option to characterise the time-dependent mechanical behaviour of viscoelastic materials. In this case, the specimen is firstly loaded at a high elongation rate of 2 s^{-1} to a given stretch level, and then held fixed. Four different stretch levels of 20%, 40%, 100% and 350% for the single-step relaxation tests are chosen, and the holding time for the stress relaxation at each test is 30 min, see Figs. 9(a) and 10(a). Comparison between experiments and simulation is shown in Figs. 9(b) and 10(b), and it can be seen that they agree with each other very well for each test. Note that the stress converges to a constant level at the end of all the single-step relaxation tests, which can be captured with excellent accuracy by the proposed model. As mentioned before, the stress measured at the end of the relaxation time can be considered as the equilibrium stress that

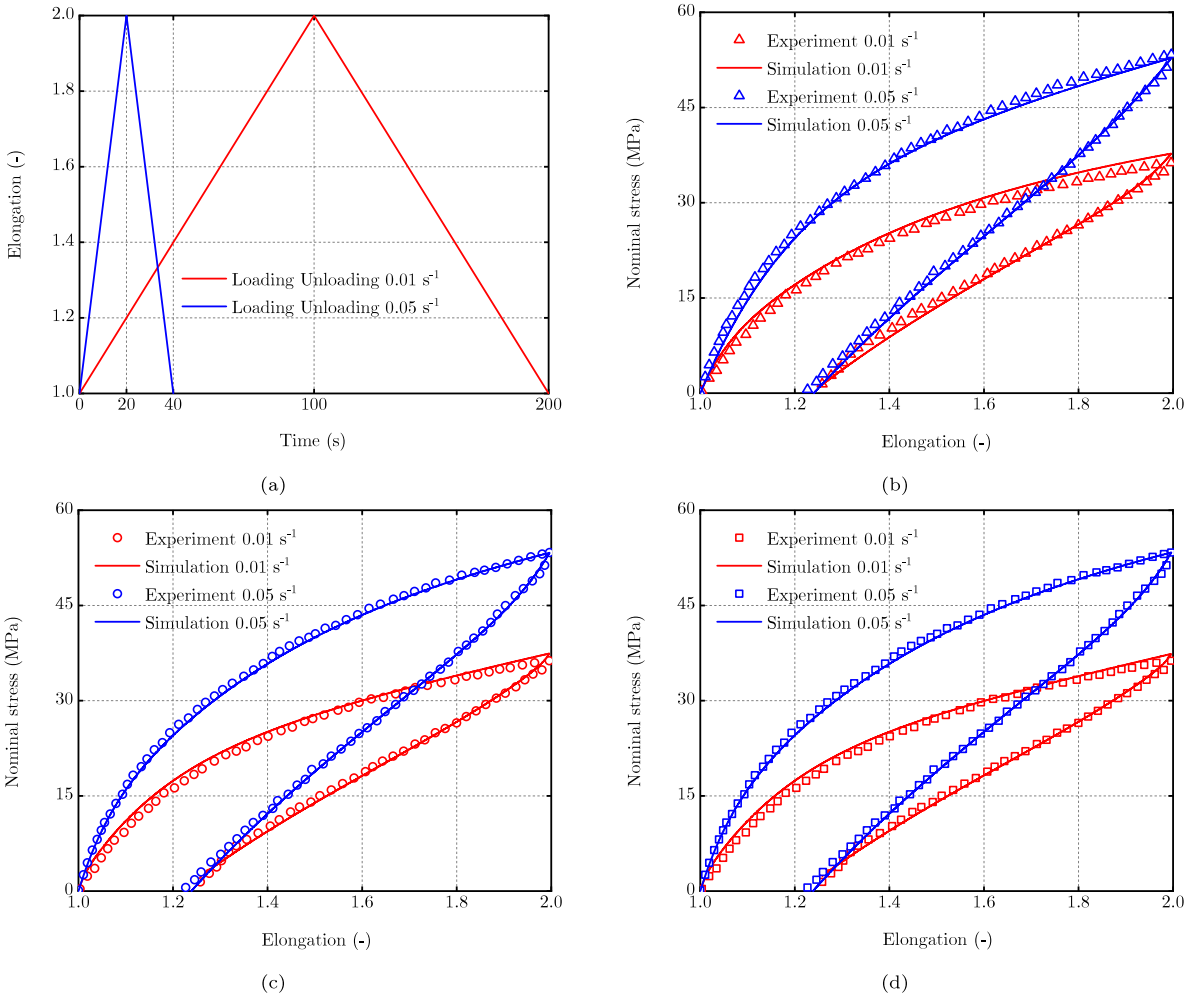

Fig. 5. (a) The loading history evolution curves and fitting nominal stress versus elongation curves using (b) two viscous branches, (c) three viscous branches and (d) four viscous branches for the loading–unloading cyclic tests at deformation level of 100% under strain rates of 0.01 s^{-1} and 0.05 s^{-1}.

Table 2
Identified viscous parameters using experimental data at deformation level of 100%.

	Two branches	Three branches	Four branches
μ_1 (kPa)	45.94	9.79	30.39
τ_1 (s)	5.13	496.31	25.13
μ_2 (kPa)	22.51	61.76	8.35
τ_2 (s)	116.83	1.23	988.22
μ_3 (kPa)	–	29.57	62.30
τ_3 (s)	–	22.95	1.27
μ_4 (kPa)	–	–	8.3e−5
τ_4 (s)	–	–	980.81

have been used for the calibration of long-term parameters. The difference between the current stress and the equilibrium stress is the overstress from the viscous contribution (Amin et al., 2006). Generally, it can be observed that higher stretch level will lead to both higher overstress and equilibrium stress. The relaxation stages for all the tests with different stretch levels agree very well with experimental observations, which can be ascribed to the suitable evolution law proposed in this work.

6.4. Validation of multi-step relaxation tests

The procedure of the multi-step relaxation test is similar to that of the previous single-step test. In this case, the specimen is firstly loaded at a stretch rate of 2 s^{-1} to the deformation level of 50% compared to the state of the previous step, and then followed by a

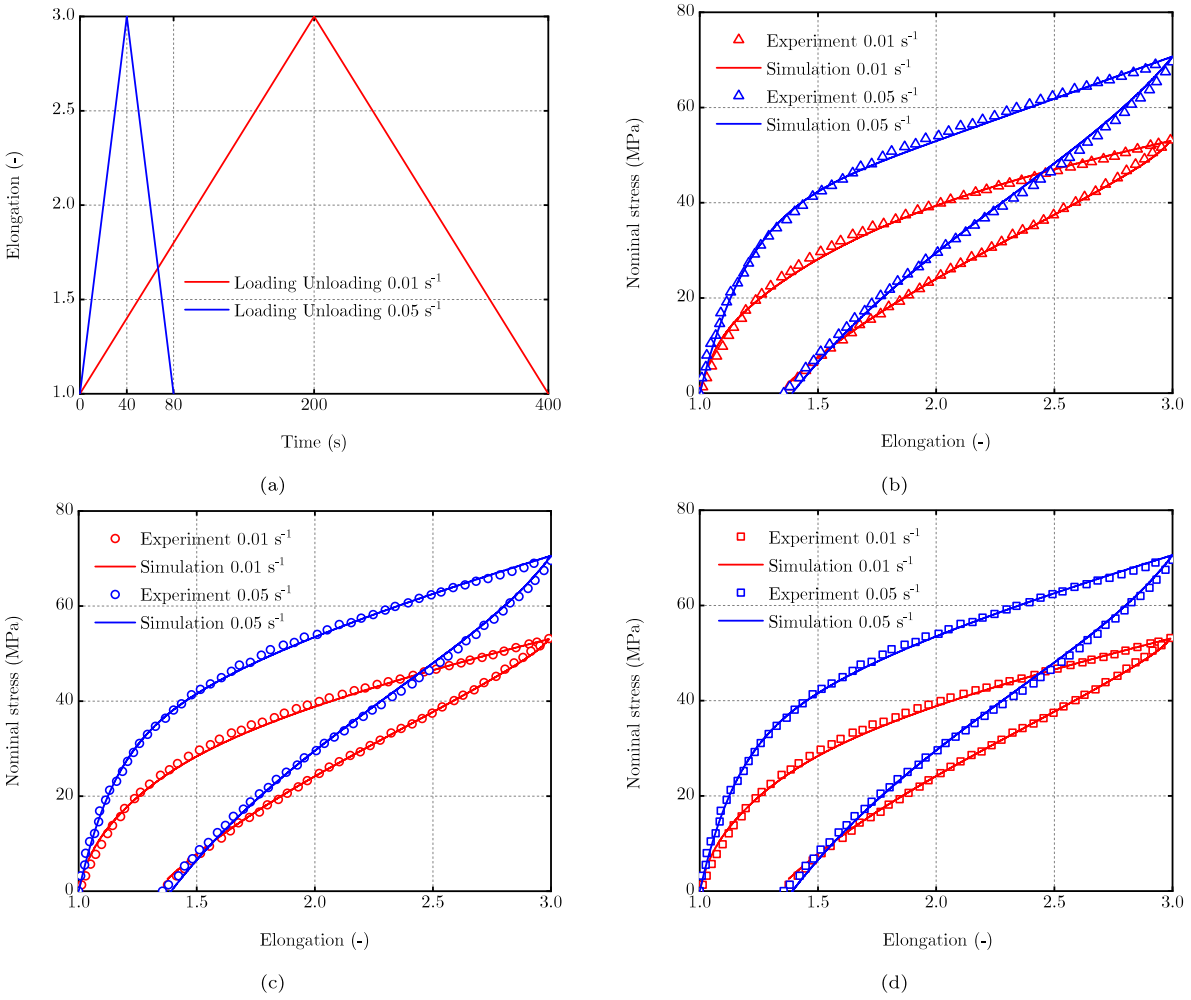

Fig. 6. (a) The loading history evolution curves and fitting nominal stress versus elongation curves using (b) two viscous branches, (c) three viscous branches and (d) four viscous branches for the loading–unloading cyclic tests at deformation level of 200% under strain rates of 0.01 s^{-1} and 0.05 s^{-1}.

Table 3
Identified viscous parameters using experimental data at deformation level of 200%.

	Two branches	Three branches	Four branches
μ_1 (kPa)	61.77	63.92	43.53
τ_1 (s)	5.95	3.52	3.60
μ_2 (kPa)	17.11	11.98	18.86
τ_2 (s)	239.65	359.67	3.64
μ_3 (kPa)	–	14.13	13.98
τ_3 (s)	–	37.02	35.86
μ_4 (kPa)	–	–	12.20
τ_4 (s)	–	–	351.24

Table 4
NRMSE for calibrations using data at different deformation levels.

	50% deformation	100% deformation	200% deformation
Two branches	0.0452	0.0301	0.0191
Three branches	0.0393	0.0203	0.0162
Four branches	0.0389	0.0201	0.0161

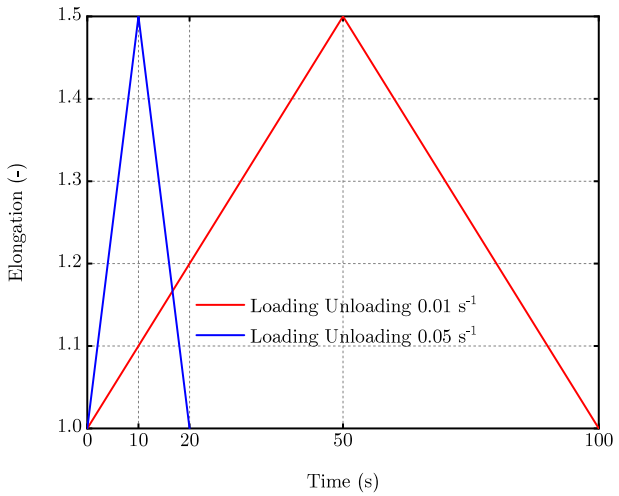

Fig. 7. (a) The loading history evolution and (b) comparison between simulation and experiments for the loading–unloading cyclic tests at the deformation level of 50% under the two loading strain rates of 0.01 s^{-1} and 0.05 s^{-1}.

holding time of 20 min for each step, as shown in Fig. 11. The comparison between simulation and experiments for the multi-step relaxation test is shown in Fig. 12, and it can be seen that the numerical predictions match with the testing data very well. The rapid stress relaxation occurs within the first few seconds at each step and after that the stress converges to the equilibrium state, which can be predicted by the model as in the case of single-step relaxation. Although the equilibrium response at the relaxation stage of each step is obtained in an asymptotic sense, such stress states are widely recognised as the equilibrium stress values at the corresponding stretch levels (Amin et al., 2006). The comparison between the equilibrium stress from the multi-step experiment and simulation is plotted in Fig. 13. A good agreement can be observed, which further demonstrates the reliability of the model.

7. Calibration and experimental validation of anisotropic viscoelasticity

For many soft biological tissues and engineering composites with an elastomeric matrix, the matrix materials are usually nearly incompressible and the neo-Hookean strain energy function (Holzapfel, 2002; Bonet et al., 2016) is adopted for the description of the isotropic elastic and viscoelastic behaviours of the myocardium, while the exponential strain energy function defined by Eq. (84) is used for the anisotropic elastic and viscoelastic modelling of the fibre family. In Section 7.1, the proposed modelling framework is carefully calibrated using the biaxial cyclic testing data of the myocardium by optimising the fitting of the numerical prediction with the experimental results. After calibration, the anisotropic viscoelastic model is validated in Section 7.2 using another two different sets of experimental data corresponding to the biaxial loading tests with different deformation levels. Besides, the numerical analysis for the biaxial cyclic tests when the loading direction varies with respect to the fibre direction is performed to show the capability

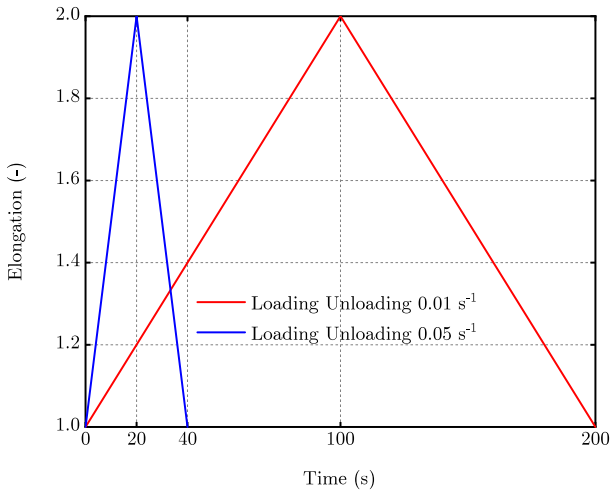

(a)

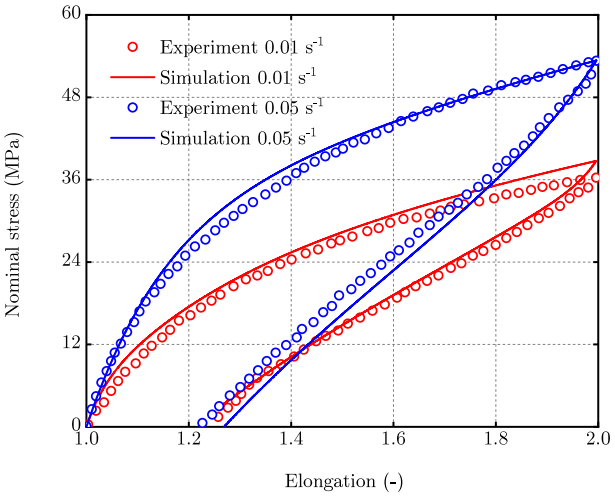

(b)

Fig. 8. (a) The loading history evolution and (b) comparison between simulation and experiments for the loading–unloading cyclic tests at the deformation level of 100% under the two loading strain rates of 0.01 s^{-1} and 0.05 s^{-1}.

of this new theory for the modelling of anisotropic viscous effects. In Section 7.3, the last numerical example considers the biaxial stretching and the subsequent relaxation behaviour of the soft biological tissue, in which we investigate the time history evolution of stress, internal variables and rate of dissipation corresponding to both the isotropic and anisotropic parts.

7.1. Calibration

According to the experimental studies (Sommer et al., 2015b,a), the equibiaxial cyclic test was conducted on the thin square samples with the loading directions parallel and vertical to the fibre orientation, as shown in Fig. 14(a). The loading strain rate is 0.002 s^{-1}, and the deformations along the fibre direction and cross-fibre directions are both stretched to 10% at the same time before the subsequent unloading, see Fig. 14(b). Due to the low loading speed, it is assumed that the elastic behaviour of the soft biological tissue is characterised by the average of the loading and unloading paths of the cyclic test as the hysteresis vanish when the strain rate approaches to zero. Hence, the average between the two paths will be treated as the elastic behaviour of this material in the following. The proposed model is calibrated with the equibiaxial testing data by assuming idealised kinematics and incompressibility, and the deformation gradient $\boldsymbol{F}$ is also defined by (91), where λ_L denotes the time dependent amount of stretch along either the fibre direction or the cross-fibre direction. It is assumed that there is only isotropic viscous contribution to the mechanical response in the cross-fibre direction during the equibiaxial cyclic test, and so the experimental data in this regard can be used for the calibration of isotropic viscous parameters while isolating from the anisotropic effects of the one-dimensional fibre family. After the calibration of isotropic viscous model, the anisotropic viscous parameters can be determined by fitting the

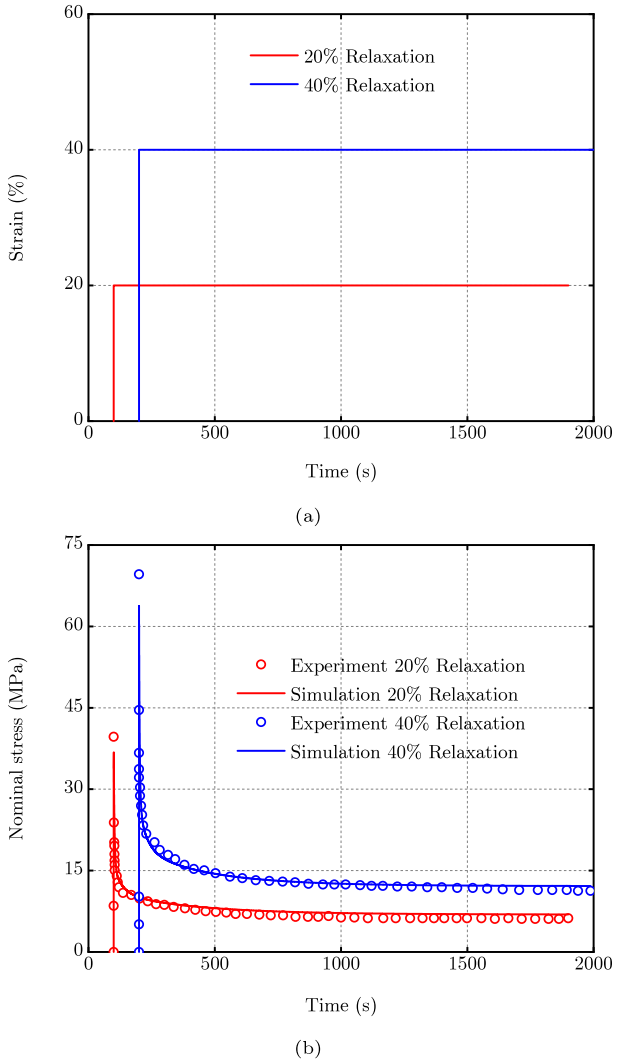

Fig. 9. (a) The loading history evolution and (b) comparison between simulation and experiments for the single-step relaxation tests at stretch levels of 20% and 40%. For better illustration, the two cases have been separated from each other by 100 s.

Table 5
Identified isotropic viscous parameters using experimental data in the cross-fibre direction.

	One branch	Two branches	Three branches	Four branches
μ_1 (kPa)	98.9	46.95	28.28	23.86
τ_1 (s)	0.7678	0.8289	0.9567	0.7285
μ_2 (kPa)	–	45.84	29.16	23.23
τ_2 (s)	–	0.8253	0.8681	0.8981
μ_3 (kPa)	–	–	28.94	23.6
τ_3 (s)	–	–	0.8431	0.8289
μ_4 (kPa)	–	–	–	24.6
τ_4 (s)	–	–	–	0.7706

numerical prediction with the experimental data in the fibre direction in which both the anisotropic and isotropic viscous effects are included. It should be pointed out that the isotropic viscous parameters are kept fixed when calibrating the anisotropic viscous parameters in a sequential manner.

To identify the isotropic viscous parameters, it is imperative to firstly ascertain the number of viscous branches or Maxwell elements, which is typically essential for an accurate characterisation of the nonlinear viscoelastic material behaviour. Each isotropic viscous branch contains two parameters that need to be determined corresponding to the matrix contribution, i.e. the viscous modulus μ_α^{m} and the relaxation time τ_α^{m}. The experimental data acquired from the equibiaxial cyclic test of the myocardium in

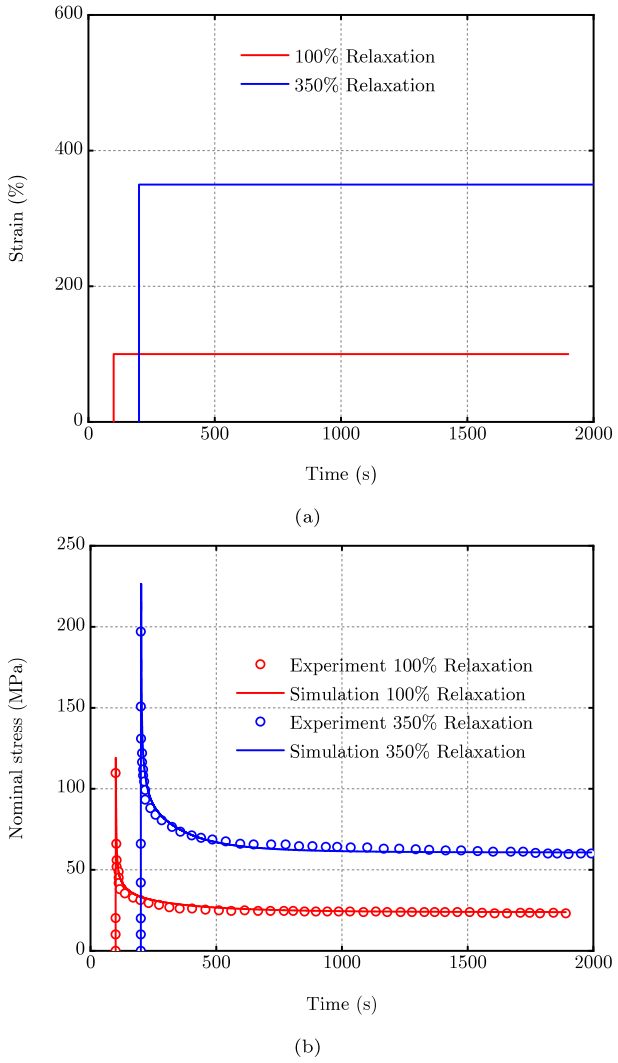

Fig. 10. (a) The loading history evolution and (b) comparison between simulation and experiments for the single-step relaxation tests at stretch levels of 100% and 350%. For better illustration, the two cases have been separated from each other by 100 s.

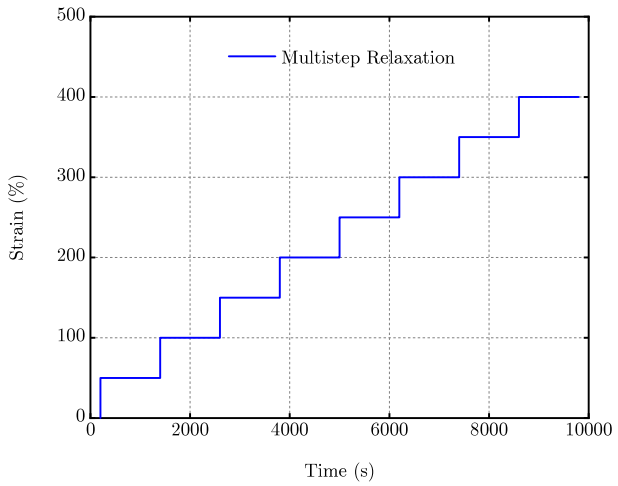

Fig. 11. The loading history evolution for the multi-step relaxation test.

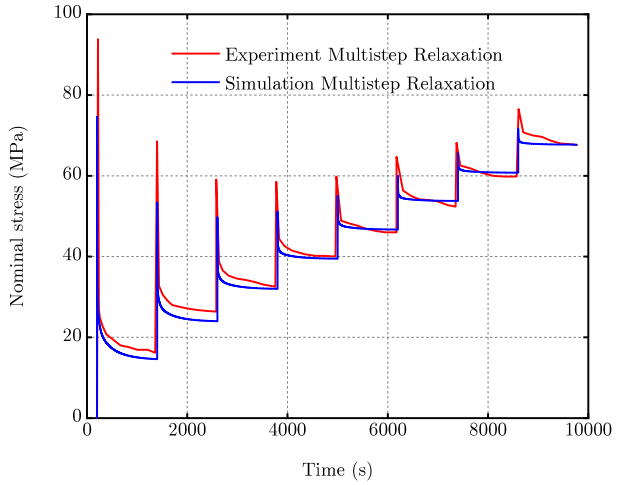

Fig. 12. Comparison between simulation and experiments for the multi-step relaxation test.

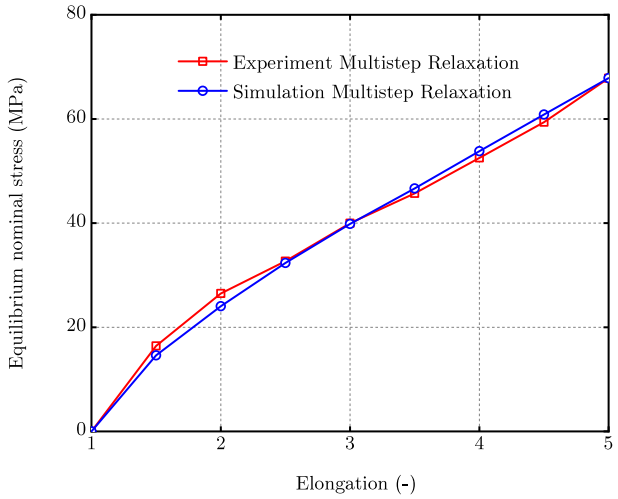

Fig. 13. Comparison of the equilibrium stress values between simulation and experiments for the multi-step relaxation test.

Table 6
Identified anisotropic viscous parameters using experimental data in the fibre direction.

	One branch	Two branches	Three branches	Four branches
μ_1 (kPa)	99.6	79.75	66.28	44.45
τ_1 (s)	0.9777	0.6255	0.4992	0.5619
μ_2 (kPa)	–	79.35	65.83	43.52
τ_2 (s)	–	0.627	0.5115	0.6171
μ_3 (kPa)	–	–	66.17	43.65
τ_3 (s)	–	–	0.506	0.5441
μ_4 (kPa)	–	–	–	43.75
τ_4 (s)	–	–	–	0.5595

the cross-fibre direction will be utilised for the construction of the objective function during the parameter optimisation process. The isotropic viscous parameters μ_α^{m} and τ_α^{m} are obtained by minimising the difference between the loading–unloading Cauchy stress versus elongation curves obtained from both experiments and numerical prediction. As pointed out in Linder et al. (2011), this optimisation methodology is referred to as simultaneous minimisation for the purpose of parameter identification. The fittings with one, two, three and four isotropic viscous branches for the loading–unloading experimental data in the cross-fibre direction of the equibiaxial test at the deformation level of 10% are shown in Fig. 15. It can be seen that the increase in the number of isotropic viscous branches from one to four does not significantly improve the fitting accuracy. The optimised parameter sets using `MatLab` built-in optimisation routine `lsqnonlin` (Anon, 2024) are listed in Table 5. Hence, it is concluded here that one isotropic viscous

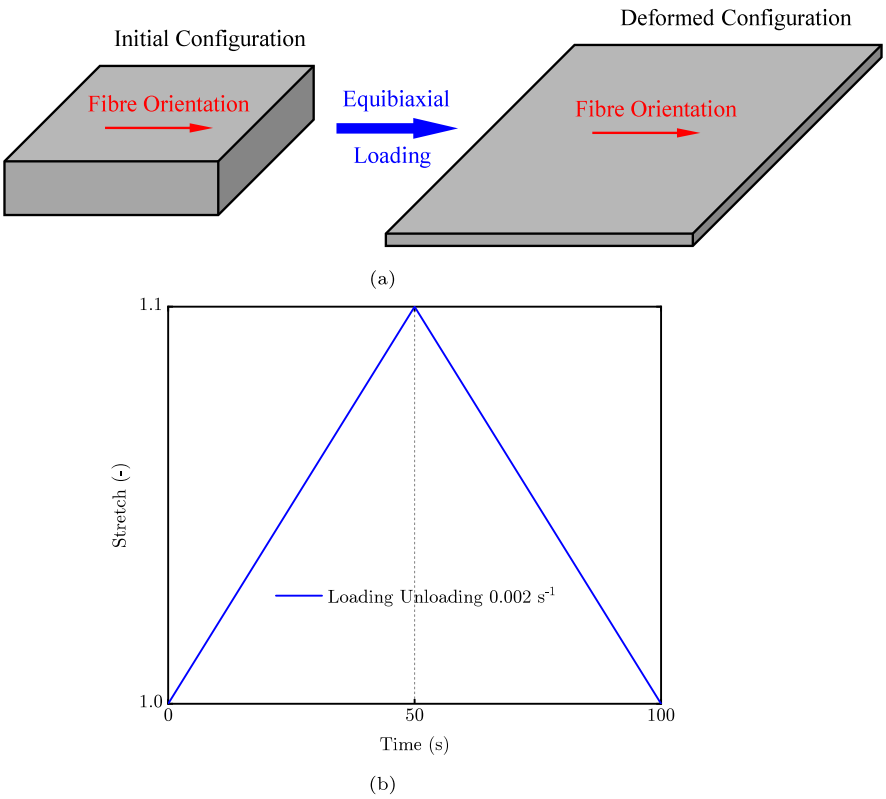

Fig. 14. (a) The schematic of the initial and deformed configurations and (b) the loading history curve in both the fibre and cross-fibre directions of the equibiaxial cyclic test.

Maxwell element is able to describe the viscoelastic behaviour of the equibiaxial cyclic test in the cross-fibre direction, and the identified parameter values corresponding to one isotropic viscous branch will be used for the subsequent calibration. Analogously, the anisotropic viscous parameter values can be obtained from the optimisation process by fitting the numerical prediction with the experimental data of the equibiaxial cyclic test in the fibre direction. Fig. 16 shows the fittings of one, two, three and four anisotropic viscous branches with the loading–unloading experimental data in the fibre direction of the equibiaxial test at the deformation level of 10%. The optimised parameter sets corresponding to the anisotropic viscous part are listed in Table 6. We can see that there is also no significant difference of increasing the number of anisotropic Maxwell elements for the accurate modelling of the viscoelastic response in the fibre direction. Therefore, it is assumed that both the isotropic and anisotropic viscous responses can be predicted with enough accuracy using only one viscous branch, and the identified parameters will be used to validate the proposed model with other experimental data and perform some numerical tests in the following.

7.2. Biaxial cyclic loading and experimental validation

In this section, the experimental results for the equibiaxial cyclic tests at deformation levels of 12.5% and 15% are used to validate the calibrated model, and the comparison between the numerical prediction and experimental results on the Cauchy stress versus elongation of the equibiaxial cyclic test are shown in Fig. 17 and Fig. 18, respectively. Due to the reinforcement in the fibre direction, it can be seen that the Cauchy stress value is obviously higher than the counterpart in the cross-fibre direction when reaching the same deformation for both cases. Besides, the higher peak stress values in both the fibre and cross-fibre directions can be observed for the equibiaxial cyclic test with the deformation level of 15% due to it larger stretch compared with the other case. Although there is slight difference between simulation and experiments, the overall prediction of the model for the two equibiaxial cyclic tests in both the cross-fibre direction and fibre direction is very good. It should be pointed out that the loading–unloading cyclic tests are typical in case of the characterisation of rate-dependent behaviour of viscoelastic biological materials. The excellent performance of the proposed model to predict the dissipative behaviour with varying hysteresis loops for the equibiaxial cyclic tests at two deformation levels clearly demonstrates its effectiveness.

To further showcase its capability for the prediction of anisotropic viscous effects, the numerical analysis of the equibiaxial cyclic tests with the deformation level of 10% when the two loading directions in the equibiaxial test are not aligned with the fibre and cross-fibre directions are performed. In case there is a rotation of the fibre family with respect to the horizontal loading direction, the mechanical responses in the horizontal and vertical directions may or may not be different from each other. The predicted

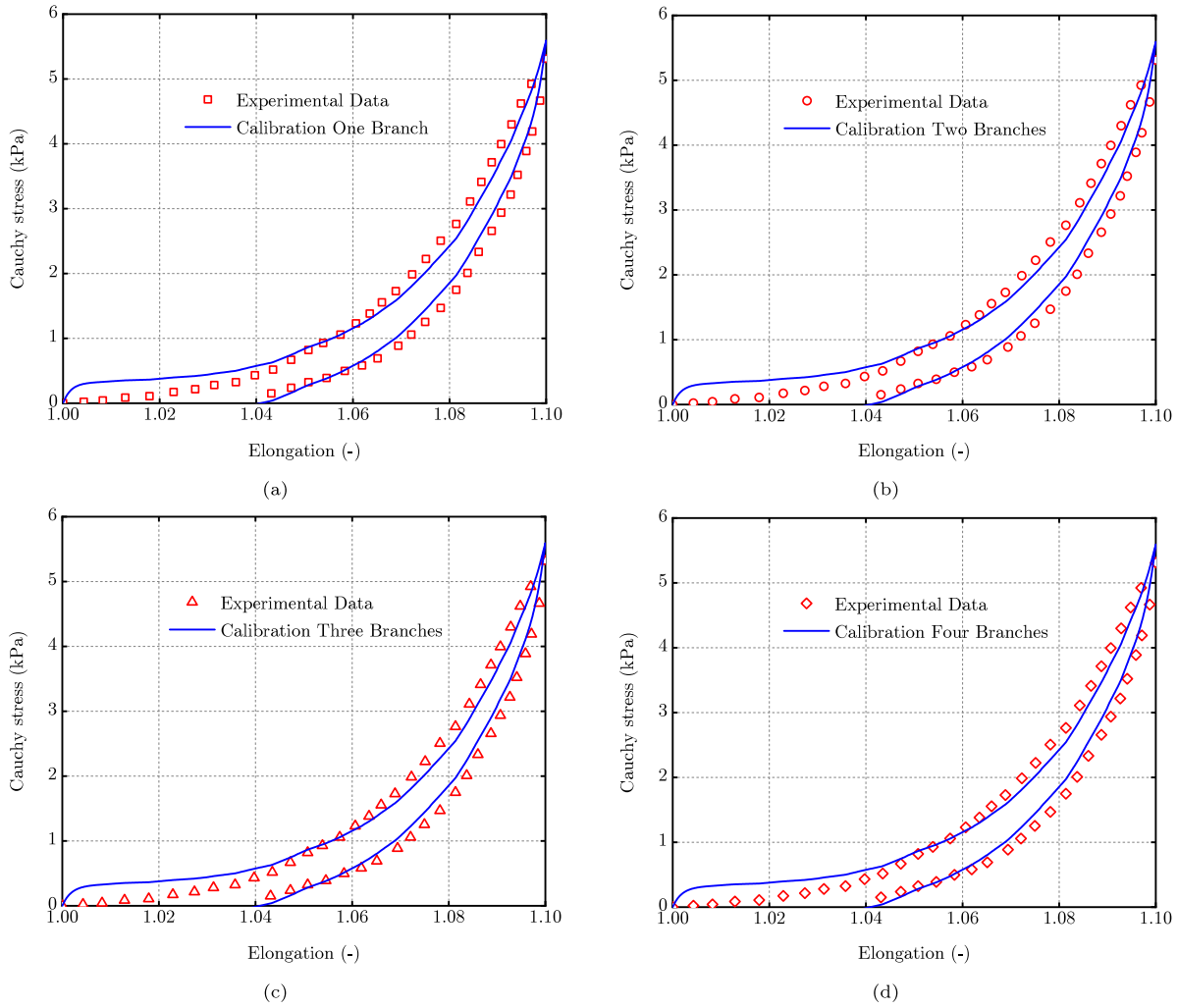

Fig. 15. The fitting Cauchy stress versus elongation curves using (a) one isotropic viscous branch, (b) two isotropic viscous branches, (c) three isotropic viscous branches and (d) four isotropic viscous branches for the equibiaxial cyclic test at deformation level of 10% in the cross-fibre direction.

equibiaxial loading–unloading curves with the deformation of 10% in the horizontal and vertical directions when the fibre direction rotates with respect to the horizontal direction at 0°, 22.5°, 67.5° and 90° are plotted in Fig. 19. Note that the vertical curves are generally below the corresponding horizontal curves in the two numerical tests with rotation angles equal to 0° and 22.5°, while this tendency is reversed in the other two numerical tests with rotation angles equal to 67.5° and 90°, which mainly depends on the anisotropic effects from the fibre contribution.

7.3. Relaxation test

The relaxation test is another alternative option to characterise the time-dependent mechanical behaviour of viscoelastic materials. In this section, we perform the numerical analysis of the equibiaxial relaxation tests in which the deformation in both the cross-fibre and fibre directions are firstly stretched to 10% at a high strain rate and then kept constant for twenty minutes, see Fig. 20. The predicted stress relaxation curves in the fibre and cross-fibre directions are plotted in Fig. 21. It can be observed that the peak stress and equilibrium stress values of the numerical prediction in the fibre direction are both higher than the counterparts in the cross-fibre direction, which can also be attributed to the reinforcement of the fibre family. The time history evolution curves of the total stretch and internal variables in both the fibre and cross-fibre directions are plotted in Fig. 22. In the cross-fibre direction, there is only one internal variable corresponding to the isotropic viscous part, while in the fibre direction, another internal variable corresponding to the anisotropic viscous part exists. As can be seen from Fig. 22, the internal variables corresponding to both the isotropic and anisotropic viscous parts gradually increase from the initial value of 1.0 to the maximum elongation value of 1.1, whereas the total stretch evolves according to the loading curve. Moreover, the rates of isotropic and anisotropic viscous dissipation

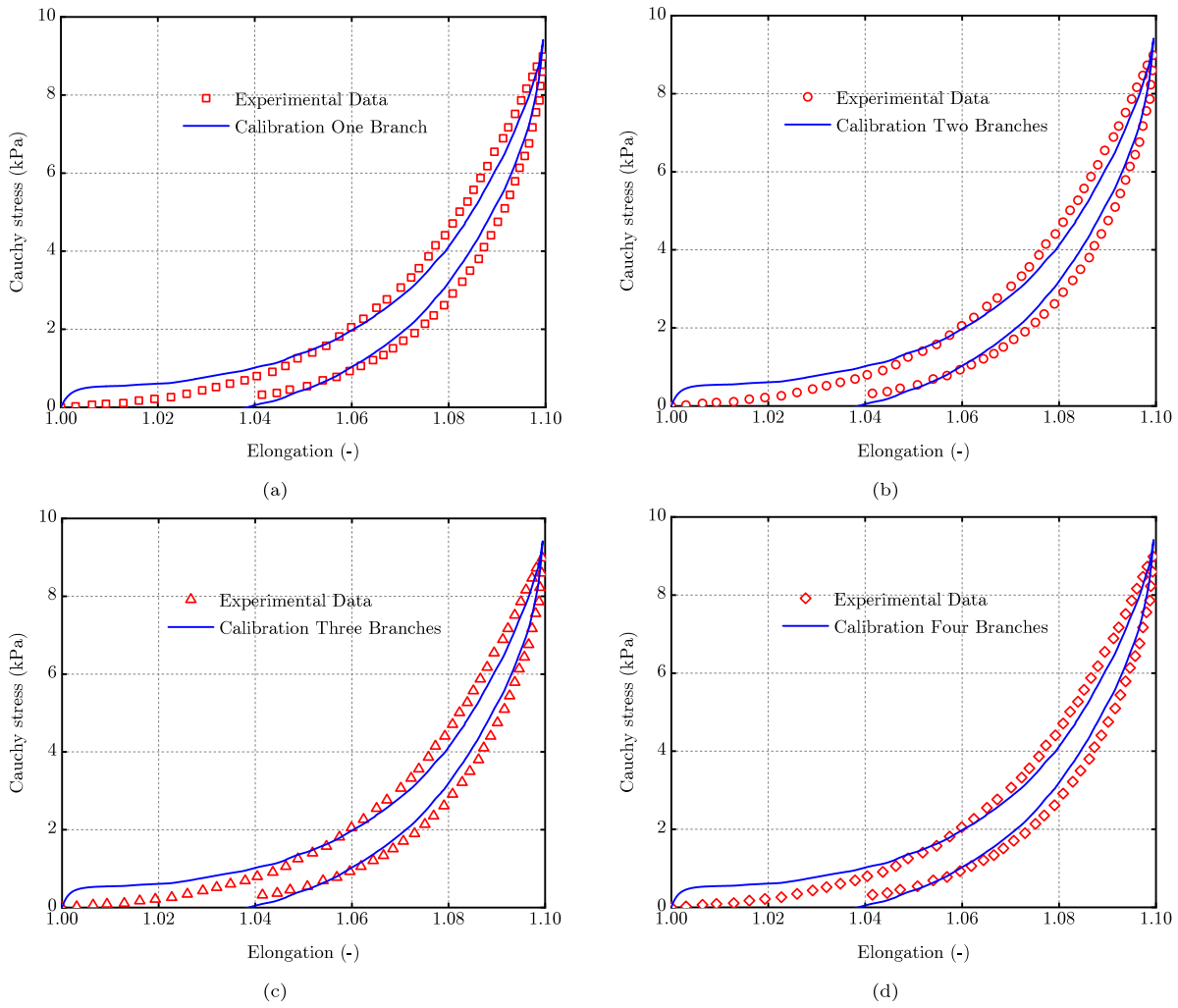

Fig. 16. The fitting Cauchy stress versus elongation curves using (a) one anisotropic viscous branch, (b) two anisotropic viscous branches, (c) three anisotropic viscous branches and (d) four anisotropic viscous branches for the equibiaxial cyclic test at deformation level of 10% in the fibre direction.

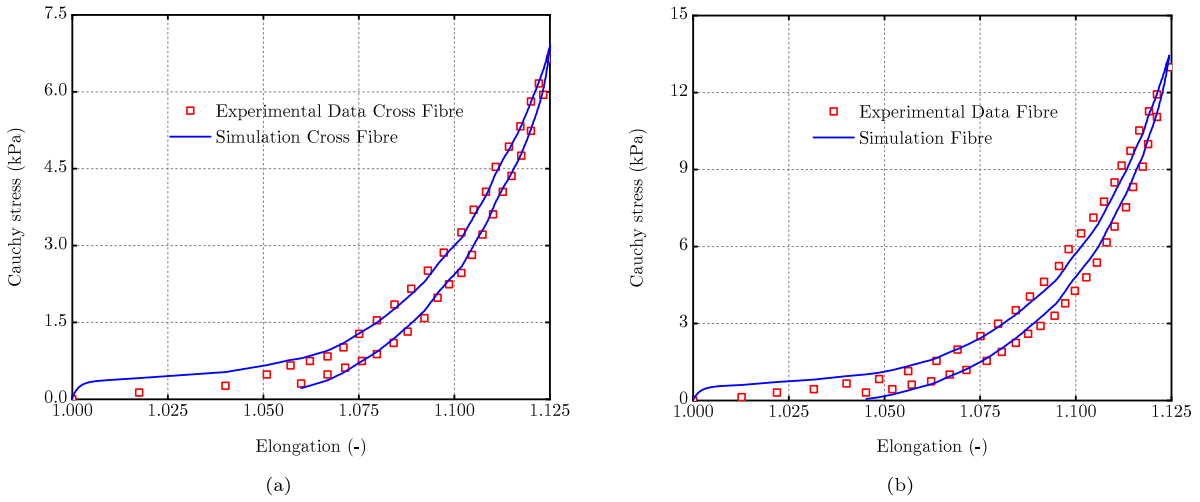

Fig. 17. The comparison between the numerical prediction and experimental results on the Cauchy stress versus elongation of the equibiaxial cyclic test at the deformation level of 12.5% in the cross-fibre direction (a) and fibre direction (b).

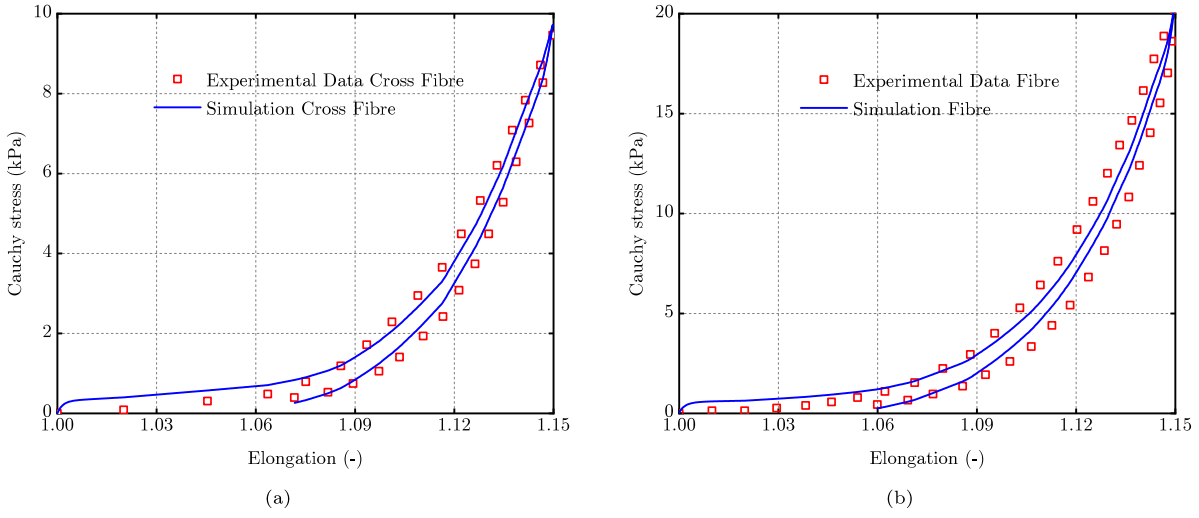

Fig. 18. The comparison between the numerical prediction and experimental results on the Cauchy stress versus elongation of the equibiaxial cyclic test at the deformation level of 15% in the cross-fibre direction (a) and fibre direction (b).

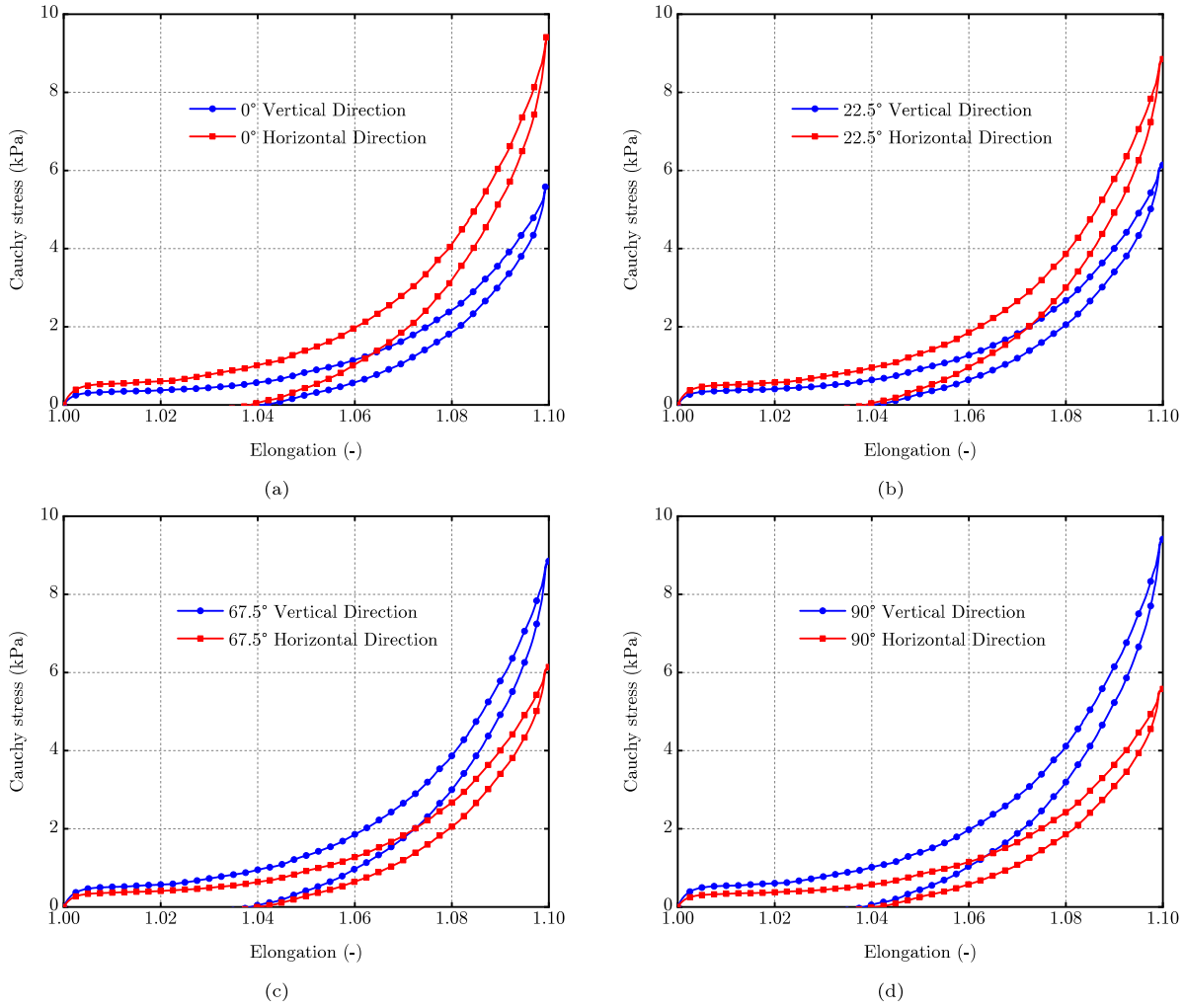

Fig. 19. The predicted equibiaxial loading–unloading curves with the deformation of 10% in the horizontal and vertical directions when the fibre direction rotates with respect to the horizontal direction at (a) 0°, (b) 22.5°, (c) 67.5°, and (d) 90°.

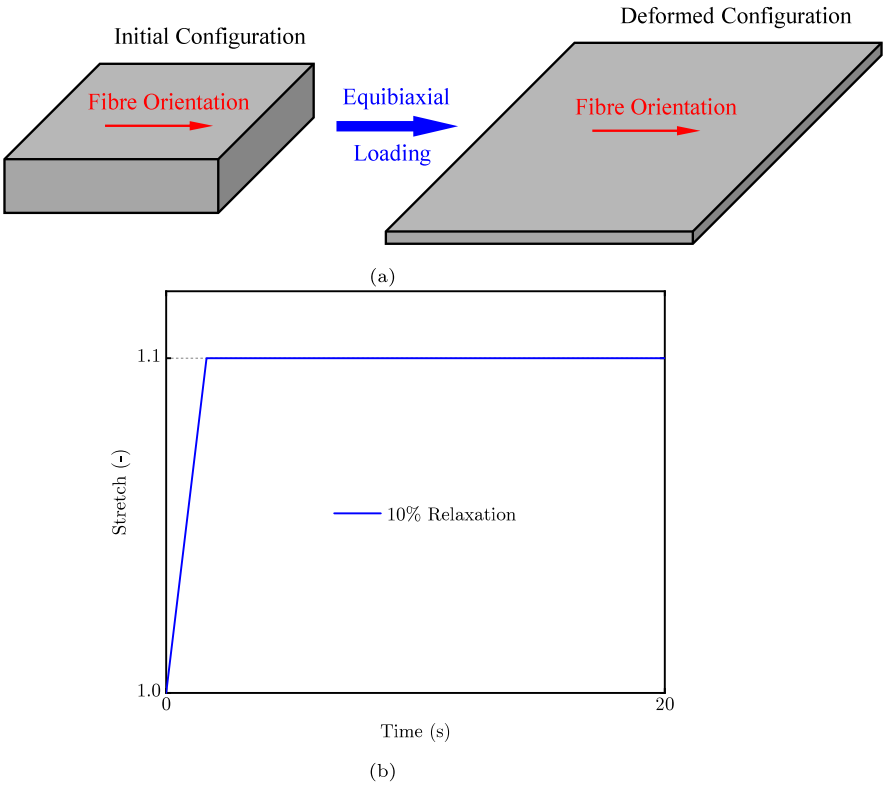

Fig. 20. (a) The schematic of the initial and deformed configurations and (b) the loading history curve in both the fibre and cross-fibre directions of the equibiaxial relaxation test.

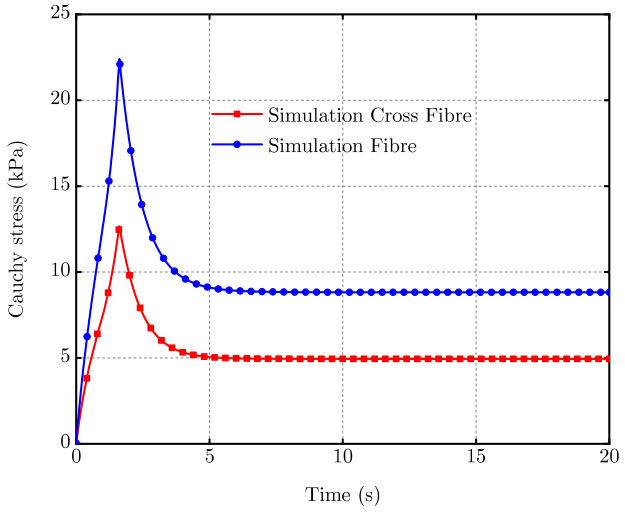

Fig. 21. The predicted stress relaxation curves of the equibiaxial relaxation test in the fibre and cross-fibre directions.

curves are shown in Fig. 23(a) and Fig. 23(b), respectively. Note that positive rates of energy dissipation corresponding to both the isotropic and anisotropic viscous parts are ensured before reaching the equilibrium during the equibiaxial relaxation test, which has also been mathematically proved before. To further study the anisotropic viscous effects on the equibiaxial relaxation test, the numerical analysis of the equibiaxial relaxation tests when the two loading directions are not aligned with the fibre and cross-fibre directions are also performed, and the predicted relaxation curves with the rotation angle of 15°, 30°, 60° and 75° are plotted in Fig. 24. Due to the anisotropic effects, the vertical stress relaxation curves are generally below the corresponding horizontal curves

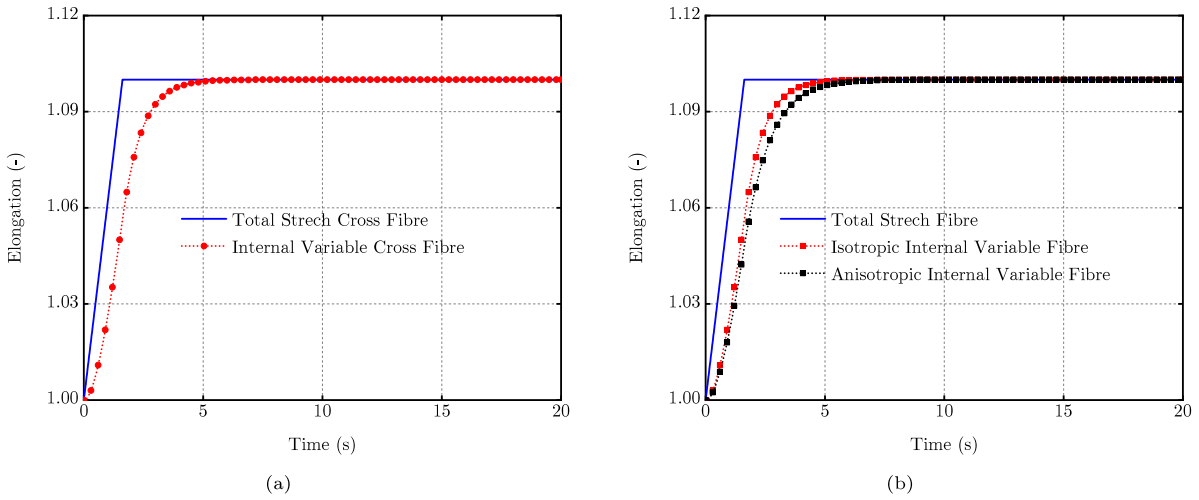

Fig. 22. The time history evolution curves of the total stretch and internal variables of the equibiaxial relaxation test in the fibre and cross-fibre directions.

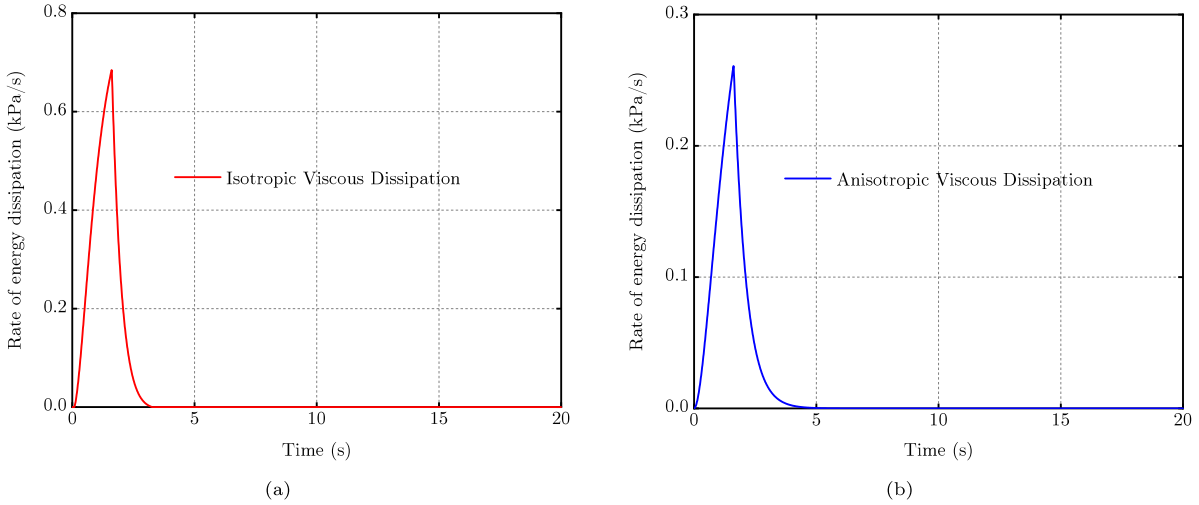

Fig. 23. The time history evolution curves of the rates of isotropic and anisotropic viscous dissipation of the equibiaxial relaxation test.

in the two numerical tests with rotation angles equal to 15° and 30°, while the opposite tendency can be observed in the other two numerical tests with rotation angles equal to 60° and 75°.

8. Concluding remarks

Starting from a classical one-dimensional Maxwell rheological model, this paper has presented a large strain modelling framework for viscoelasticity in three-dimensional continua. Similar to traditional approaches, the framework adopts a multiplicative decomposition of the deformation gradient into elastic and viscous contributions for each of the Maxwell (non-equilibrium) elements. To ensure thermodynamic compliance, that is, positive energy dissipation, a novel rate-type relaxation law for the evolution of internal variables is revisited (Bonet, 2001), which gives the rate of the elastic stress tensor of the viscous element, at constant total deformation, in terms of the relaxation time parameter and the current stress. Due to the volume-preserving constraint for many viscoelastic materials (i.e. polymers), the evolution law is further modified, which also ensures the thermodynamic consistency in the case of strict incompressibility. For ease of computational implementation, the rate form evolution laws are integrated in time via a standard backward Euler algorithm, resulting in an incremental return mapping type of approach, facilitating the link between modelling of viscoelasticity and elastoplasticity. The internal state strain viscous variables can finally be recovered via a simple Newton–Raphson type of iteration scheme. Crucially, for the case of some prototypical user-defined non-equilibrium strain energy densities (i.e. Saint-Venant Kirchhoff, incompressible neo-Hookean), closed-form solutions can be obtained. Finally, by taking advantage of a frame invariant stress free configuration, the formulation is then extended for the consideration of anisotropy.

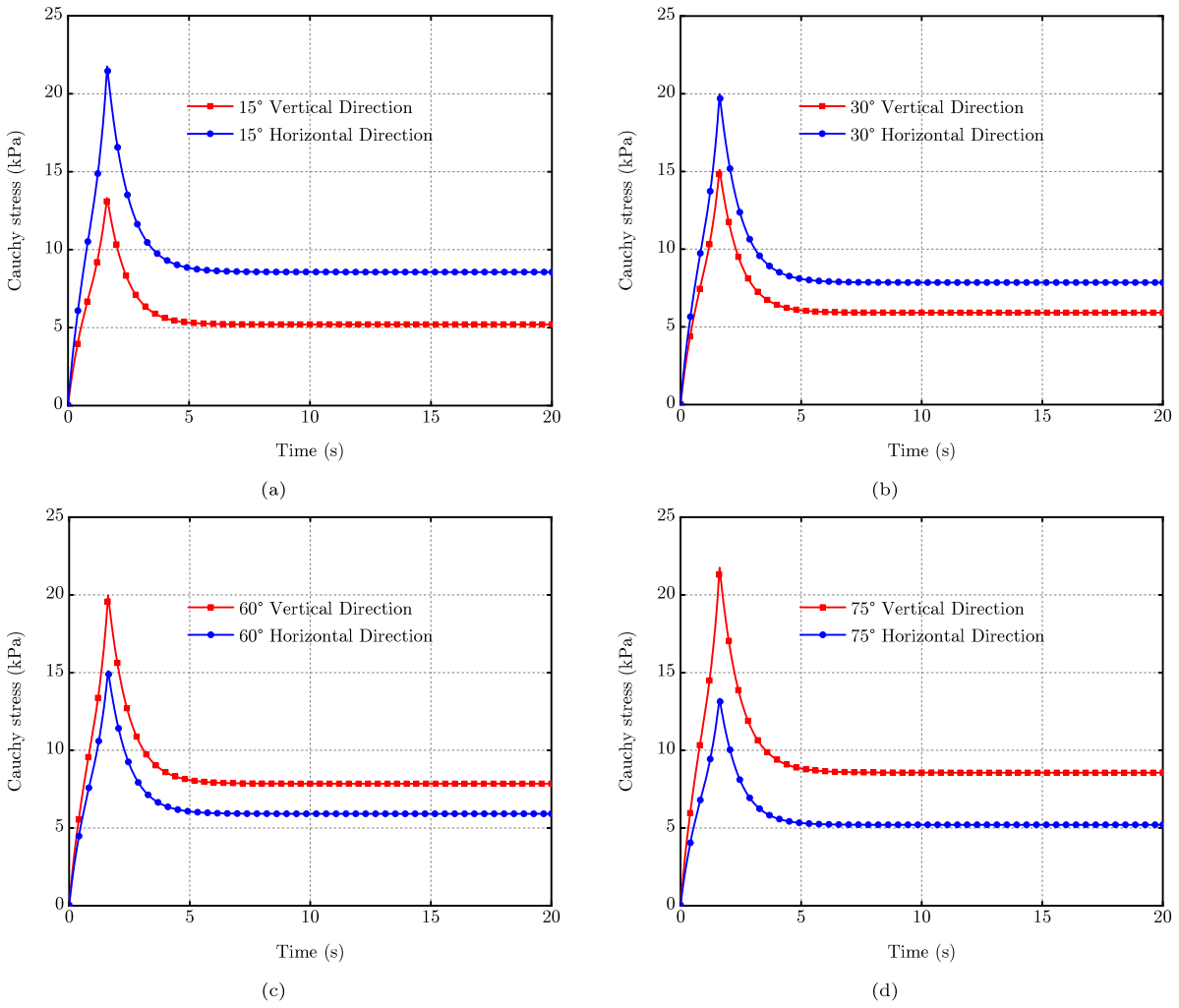

Fig. 24. The predicted equibiaxial relaxation curves in the horizontal and vertical directions when the fibre direction rotates with respect to the horizontal direction at (a) 15°, (b) 30°, (c) 60°, and (d) 75°.

Although the framework is pursued for the simple case of a single transversely isotropic invariant contribution with corresponding closed-form solution, the methodology is also extended to the consideration of the second transversely isotropic invariant, multiple families of fibres, or even more complex symmetry groups.

To validate the formulation, a specialised form with an eight-chain (long-term) strain energy density functional and a simple neo-Hookean (non-equilibrium) strain energy density functional have been adopted for the calibration and verification with available experimental data of soft viscoelastic VHB 4910 polymers. It was found that the simulation results match very well with the testing data from different types of viscoelastic experiments, including the loading–unloading cyclic tests, single-step relaxation tests and multi-step relaxation tests, including anisotropic scenarios. The good agreement clearly demonstrates the effectiveness of the proposed theory. Extension of the presented framework in the context of electro-mechanics will be the next step of this research, paving the way for the comprehensive time-dependent modelling of anisotropic Electro-Active Polymers for soft robotics applications.

CRediT authorship contribution statement

Zeng Liu: Writing – original draft, Validation, Software, Methodology, Formal analysis, Data curation. **Rogelio Ortigosa:** Writing – review & editing, Validation, Software, Resources, Methodology, Funding acquisition, Formal analysis. **Antonio J. Gil:** Writing – review & editing, Visualization, Methodology, Investigation, Funding acquisition, Formal analysis. **Javier Bonet:** Writing – review & editing, Writing – original draft, Supervision, Resources, Project administration, Methodology, Investigation, Funding acquisition, Formal analysis, Conceptualization.

Declaration of competing interest

The authors declare the following financial interests/personal relationships which may be considered as potential competing interests: Javier Bonet reports financial support was provided by Spain Ministry of Science and Innovation. Rogelio Ortigosa reports financial support was provided by Spain Ministry of Science and Innovation. Rogelio Ortigosa reports financial support was provided by Autonomous Community of the Region of Murcia. Antonio J. Gil reports financial support was provided by The Leverhulme Trust. Antonio J. Gil reports financial support was provided by Defence Science and Technology Laboratory. If there are other authors, they declare that they have no known competing financial interests or personal relationships that could have appeared to influence the work reported in this paper.

Acknowledgements

The authors acknowledge funding received from grants PID2022-141957OB-C21 and PID2022-141957OA-C22 financed by MCIN/AEI /10.13039/501100011033/ FEDER, UE. R. Ortigosa also acknowledges the support provided by the Autonomous Community of the Region of Murcia, Spain, through the programme for the development of scientific and technical research by competitive groups (21996/PI/22), included in the Regional Program for the Promotion of Scientific and Technical Research of Fundación Séneca - Agencia de Ciencia y Tecnología de la Región de Murcia. A. J. Gil wishes to acknowledge the support provided by the Defence, Science and Technology Laboratory (Dstl) and The Leverhulme Trust Foundation (UK) through a Leverhulme Fellowship. The authors also acknowledge the useful discussions with colleagues Alberto García González and Max Barillas Velásquez from UPC-CIMNE, Jesús Martínez Frutos from Technical University of Cartagena, and graphical support by Nathan Ellmer from Swansea University.

Appendix A. Alternative derivation of the Lagrange multiplier in incompressible viscoelasticity

An alternative expression for the Lagrange multiplier λ_α can be obtained by making use of the kinetic constraint Eq. (41). Indeed, time derivative of (41) yields

$$\begin{aligned} 0 &= \left.\frac{\mathrm{d}\boldsymbol{S}'_{\mathrm{e}_\alpha}}{\mathrm{d}t}\right|_{\boldsymbol{F}=\text{const}} : \boldsymbol{C}_{\mathrm{e}_\alpha} + \boldsymbol{S}'_{\mathrm{e}_\alpha} : \left.\frac{\mathrm{d}\boldsymbol{C}_{\mathrm{e}_\alpha}}{\mathrm{d}t}\right|_{\boldsymbol{F}=\text{const}} \\ &= \left.\frac{\mathrm{d}\boldsymbol{S}'_{\mathrm{e}_\alpha}}{\mathrm{d}t}\right|_{\boldsymbol{F}=\text{const}} : \boldsymbol{C}_{\mathrm{e}_\alpha} + \boldsymbol{S}'_{\mathrm{e}_\alpha} : 2\bar{\mathbb{C}}^{-1}_{\mathrm{e}_\alpha} : \left.\frac{\mathrm{d}\boldsymbol{S}'_{\mathrm{e}_\alpha}}{\mathrm{d}t}\right|_{\boldsymbol{F}=\text{const}} \\ &= \left.\frac{\mathrm{d}\boldsymbol{S}'_{\mathrm{e}_\alpha}}{\mathrm{d}t}\right|_{\boldsymbol{F}=\text{const}} : \left(\boldsymbol{C}_{\mathrm{e}_\alpha} + 2\bar{\mathbb{C}}^{-1}_{\mathrm{e}_\alpha} : \boldsymbol{S}'_{\mathrm{e}_\alpha}\right) \\ &= -\frac{1}{\tau_\alpha}\left(\boldsymbol{S}'_{\mathrm{e}_\alpha} - \lambda_{\mathrm{e}_\alpha}\boldsymbol{C}^{-1}_{\mathrm{e}_\alpha}\right) : \left(\boldsymbol{C}_{\mathrm{e}_\alpha} + 2\bar{\mathbb{C}}^{-1}_{\mathrm{e}_\alpha} : \boldsymbol{S}'_{\mathrm{e}_\alpha}\right), \end{aligned} \tag{92}$$

where Eqs. (44) and (45) have been used in the second and fourth lines of above Eq. (92), respectively. As a result, re-arrangement of the last line of Eq. (92) results into

$$\lambda_\alpha = \frac{2\boldsymbol{S}'_{\mathrm{e}_\alpha} : \bar{\mathbb{C}}^{-1}_{\mathrm{e}_\alpha} : \boldsymbol{S}'_{\mathrm{e}_\alpha}}{3 + 2\boldsymbol{C}^{-1}_{\mathrm{e}_\alpha} : \bar{\mathbb{C}}^{-1}_{\mathrm{e}_\alpha} : \boldsymbol{S}'_{\mathrm{e}_\alpha}}. \tag{93}$$

Note that the time derivative of the deviatoric condition Eq. (41) can also be written as

$$\begin{aligned} 0 &= \left.\frac{\mathrm{d}\boldsymbol{S}'_{\mathrm{e}_\alpha}}{\mathrm{d}t}\right|_{\boldsymbol{F}=\text{const}} : \boldsymbol{C}_{\mathrm{e}_\alpha} + \boldsymbol{S}'_{\mathrm{e}_\alpha} : \left.\frac{\mathrm{d}\boldsymbol{C}_{\mathrm{e}_\alpha}}{\mathrm{d}t}\right|_{\boldsymbol{F}=\text{const}} \\ &= \left(\frac{1}{2}\mathbb{C}_{\mathrm{e}_\alpha} : \boldsymbol{C}_{\mathrm{e}_\alpha} + \boldsymbol{S}'_{\mathrm{e}_\alpha}\right) : \left.\frac{\mathrm{d}\boldsymbol{C}_{\mathrm{e}_\alpha}}{\mathrm{d}t}\right|_{\boldsymbol{F}=\text{const}}. \end{aligned} \tag{94}$$

Recalling Eq. (39), the above Eq. (94) implies that

$$\frac{1}{2}\mathbb{C}_{\mathrm{e}_\alpha} : \boldsymbol{C}_{\mathrm{e}_\alpha} + \boldsymbol{S}'_{\mathrm{e}_\alpha} = g\boldsymbol{C}^{-1}_{\mathrm{e}_\alpha}, \tag{95}$$

for any arbitrary constant g, and it can be alternatively expressed as

$$\mathbb{C}^{-1}_{\mathrm{e}_\alpha} : \boldsymbol{S}'_{\mathrm{e}_\alpha} = -\frac{1}{2}\boldsymbol{C}_{\mathrm{e}_\alpha} + g\mathbb{C}^{-1}_{\mathrm{e}_\alpha} : \boldsymbol{C}^{-1}_{\mathrm{e}_\alpha}. \tag{96}$$

By substituting Eq. (96) into Eq. (93), we can get

$$\begin{aligned}\lambda_\alpha &= \frac{2\boldsymbol{S}'_{\mathrm{e}_\alpha} : \left(-\frac{1}{2}\boldsymbol{C}_{\mathrm{e}_\alpha} + g\mathbb{C}^{-1}_{\mathrm{e}_\alpha} : \boldsymbol{C}^{-1}_{\mathrm{e}_\alpha}\right)}{3 + 2\boldsymbol{C}^{-1}_{\mathrm{e}_\alpha} : \left(-\frac{1}{2}\boldsymbol{C}_{\mathrm{e}_\alpha} + g\mathbb{C}^{-1}_{\mathrm{e}_\alpha} : \boldsymbol{C}^{-1}_{\mathrm{e}_\alpha}\right)} \\ &= \frac{2g\boldsymbol{S}'_{\mathrm{e}_\alpha} : \mathbb{C}^{-1}_{\mathrm{e}_\alpha} : \boldsymbol{C}^{-1}_{\mathrm{e}_\alpha}}{3 - 3 + 2g\boldsymbol{C}^{-1}_{\mathrm{e}_\alpha} : \mathbb{C}^{-1}_{\mathrm{e}_\alpha} : \boldsymbol{C}^{-1}_{\mathrm{e}_\alpha}} \\ &= \frac{\boldsymbol{S}'_{\mathrm{e}_\alpha} : \mathbb{C}^{-1}_{\mathrm{e}_\alpha} : \boldsymbol{C}^{-1}_{\mathrm{e}_\alpha}}{\boldsymbol{C}^{-1}_{\mathrm{e}_\alpha} : \mathbb{C}^{-1}_{\mathrm{e}_\alpha} : \boldsymbol{C}^{-1}_{\mathrm{e}_\alpha}},\end{aligned} \tag{97}$$

which is exactly Eq. (46).

Appendix B. Tangent modulus of the compressible case

For the computational (i.e. Finite Element Method) implementation of the proposed large strain viscoelastic theory, the tangent constitutive operator[11] needs to be derived to ensure the convergence performance of the global Newton–Raphson iterative solution scheme, as pointed out in Bonet et al. (2016). This tangent operator measures the change of stress with respect to the total strain in the reference configuration, which can be defined by

$$\mathbb{C} = \mathbb{C}_\infty + \sum_\alpha \mathbb{C}_\alpha = 2\frac{\partial \boldsymbol{S}_\infty}{\partial \boldsymbol{C}} + \sum_\alpha 2\frac{\partial \boldsymbol{S}_\alpha}{\partial \boldsymbol{C}}. \tag{98}$$

As an example, in case[12] that the long-term material response can be described by the compressible neo-Hookean model, the tangent operator $\mathbb{C}_\infty$ is obtained as

$$\mathbb{C}_\infty = \lambda_\infty \boldsymbol{C}^{-1} \otimes \boldsymbol{C}^{-1} + 2(\mu_\infty - \lambda_\infty \ln J)\mathbb{K}, \tag{99}$$

where λ_∞ and μ_∞ are Lamé material parameters, and the fourth order tensor $\mathbb{K}$ is given by

$$\mathbb{K} = -\frac{\partial \boldsymbol{C}^{-1}}{\partial \boldsymbol{C}}; \quad (\mathbb{K})_{IJKL} = \frac{1}{2}\left(\left(\boldsymbol{C}^{-1}\right)_{IK}\left(\boldsymbol{C}^{-1}\right)_{JL} + \left(\boldsymbol{C}^{-1}\right)_{IL}\left(\boldsymbol{C}^{-1}\right)_{JK}\right). \tag{100}$$

The evaluation of the α-viscous contribution $\mathbb{C}_\alpha$ to the tangent modulus is not immediate, since the change of the state variables $\boldsymbol{C}_{\mathrm{e}_\alpha}$ arising from the change of the strain tensor $\boldsymbol{C}$ needs also to be taken into account. By recalling Eq. (19), the viscous tangent operator $\mathbb{C}_\alpha$ is given by

$$\mathbb{C}_\alpha = 2\frac{\partial \boldsymbol{S}_\alpha}{\partial \boldsymbol{C}} = 2\frac{\partial\left(\boldsymbol{U}^{-1}_{\mathrm{v}_\alpha}\boldsymbol{S}_{\mathrm{e}_\alpha}\boldsymbol{U}^{-1}_{\mathrm{v}_\alpha}\right)}{\partial \boldsymbol{C}}, \tag{101}$$

and its index form can be presented as

$$(\mathbb{C}_\alpha)_{IJKL} = 2\left((\mathbb{B})_{IPKL}(\boldsymbol{S}_{\mathrm{e}_\alpha})_{PQ}(\boldsymbol{U}^{-1}_{\mathrm{v}_\alpha})_{QJ} + (\boldsymbol{U}^{-1}_{\mathrm{v}_\alpha})_{IP}(\mathbb{A})_{PQKL}(\boldsymbol{U}^{-1}_{\mathrm{v}_\alpha})_{QJ} + (\boldsymbol{U}^{-1}_{\mathrm{v}_\alpha})_{IP}(\boldsymbol{S}_{\mathrm{e}_\alpha})_{PQ}(\mathbb{B})_{QJKL}\right), \tag{102}$$

where the fourth order tensors $\mathbb{A}$ and $\mathbb{B}$ read

$$\mathbb{A} = \frac{\partial \boldsymbol{S}_{\mathrm{e}_\alpha}}{\partial \boldsymbol{C}}; \qquad \mathbb{B} = \frac{\partial \boldsymbol{U}^{-1}_{\mathrm{v}_\alpha}}{\partial \boldsymbol{C}}. \tag{103}$$

The calculation of the tensor $\mathbb{A}$ can be obtained via the use of Eq. (34), as the differentiation of the final stress can be related to the differentiation of the instantaneous stress that keeps the internal state variables $\boldsymbol{U}_{\mathrm{v}_\alpha}$ constant. In this way, the tangent operator $\mathbb{A}$ can be determined by

$$\mathbb{A} = \frac{\partial \boldsymbol{S}_{\mathrm{e}_\alpha}}{\partial \boldsymbol{C}} = \gamma_\alpha \frac{\partial \boldsymbol{S}^*_{\mathrm{e}_\alpha}}{\partial \boldsymbol{C}}. \tag{104}$$

To determine the tensor $\mathbb{B}$, note firstly that the differentiation of $\boldsymbol{C}_{\mathrm{e}_\alpha}$ with respect to $\boldsymbol{C}$, by recalling Eq. (13), can be derived as

$$\frac{\partial \boldsymbol{C}_{\mathrm{e}_\alpha}}{\partial \boldsymbol{C}} = \frac{\partial \hat{\boldsymbol{C}}_{\mathrm{e}_\alpha}(\boldsymbol{C},\ \boldsymbol{U}^{-1}_{\mathrm{v}_\alpha})}{\partial \boldsymbol{C}} = \mathbb{E} + \mathbb{F} : \mathbb{B}, \tag{105}$$

where the fourth order tensors $\mathbb{E}$ and $\mathbb{F}$ read

$$\mathbb{E} = \left.\frac{\partial \hat{\boldsymbol{C}}_{\mathrm{e}_\alpha}}{\partial \boldsymbol{C}}\right|_{\boldsymbol{U}^{-1}_{\mathrm{v}_\alpha}=\mathrm{const}}; \quad \mathbb{F} = \left.\frac{\partial \hat{\boldsymbol{C}}_{\mathrm{e}_\alpha}}{\partial \boldsymbol{U}^{-1}_{\mathrm{v}_\alpha}}\right|_{\boldsymbol{C}=\mathrm{const}}, \tag{106}$$

[11] The geometric contribution to the tangent operator can be found in standard textbooks (Bonet et al., 2016).

[12] Notice that this is not a restriction of the theory, but any other constitutive law is acceptable.

with the index forms given by

$$(\mathbb{E})_{IJKL} = \frac{1}{2}\left((\boldsymbol{U}^{-1}_{\mathrm{v}_\alpha})_{IK}(\boldsymbol{U}^{-1}_{\mathrm{v}_\alpha})_{LJ} + (\boldsymbol{U}^{-1}_{\mathrm{v}_\alpha})_{IL}(\boldsymbol{U}^{-1}_{\mathrm{v}_\alpha})_{KJ}\right); \tag{107a}$$

$$(\mathbb{F})_{IJKL} = \frac{1}{2}\left(\delta_{IK}(\boldsymbol{C}\boldsymbol{U}^{-1}_{\mathrm{v}_\alpha})_{LJ} + \delta_{IL}(\boldsymbol{C}\boldsymbol{U}^{-1}_{\mathrm{v}_\alpha})_{KJ} + \delta_{JL}(\boldsymbol{U}^{-1}_{\mathrm{v}_\alpha}\boldsymbol{C})_{IK} + \delta_{JK}(\boldsymbol{U}^{-1}_{\mathrm{v}_\alpha}\boldsymbol{C})_{IL}\right), \tag{107b}$$

and the tensor $\mathbb{B}$ is calculated as

$$\mathbb{B} = \mathbb{F}^{-1} : \left(\frac{\partial \boldsymbol{C}_{\mathrm{e}_\alpha}}{\partial \boldsymbol{C}} - \mathbb{E}\right). \tag{108}$$

By the use of Eq. (34) again, we can obtain

$$\frac{\partial \boldsymbol{S}_{\mathrm{e}_\alpha}}{\partial \boldsymbol{C}} = \frac{\partial \boldsymbol{S}_{\mathrm{e}_\alpha}}{\partial \boldsymbol{C}_{\mathrm{e}_\alpha}} : \frac{\partial \boldsymbol{C}_{\mathrm{e}_\alpha}}{\partial \boldsymbol{C}} = \gamma_\alpha \frac{\partial \boldsymbol{S}^*_{\mathrm{e}_\alpha}}{\partial \boldsymbol{C}}, \tag{109}$$

and recalling the definition of $\mathbb{C}_{\mathrm{e}_\alpha}$, we can finally obtain

$$\frac{\partial \boldsymbol{C}_{\mathrm{e}_\alpha}}{\partial \boldsymbol{C}} = 2\gamma_\alpha \mathbb{C}^{-1}_{\mathrm{e}_\alpha} : \frac{\partial \boldsymbol{S}^*_{\mathrm{e}_\alpha}}{\partial \boldsymbol{C}}. \tag{110}$$

Appendix C. Tangent modulus of the incompressible case

The derivation of the tangent modulus is similar to that of the compressible formulation described in Appendix B. To fully determine the viscous tangent operators, the fourth order operators $\mathbb{A}$ and $\mathbb{B}$ need to be adapted, which are given by

$$\mathbb{A} = \frac{\partial \boldsymbol{S}'_{\mathrm{e}_\alpha}}{\partial \boldsymbol{C}} = \frac{\partial \boldsymbol{S}'_{\mathrm{e}_\alpha}}{\partial \boldsymbol{C}_{\mathrm{e}_\alpha}} : \frac{\partial \boldsymbol{C}_{\mathrm{e}_\alpha}}{\partial \boldsymbol{C}} = \mathbb{C}_{\mathrm{e}_\alpha} : \frac{\partial \boldsymbol{C}_{\mathrm{e}_\alpha}}{\partial \boldsymbol{C}}; \tag{111a}$$

$$\mathbb{B} = \frac{\partial \boldsymbol{U}^{-1}_{\mathrm{v}_\alpha}}{\partial \boldsymbol{C}} = \mathbb{F}^{-1} : \left(\frac{\partial \boldsymbol{C}_{\mathrm{e}_\alpha}}{\partial \boldsymbol{C}} - \mathbb{E}\right), \tag{111b}$$

where the fourth order tensor $\frac{\partial \boldsymbol{C}_{\mathrm{e}_\alpha}}{\partial \boldsymbol{C}}$ can be derived using the incompressibility constraint given by Eq. (50). Differentiation of the left-hand side of Eq. (50) with respect to the right Cauchy–Green tensor $\boldsymbol{C}$ leads to

$$\frac{\partial(\det \boldsymbol{C}_{\mathrm{e}_\alpha})}{\partial \boldsymbol{C}} = \frac{\partial(\det \boldsymbol{C}_{\mathrm{e}_\alpha})}{\partial \boldsymbol{C}_{\mathrm{e}_\alpha}} : \frac{\partial \boldsymbol{C}_{\mathrm{e}_\alpha}}{\partial \boldsymbol{C}} = J^2 \boldsymbol{C}^{-1}_{\mathrm{e}_\alpha} : \frac{\partial \boldsymbol{C}_{\mathrm{e}_\alpha}}{\partial \boldsymbol{C}}. \tag{112}$$

Compared to the differentiation of the right-hand side of Eq. (50) with respect to the right Cauchy–Green tensor $\boldsymbol{C}$, the fourth order tensor $\frac{\partial \boldsymbol{C}_{\mathrm{e}_\alpha}}{\partial \boldsymbol{C}}$ can be deduced from the following relationship

$$\boldsymbol{C}^{-1}_{\mathrm{e}_\alpha} : \frac{\partial \boldsymbol{C}_{\mathrm{e}_\alpha}}{\partial \boldsymbol{C}} = \boldsymbol{C}^{-1}. \tag{113}$$

Data availability

Data will be made available on request.

References

Amin, A., Lion, A., Sekita, S., Okui, Y., 2006. Nonlinear dependence of viscosity in modeling the rate-dependent response of natural and high damping rubbers in compression and shear: Experimental identification and numerical verification. Int. J. Plast. 22 (9), 1610–1657.

Anand, L., 1985. Constitutive equations for hot-working of metals. Int. J. Plast. 1 (3), 213–231.

Anon, 2024. Mathworks MATLAB oprimization toolbox. https://uk.mathworks.com/help/optim/ug/fmincon.html. (Accessed 01 June 2024).

Arruda, E.M., Boyce, M.C., 1993. A three-dimensional constitutive model for the large stretch behavior of rubber elastic materials. J. Mech. Phys. Solids 41 (2), 389–412.

Bergström, J., Boyce, M., 1998. Constitutive modeling of the large strain time-dependent behavior of elastomers. J. Mech. Phys. Solids 46 (5), 931–954.

Bischoff, J., Arruda, E., Grosh, K., 2002. A microstructurally based orthotropic hyperelastic constitutive law. J. Appl. Mech. 69 (5), 570–579.

Bischoff, J.E., Arruda, E.M., Grosh, K., 2004. A rheological network model for the continuum anisotropic and viscoelastic behavior of soft tissue. Biomech. Model. Mechanobiol. 3, 56–65.

Bonet, J., 2001. Large strain viscoelastic constitutive models. Int. J. Solids Struct. 38 (17), 2953–2968.

Bonet, J., Gil, A.J., Wood, R.D., 2016. Nonlinear Solid Mechanics for Finite Element Analysis: Startics. Cambridge University Press.

Budday, S., Sommer, G., Haybaeck, J., Steinmann, P., Holzapfel, G.A., Kuhl, E., 2017. Rheological characterization of human brain tissue. Acta Biomater. 60, 315–329.

Chockalingam, S., Roth, C., Henzel, T., Cohen, T., 2021. Probing local nonlinear viscoelastic properties in soft materials. J. Mech. Phys. Solids 146, 104172.

Ciambella, J., Nardinocchi, P., 2021. A structurally frame-indifferent model for anisotropic visco-hyperelastic materials. J. Mech. Phys. Solids 147, 104247.

Clifton, R.J., Wang, X., Jiao, T., 2016. A physically-based, quasilinear viscoelasticity model for the dynamic response of polyurea. J. Mech. Phys. Solids 93, 8–15.

Dal, H., Gültekin, O., Açıkgöz, K., 2020. An extended eight-chain model for hyperelastic and finite viscoelastic response of rubberlike materials: Theory, experiments and numerical aspects. J. Mech. Phys. Solids 145, 104159.

Dusane, A.R., Lenarda, P., Paggi, M., 2023. Computational modeling of viscoelastic backsheet materials for photovoltaics. Mech. Mater. 186, 104810.
Eleni, P.N., Perivoliotis, D., Dragatogiannis, D.A., Krokida, M.K., Polyzois, G.L., Charitidis, C.A., Ziomas, I., Gettleman, L., 2013. Tensile and microindentation properties of maxillofacial elastomers after different disinfecting procedures. J. Mech. Behav. Biomed. Mater. 28, 147–155.
Ellmer, N., Ortigosa, R., Martínez-Frutos, J., Gil, A.J., 2024. Gradient enhanced gaussian process regression for constitutive modelling in finite strain hyperelasticity. Comput. Methods Appl. Mech. Engrg. 418, 116547. http://dx.doi.org/10.1016/j.cma.2023.116547, URL https://www.sciencedirect.com/science/article/pii/S0045782523006710.
Ericksen, J.L., Rivlin, R., 1997. Large elastic deformations of homogeneous anisotropic materials. In: Collected Papers of RS Rivlin: Volume I and II. Springer, pp. 467–487.
Freed, A.D., Rajagopal, K., 2016. A viscoelastic model for describing the response of biological fibers. Acta Mech. 227, 3367–3380.
Garcia-Blanco, E., Ortigosa, R., Gil, A.J., Bonet, J., 2019a. Towards an efficient computational strategy for electro-activation in cardiac mechanics. Comput. Methods Appl. Mech. Engrg. 356, 220–260. http://dx.doi.org/10.1016/j.cma.2019.06.042, URL https://www.sciencedirect.com/science/article/pii/S0045782519303871.
Garcia-Blanco, E., Ortigosa, R., Gil, A.J., Lee, C.H., Bonet, J., 2019b. A new computational framework for electro-activation in cardiac mechanics. Comput. Methods Appl. Mech. Engrg. 348, 796–845. http://dx.doi.org/10.1016/j.cma.2019.01.042.
Ghosh, K., Lopez-Pamies, O., 2021. On the two-potential constitutive modeling of dielectric elastomers. Meccanica 56, 1505–1521.
Gurtin, M.E., 1968. On the thermodynamics of materials with memory. Arch. Ration. Mech. Anal. 28, 40–50.
Gurtin, M.E., Fried, E., Anand, L., 2010. The Mechanics and Thermodynamics of Continua. Cambridge University Press.
Haupt, P., Lion, A., 2002. On finite linear viscoelasticity of incompressible isotropic materials. Acta Mech. 159 (1), 87–124.
Holthusen, H., Rothkranz, C., Lamm, L., Brepols, T., Reese, S., 2023. Inelastic material formulations based on a co-rotated intermediate configuration—Application to bioengineered tissues. J. Mech. Phys. Solids 172, 105174. http://dx.doi.org/10.1016/j.jmps.2022.105174.
Holzapfel, G.A., 1996. On large strain viscoelasticity: continuum formulation and finite element applications to elastomeric structures. Internat. J. Numer. Methods Engrg. 39 (22), 3903–3926.
Holzapfel, G.A., 2002. Nonlinear Solid Mechanics: a Continuum Approach for Engineering Science. Kluwer Academic Publishers Dordrecht.
Holzapfel, G.A., Gasser, T.C., Ogden, R.W., 2000. A new constitutive framework for arterial wall mechanics and a comparative study of material models. J. Elast. Phys. Sci. Solids 61, 1–48.
Horák, M., Gil, A.J., Ortigosa, R., Kružík, M., 2023. A polyconvex transversely-isotropic invariant-based formulation for electro-mechanics: Stability, minimisers and computational implementation. Comput. Methods Appl. Mech. Engrg. 403, 115695.
Hossain, M., Vu, D.K., Steinmann, P., 2012. Experimental study and numerical modelling of VHB 4910 polymer. Comput. Mater. Sci. 59, 65–74.
Huber, N., Tsakmakis, C., 2000. Finite deformation viscoelasticity laws. Mech. Mater. 32 (1), 1–18.
Humphrey, J.D., Rajagopal, K., 2002. A constrained mixture model for growth and remodeling of soft tissues. Math. Models Methods Appl. Sci. 12 (03), 407–430.
Kröner, E., 1959. Allgemeine kontinuumstheorie der versetzungen und eigenspannungen. Arch. Ration. Mech. Anal. 4, 273–334.
Kumar, A., Lopez-Pamies, O., 2016. On the two-potential constitutive modeling of rubber viscoelastic materials. C. R. Mec. 344 (2), 102–112.
Lee, E.H., 1969. Elastic-plastic deformation at finite strains. J. Appl. Mech. 36, 1–6.
Lenarda, P., Paggi, M., 2022. A computational framework for rheologically complex thermo-visco-elastic materials. Int. J. Solids Struct. 236, 111297.
Li, X., Tao, J., Landauer, A.K., Franck, C., Henann, D.L., 2022. Large-deformation constitutive modeling of viscoelastic foams: Application to a closed-cell foam material. J. Mech. Phys. Solids 161, 104807.
Limbert, G., Middleton, J., 2004. A transversely isotropic viscohyperelastic material: Application to the modeling of biological soft connective tissues. Int. J. Solids Struct. 41 (15), 4237–4260.
Linder, C., Tkachuk, M., Miehe, C., 2011. A micromechanically motivated diffusion-based transient network model and its incorporation into finite rubber viscoelasticity. J. Mech. Phys. Solids 59 (10), 2134–2156.
Liu, H., Holzapfel, G.A., Skallerud, B.H., Prot, V., 2019. Anisotropic finite strain viscoelasticity: Constitutive modeling and finite element implementation. J. Mech. Phys. Solids 124, 172–188.
Liu, J., Latorre, M., Marsden, A.L., 2021. A continuum and computational framework for viscoelastodynamics: I. finite deformation linear models. Comput. Methods Appl. Mech. Engrg. 385, 114059.
Liu, Z., Reinoso, J., Paggi, M., 2022. Hygro-thermo-mechanical modeling of thin-walled photovoltaic laminates with polymeric interfaces. J. Mech. Phys. Solids 169, 105056.
Lubliner, J., 1985. A model of rubber viscoelasticity. Mech. Res. Commun. 12 (2), 93–99.
Martínez-Frutos, J., Ortigosa, R., Gil, A.J., 2021a. A convex multi-variable based computational framework for multilayered electro-active polymers. Comput. Methods Appl. Mech. Engrg. 374, 113567.
Martínez-Frutos, J., Ortigosa, R., Gil, A.J., 2021b. In-silico design of electrode meso-architecture for shape morphing dielectric elastomers. J. Mech. Phys. Solids 157, 104594.
Naghdabadi, R., Baghani, M., Arghavani, J., 2012. A viscoelastic constitutive model for compressible polymers based on logarithmic strain and its finite element implementation. Finite Elem. Anal. Des. 62, 18–27.
Nedjar, B., 2007. An anisotropic viscoelastic fibre–matrix model at finite strains: continuum formulation and computational aspects. Comput. Methods Appl. Mech. Engrg. 196 (9–12), 1745–1756.
Nguyen, T.D., Jones, R.E., Boyce, B.L., 2007. Modeling the anisotropic finite-deformation viscoelastic behavior of soft fiber-reinforced composites. Int. J. Solids Struct. 44 (25–26), 8366–8389.
Ortigosa, R., Martínez-Frutos, J., Gil, A.J., 2022a. Viscoelastic up-scaling rank-one effects in in-silico modelling of electro-active polymers. Comput. Methods Appl. Mech. Engrg. 389, 114358.
Ortigosa, R., Martínez-Frutos, J., Gil, A.J., 2023. Programming shape-morphing electroactive polymers through multi-material topology optimisation. Appl. Math. Model. 118, 346–369.
Ortigosa, R., Martínez-Frutos, J., Mora-Corral, C., Pedregal, P., Periago, F., 2022b. Optimal control and design of magnetic field-responsive smart polymer composites. Appl. Math. Model. 103, 141–161.
Pioletti, D.P., Rakotomanana, L., Benvenuti, J.-F., Leyvraz, P.-F., 1998. Viscoelastic constitutive law in large deformations: application to human knee ligaments and tendons. J. Biomech. 31 (8), 753–757.
Reese, S., Govindjee, S., 1997. Theoretical and numerical aspects in the thermo-viscoelastic material behaviour of rubber-like polymers. Mech. Time-Depend. Mater. 1, 357–396.
Reese, S., Govindjee, S., 1998. A theory of finite viscoelasticity and numerical aspects. Int. J. Solids Struct. 35 (26–27), 3455–3482.
Sadik, S., Yavari, A., 2024. Nonlinear anisotropic viscoelasticity. J. Mech. Phys. Solids 182, 105461.
Sansour, C., 2008. On the physical assumptions underlying the volumetric-isochoric split and the case of anisotropy. Eur. J. Mech. A Solids 27 (1), 28–39.
Sidoroff, F., 1974. Un modèle viscoélastique non linéaire avec configuration intermédiaire. J Méc. 13 (4), 679–713.
Simo, J.C., 1987. On a fully three-dimensional finite-strain viscoelastic damage model: Formulation and computational aspects. Comput. Methods Appl. Mech. Engrg. 60 (2), 153–173.
Simo, J.C., 1988. A framework for finite strain elastoplasticity based on maximum plastic dissipation and the multiplicative decomposition: Part I. Continuum formulation. Comput. Methods Appl. Mech. Engrg. 66 (2), 199–219.

Simo, J., Hughes, T., 1998. Computational Inelasticity. Springer, New York.
Simo, J.C., Miehe, C., 1992. Associative coupled thermoplasticity at finite strains: Formulation, numerical analysis and implementation. Comput. Methods Appl. Mech. Engrg. 98 (1), 41–104.
Sommer, G., Haspinger, D.C., Andrä, M., Sacherer, M., Viertler, C., Regitnig, P., Holzapfel, G.A., 2015a. Quantification of shear deformations and corresponding stresses in the biaxially tested human myocardium. Ann. Biomed. Eng. 43, 2334–2348.
Sommer, G., Schriefl, A.J., Andrä, M., Sacherer, M., Viertler, C., Wolinski, H., Holzapfel, G.A., 2015b. Biomechanical properties and microstructure of human ventricular myocardium. Acta Biomater. 24, 172–192.
Valentin, A., Humphrey, J.D., Holzapfel, G.A., 2013. A finite element-based constrained mixture implementation for arterial growth, remodeling, and adaptation: Theory and numerical verification. Int. J. Numer. Methods Biomed. Eng. 29 (8), 822–849.
Wijaya, I.P., Lopez-Pamies, O., Masud, A., 2023. A unified determinant-preserving formulation for compressible/incompressible finite viscoelasticity. J. Mech. Phys. Solids 177, 105312.
Wollner, M.P., Terzano, M., Rolf-Pissarczyk, M., Holzapfel, G.A., 2023. A general model for anisotropic pseudo-elasticity and viscoelasticity at finite strains. J. Mech. Phys. Solids 180, 105403.
Zheng, Q.-S., 1994. Theory of representations for tensor functions—A unified invariant approach to constitutive equations. Appl. Mech. Rev. 47 (11), 545–587. http://dx.doi.org/10.1115/1.3111066.